Temporal and Spatial Evolution of the Izu Island Arc, Japan in Terms of Sr-Nd-Pb Isotope Geochemistry

Dissertation

zur Erlangung des Doktorgrades

der Mathematisch-Naturwissenschaftlichen Fakultät

der Christian-Albrechts-Universität

zu Kiel

vorgelegt von

Angelika Schmidt

Kiel 2001

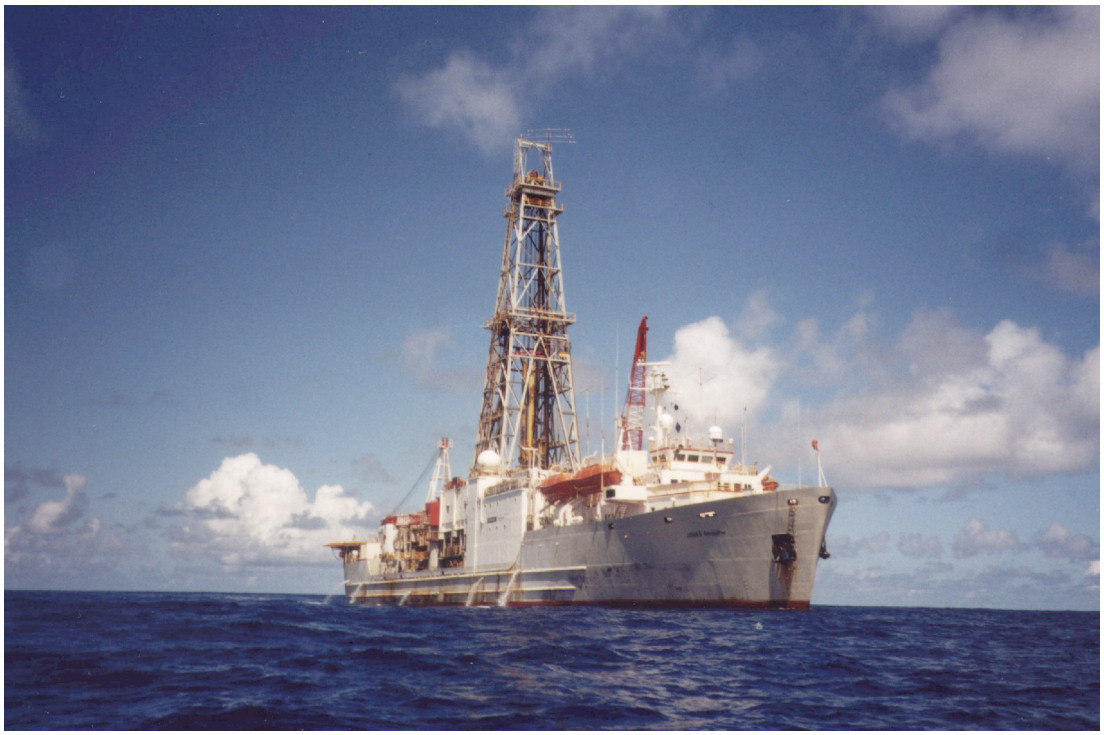

JOIDES Resolution bei der Probennahme im Pazifik 1999

Für

S. Bossan, E. Sehr, D. Beushausen,

A. de Haan, P. Ganske und R. Klemd -

die wichtigsten Lehrer, die ich hatte.

Referent: Prof. Dr. Kaj Hoernle

Korreferent: Dr. habil Matthias Hort

Tag der Disputation: 5. Juli 2001

zum Druck genehmigt: Kiel, den

Erklärung

Hiermit erkläre ich, die vorliegende Dissertation selbstständig und ohne unerlaubte Hilfen erstellt zu haben. Desweiteren habe ich weder diese noch eine ähnliche Arbeit an einer anderen Hochschule oder Abteilung im Rahmen eines Prüfungsverfahrens vorgelegt, veröffentlicht oder zur Veröffentlichung vorgelegt.

Kiel, den 5. Juni 2001

(Angelika Schmidt)

Danksagung

Der offizielle Teil

Ich möchte mich herzlich bei Prof. Kaj Hoernle und Dr. Susanne M. Straub bedanken, die mir durch die Idee und das Stellen des Erstantrages die Grundlage zur Bearbeitung dieses Themas geschaffen haben. Beide haben durch ihre Diskussionsbereitschaft und eigenen Ideen erheblich zum Gelingen dieser Arbeit beigetragen.

Ich danke ausserdem Dr. habil. Matthias Hort, der freundlicherweise die Korefferenz dieser Arbeit übernommen hat. Ihm möchte ich zudem für die vielen Male, die er mir zugehört hat, herzlich danken.

Für die Einarbeitung und Unterstützung im GEOMAR Isotopenlabor möchte ich mich bei Prof. Kaj Hoernle, Dr. Evelyn Zuleger, Dr. Folkmar Hauff und Silke Vetter bedanken. Die Isotopengeochemie und Isotopenmessung stellen die Grundlage dieser Arbeit dar und ohne die Hilfestellung dieser Personen wäre diese Arbeit niemals möglich gewesen. Ich bin der festen Überzeugung, dass das „TIMS“ nicht nur hochkompliziert ist, sondern auch über ein Eigenleben verfügt, dass nur wenige Leute in den Griff bekommen, zu denen Evi und Folkmar auf jeden Fall gehören.

Ein dickes Dankeschön geht an Dr. Paul van den Bogaard und Dr. Carsten Schirnick (beide GEOMAR), die mich bei der Probenauswahl und Aufbereitung für die $^{40}Ar/^{39}Ar$ Alterdatierung angeleitet haben. Ich danke Paul van den Bogaard ausserdem dafür, dass er die Altersdatierungen nicht nur durchgeführt, sondern sich auch viele Gedanken über deren Ergebnisse gemacht hat. Carsten Schirnick danke ich für die Beantwortung von etwa 100 Fragen sowie mindestens doppelt so vieler anderer Dinge, von denen er sicherlich weiss, was ich meine und die mir sehr geholfen haben.

Ebenfalls bedanken möchte ich mich bei Dr. Dieter Garbe-Schönberg und Heidi Blaschek (Universität Kiel) für die extrem freundliche Atmosphäre, Anleitung und Durchführung der ICP-MS Analysen sowie die Hilfe bei der Interpretation der Daten.

Dem Ocean Drilling Programm (ODP) und der Bundesanstalt für Geowissenschaften und Rohstoffe (BGR) danke ich dafür, dass sie mir die Teilnahme an ODP Leg 185 ermöglicht haben, das interessante Proben und Erfahrungen geliefert hat.

Ein Teil der bearbeiteten Proben wurde von Jim Gill, Fred Hochstaedter (beide University of California, Santa Cruz, USA) und Charlie Langmuir (Lamont Doherty Earth Observatory of Columbia University, USA) zur Verfügung gestellt. Ich danke ihnen dafür sowie für die rege Kooperation. Vom wissenschaftlichen Austausch mit Terry Plank und Katie Kelley (beide Boston University, USA), John Ludden (CRPG-CNRS, Nancy, Frankreich) sowie Julian Pearce (Cardiff University, UK) hat diese Arbeit wertvolle Anregungen erhalten.

Meine Arbeit wurde durch die Deutsche Forschungsgemeinschft (DFG) in den Projekten Ho1833/3 und 1833/7 gefördert.

Der persönliche Teil

Ich danke Kaj immens dafür, dass er das hier mit mir durchgezogen hat. Ich weiss, dass sowohl er, als auch Susanne nicht glücklich mit der Situation sind, aber ehrlich gesagt ist das keiner der Beteiligten! Ich weiss seine Unterstützung daher ganz besonders zu schätzen und es bedeutet mir viel, dass wir es tatsächlich -zumindest bis hier- geschafft haben!

Ich möchte außerdem Silke und Folkmar dafür danken, dass sie zugesagt haben die Chemie und Isotopenanalysen an meiner statt für die verbliebenen Leg 185 Proben zu übernehmen und ich verspreche bei der Auswertung der Daten mitzuarbeiten soviel es geht.

Einfach nur dafür dass es sie gibt danke ich O.T.T.O., Mari, Marco, Timo, Marion, Martin, Hendrick, Christoph, allen treuen Bremern (insbesondere Olli, Nici, Tina, Ralf G., Jens, Tanja, Tiffy, Michl, Britta, Eschti, Sascha, Michael, Natascha, Martin und Wieby) sowie allen werdenden oder frisch gewordenen Müttern und Vätern.

Ich danke meinen Volleyballern und meinem Chor dafür, dass sie mir so viele schöne Stunden in Kiel *ohne* Wissenschaft beschert haben!

Schon immer danken wollte ich den Erfindern von Internet und email, sowie dem Erfinder gelatinefreier Gummibärchen. Überlebenswichtig war im letzten Monat zudem die „5 Minuten Terrine“, so dass auch deren Erfinder mein Dank gebührt!

Desweiteren danke ich allen, die Teile dieser Arbeit Korrektur gelesen haben oder ihre Hilfe angeboten haben. Ich danke ausserdem allen, die mich getröstet haben ohne mir zu sagen was die *einzig richtige* Möglichkeit ist, die mich in den Arm nehmen konnten *ohne* konstruktive Besserungsvorschläge zu machen, die mir in die Augen gesehen haben und mir glaubhaft versichert haben: „Du schaffst das schon“, die wirklich für mich da waren, oder mir zumindest das Gefühl gegeben haben, dass sie da wären, wenn es hart auf hart kommt, und allen, die nicht müde geworden sind sich mein Gejammer anzuhören! Ich danke in diesem Zusammenhang besonders Geesche, Malte, Sönke, Sandra, Bea, Britta, Judith, Reinhard, Annie, Svend, 2 x Matthias H., Susi, Nico, Lothar, 2 x Ralf S., Alex, Carsten, Frau Herden und allen, die ich vergessen habe. Helge danke ich für den Fisch und Jörg für die 100.000 aufmunternden Worte per Telefon und email aus dem Land der unbegrenzten Möglichkeiten.

Ralf kann ich leider für fast nichts danken, außer dafür, dass er mir in den letzten Tagen das Gefühl gegeben hat, dass doch noch alles gut wird, was ich zwar nicht glaube, wodurch ich aber endlich wieder schlafen und klarer denken konnte.

Von ganzem Herzen danke ich meiner Mutter für 29 Jahre Freundschaft und bedingungsloses zu mir stehen sowie meinem Kind für seinen Lebenswillen, den er oder sie ganz sicher von mir hat!

Dankeschön!

Zusammenfassung

Die zeitliche und räumliche Entwicklung des Izu Inselbogensystems

Das südlich von Japan gelegene Izu-Bonin Inselbogensystem befindet sich an einer der aktivsten Plattengrenzen der Erde. Die Pazifische Platte wird hier unter die Philippinische Platte subduziert, was zu aktivem Inselbogenvulkanismus führt. Seit Beginn der Subduktion im Mittleren Eozän wechseln Phasen von Arc Front Vulkanismus mit Phasen von Backarc Rifting und Spreading. Die Zeugen der explosiven vulkanischen Aktivität finden sich außer in den subaerischen Vulkanen auch in submarinen Aschelagen am Meeresboden, die in mehreren Ausfahrten des internationalen Bohrprogrammes Deep Sea Drilling Project/Ocean Drilling Programm (DSDP/ODP) erbohrt wurden. Im Gegensatz zu den subaerischen Vulkankegeln, die hohen Erosionsraten und intensiver Verwitterung unterliegen, überliefern die submarinen Aschelagen die vulkanische Aktivität seit Beginn des explosiven Vulkanismus. Eigene $^{40}Ar/^{39}Ar$-Laserdatierungen und Stufenheizungsexperimente an Einzelkristallen und Gläsern dieser Aschelagen, sowie interpolierte Alter anhand von Sedimentationsraten in Bohrkern 782A belegen eine explosive Inselbogenaktivität von über 40 Millionen Jahren im Izu Forearc. Ein Hiatus in der vulkanischen Aktivität zu Beginn des Miozäns (23-17 Ma) teilt die Aschelagen in eine *jüngere* Gruppe mit Altern <17 Ma und eine *ältere* Gruppe mit Altern >23 Ma ein.

Die in dieser Arbeit bestimmten Sr-, Nd- und Pb-Isotopenzusammensetzungen der Aschelagen zeigen relativ geringe Variationen innerhalb der letzten 15 Millionen Jahre, deutliche Schwankungen in den Isotopenverhältnissen der älteren Gruppe und generelle Trends zu niedrigeren Nd und Pb Isotopenverhältnissen mit zunehmendem Alter.

Die räumlichen Variationen des Izu Inselbogensystems wurden an Laven der rezenten vulkanischen Front, des seit 3 Ma aktiven Rifts, des submarinen und auf 13-3 Ma datierten Rear Arcs und erbohrten Laven und Gläsern des 25-17 Ma Shikoku Backarc Beckens untersucht. Die Abfolge von vulkanischer Front, aktivem Rift, Rear Arc und Backarc Becken entspricht der räumlichen Abfolge dieser Bereiche von Ost nach West.

Spurenelement- und Isotopenzusammensetzungen zeigen deutliche geochemische Unterschiede zwischen den einzelnen Zonen des Inselbogens an. So sind die Arc Front Laven am verarmtesten in inkompatiblen Spurenelementen, am unradiogensten in den $^{143}Nd/^{144}Nd$-Verhältnissen und am radiogensten in den Sr-, und Pb-Isotopenverhältnissen. Sie überlappen mit der jüngeren Gruppe der Aschelagen.

Legt man ein Corner-Flow-Modell für die Strömung des Mantelmaterials zugrunde, so sind alle Isotopenverhältnisse durch 2-Komponentenmischung zwischen dem unterlagerndem, asthenosphärischen Mantelkeil und einer Subduktionskomponente erklärbar, die aus Fluiden der subduzierten Platte (Sediment und alterierte Ozeankruste)

besteht. Die räumlichen Unterschiede in der Geochemie weisen darauf hin, dass beide Komponenten heterogen sind. Der Mantelkeil unter der vulkanischen Front ist demnach infolge von Schmelzentzug durch Backarc Spreizen, Rear Arc- und Rift Vulkanismus stärker verarmt als im Backarc, Rear Arc und Riftbereich selbst. Gleichzeitig verarmt die Subduktionskomponente durch zunehmende Dehydrierung mit zunehmender Subduktionstiefe immer stärker in inkompatiblen Spurenelementen. Mischungsmodelle mit diesen Annahmen belegen, dass die Geochemie durch 2-Komponentenmischung erklärbar ist.

Die zeitliche geochemische Entwicklung zeigt an, dass die Verarmung des Mantelkeils unterhalb der vulkanischen Front mit Beginn des Schmelzentzugs durch Backarc Spreizen im Shikoku Becken vor etwa 25 Ma begann. Da die Aschelagen eine leichte zeitliche Verzögerung dessen anzeigen, ist anzunehmen, dass das verarmte Mantelmaterial bedingt durch die Fließgeschwindigkeit erst einige Millionen Jahre später unter die vulkanische Front gelangte. Durch den anhaltenden Schmelzentzug hinter der vulkanischen Front ist die vulkanische Front selbst seitdem verarmt, was infolge des Hiatus in der vulkanischen Aktivität jedoch erst seit etwa 17 Ma überliefert ist.

Neben dem Zustand des Mantelkeils und der Subduktionskomponente spiegeln sich auch der Eintrag in den Inselbogen und die Struktur der Subduktionszone im vulkanischen Ausstoß wider. Der Einfluß des Eintrages zeigt sich in der zeitlichen Entwicklung der Pb-Isotopenverhältnisse, die vermutlich auf einer geringeren Sedimentbedeckung und einem geringeren Alter der subduzierten Platte und damit einer geringeren Radiogenität in Pb im Eozän und Oligozän beruhen. Noch deutlicher wird die Bedeutung des Eintrages im Vergleich der Izu Arc Front mit der südlich angrenzenden Mariana Arc Front. Da im Marianen Tiefseegraben Material (Sediment und Ozeankruste) mit radiogenerer Pb-Isotopensignatur subduziert wird als im Izu Tiefseegraben, sind die Pb Isotopenverhältnisse der Marianen Arc Front deutlich radiogener als die der Izu Arc Front. Die steiler (80-90°) abtauchende Ozeanplatte unterhalb der Marianen bewirkt außerdem, dass es zu Elementrezyklierung durch (Sediment-) Schmelzen zusätzlich zu der durch Fluide kommt, wohingegen Elemente in der Izu Arc Front aufgrund des flacheren Einfallswinkels (60-70°) ausschliesslich durch Fluide rezykliert werden. Dies zeigt sich am deutlichsten in den Spurenelementmustern und Nd-Isotopenverhältnissen.

Summary

The Temporal and Spatial Evolution of the Izu Subduction System

The Izu-Bonin Island arc is located south of Japan on one of the most active plate boundaries on earth. The Pacific Plate is subducted beneath the Philippine Sea Plate resulting in active island arc volcanism. Since subduction began in the Middle Eocene, phases of arc front volcanism alternated with phases of backarc spreading, rear arc volcanism and rifting. Except in the subaerial volcanoes, explosive volcanic activity is documented in submarine volcaniclastic layers. These layers have been recovered by deep sea drilling in several cruises of the international Deep Sea Drilling Project/Ocean Drilling Program (DSDP/ODP). Because the subaerial volcanoes are subject to high erosion rates and atmospheric alteration, the submarine volcaniclastic layers contain a more complete record of the explosive volcanic activity. Our own $^{40}Ar/^{39}Ar$ laserdating and step heating experiments from single crystal and glass particles from Hole 782A in the Izu forearc, as well as interpolated ages based on sedimentation rates, reveal volcanic activity in the Izu volcanic front for more than 40 million years. Due to a hiatus in volcanic activity between 23-17 Ma, arc volcanism is split into a <17 Ma *younger* group and a >23 Ma *older* group.

The Sr, Nd and Pb isotope ratios from the volcaniclastic layers <17 Ma show nearly constant isotope ratios, while the isotope ratios of the older group show larger variations and on average tend to less radiogenic Nd and Pb isotopic compositions with age.

The spatial variations of the Izu arc system were investigated on lavas from the recent volcanic front, the active rift (<3 Ma), submarine rear arc volcanoes (13-3 Ma) and lavas and glass particles drilled in the Shikoku backarc basin (25-17 Ma). The sequence of volcanic front, rift, rear arc and backarc basin corresponds to the spatial sequence from the trench to the West.

Trace element and isotope ratios reveal distinct geochemical signatures for each zone of the arc with the volcanic front being most depleted in incompatible trace elements and showing the least radiogenic Nd isotope ratios and the most radiogenic Sr and Pb isotope ratios. The recent volcanic front shows broad overlapping with the younger volcaniclastic group.

Assuming a corner flow model for the streaming of mantle material, the isotope ratios can be explained by two component mixing between the underlying asthenospheric mantle wedge and a subduction component consisting of fluids from the subducted plate (sediments and altered oceanic crust). The spatial geochemical variations reveal that both components must be heterogeneous across the arc. The mantle wedge beneath the volcanic front is thus more depleted than behind the arc front (backarc, rear arc and rift), which we ascribe to melt extraction in the backarc, rear arc and rift region. At the same time the subduction component continuously dehydrates with increasing depths of the subducting plate resulting

in a subduction component more and more depleted in incompatible trace elements. Mixing models based on these assumptions show that the across arc geochemical differences can be explained accordingly.

The temporal geochemical evolution shows that depletion of the mantle wedge beneath the volcanic front started when the Shikoku Basin began to spread about 25 Ma ago. The volcaniclastic layers reveal a slight time delay of depletion, that suggests that the depleted material reached the magma source beneath the volcanic front a few million years later possibly due to the flow velocity of the mantle material. Subsequently there was almost continuous melt extraction behind the volcanic front. This results in the depleted mantle wedge beneath the volcanic front, which was detected only 17 million years ago due to the hiatus in volcanic activity.

With the exception of the state of enrichment or depletion of the mantle wedge and the subduction component, the input into the arc as well as the structure of the subduction zone are reflected in the arc output. The input into the arc is reflected in the temporal evolution of the Pb isotopes. These data possibly reflect a less radiogenic input in the Eocene and Oligocene due to the lesser age and smaller sediment carapace of the subducting plate, which is supported by a comparison of the recent Izu volcanic front with the southerly adjacent Mariana volcanic front. Because the input (sediment and oceanic crust) into the Mariana trench is more radiogenic in Pb, the volcanic output of the Mariana volcanic front is more radiogenic in Pb than in the Izu volcanic front. The steeper subduction angle beneath the Marianas (80-90°) results further in element recycling in (sediment-) melts in addition to fluids, whereas in the Izu arc the flatter subduction angle (60-70°) is unable to yield P-T conditions capable of generating sediment melt conditions beneath the volcanic front. This is best reflected in the trace element patterns and Nd isotope ratios.

Table of Contents

II. Across Arc variations in Trace Elements and Isotopes in the Central Izu Arc, Japan 29-62

Eocene to Recent Evolution of the Izu Arc, Japan

Schmidt, A.*, Hoernle, K., Straub, S.M. and van den Bogaard, P.
(GEOMAR Research Center, Wischhofstr. 1-3, 24148 Kiel, Germany)

Keywords: Izu arc, Sr-Nd-Pb isotopes, $^{40}Ar/^{39}Ar$ age dating

*corresponding author
Tel. (49) 431-600-2644
Fax (49) 431-600-2978

(For Submission to Journal of Petrology)

Abstract

In order to compare the geochemical evolution and sources of the Early Miocene to Eocene Izu-Bonin island arc with the Middle Miocene to Recent arc, we have dated volcaniclastic deposits (glass particles, plagioclase and hornblende phenocrysts) from ODP Site 782A with the $^{40}Ar/^{39}Ar$ method and determined Sr, Nd and Pb isotopic compositions of the same units and Recent volcanic front lavas. The age of the volcaniclastic layers range from 0.5 to 40 Ma, covering most of the Eocene to Recent arc history. The $^{40}Ar/^{39}Ar$ ages of the samples <17 Ma correspond well (within 2-sigma error) with the stratigraphic ages while the $^{40}Ar/^{39}Ar$ ages of the >23 Ma volcaniclastic layers are lower than the interpolated (based on sedimentation rates) ones. Due to a hiatus in the volcanic activity (17-23 Ma) that corresponds to the opening of the Shikoku backarc Basin, arc volcanism is split into a <17 Ma group and a >23 Ma group. The <17 Ma group shows nearly constant Sr, Nd and Pb isotopic compositions. The older group shows considerably larger variations and on average has less radiogenic Nd and Pb isotopic compositions. We interpret the differences in the Sr-Nd-Pb isotopic composition to reflect differences in the composition of the mantle wedge and in the input into the arc.

1 Introduction

Reconstructing the temporal evolution of island arcs over tens of millions of years is associated with a variety of problems, e.g. island arc volcanoes are subject to erosion, display stratigraphic gaps, can be tectonically disturbed and older eruptions are often covered by younger ones. Undisturbed volcaniclastic layers in marine sedimentary sequences, however, can potentially record the long-term evolution of magma sources in an island arc (e.g. Egeberg et al., 1992; Gill et al., 1994; Lee et al., 1995; Taylor and Nesbitt, 1998). The volcaniclastic layers drilled during ODP Leg 125 and 126 in the Izu fore- and backarc regions have been interpreted to have originated from explosive volcanism along the Izu volcanic arc (Arculus et al., 1992; Fujioka et al., 1992a; Fujioka et al., 1992b). Site 782 is located east of the subaerial volcanoes of Sumisujima and Torishima and since explosive eruptions occur almost exclusively along the volcanic front (VF) of the Izu arc, the Izu VF is the most likely source region of the volcaniclastic deposits. Some of the studied volcaniclastic layers were interpreted as primary ash-fall layers, whereas others were interpreted as secondary in origin (turbidity currents, bottom flows etc.) during Leg 125 (Fryer et al., 1990). Gill et al. (1994) showed that turbidities preserve many geochemical traits of their sources whose potential diversity is an advantage when studying the average geochemical characteristics of volcanism. Sedimentation rates and biostratigraphy may also isolate the age of a single volcaniclastic layer. In this study, $^{40}Ar/^{39}Ar$ age data was obtained to supplement the biostratigraphic age information on the Eocene to Pleistocene

volcaniclastic deposits. Twenty-five distinct volcaniclastic layers from Hole 782A have been investigated for Sr, Nd and Pb isotopes, in order to characterize the temporal evolution of the Izu arc from Eocene to Pleistocene.

2 Geological Evolution of the Izu Arc

The Izu-Bonin or Izu-Ogasawara island arc extends from Honshu Japan to the Bonin islands, that are sometimes denoted as Volcano arc (Fig. 1). The present-day tectonic configuration of the Izu-Bonin volcanic arc comprises (from east to west) 1) the trench, 2) the forearc region (between the trench axis and the active volcanic front), 3) the active VF, 4) the active Izu-Bonin rifts, 5) several inactive rear arc (RA) chains of seamount volcanoes, and 6) the Shikoku marginal basin, a Miocene backarc basin (Fig. 1). Subduction is currently taking place with velocities between 8 and 10 cm per year to the northwest (Fryer and Pearce, 1992). The arc evolution began in the early-middle Eocene when westward subduction of Pacific lithosphere began beneath the West Philippine plate (Karig and Moore, 1975). Rifting split the arc in the middle Oligocene and subsequent backarc spreading in the early Miocene isolated the Palau-Kyushu remnant arc from the active Izu arc system, forming the Shikoku Basin (Kobayashi and Nakada, 1979). Volcanic activity started to decrease in intensity at 27 Ma and was at a minimum between 23-17 Ma, with no record of explosive volcanism during early spreading of the Shikoku Basin (23-20 Ma; Taylor et al., 1990). Backarc spreading behind the Izu-Bonin ceased at 17-15 Ma, but volcanism resumed at the Izu VF. At the same time RA volcanism started. K-Ar age dating yields ages between 12.5 and 2.9 Ma for the RA volcanoes (Ishizuka et al., 1998). Except for VF volcanism, recent volcanic activity occurs within 10-15 km west of the VF in a series of rift basins that started opening about 2.8 Ma ago (Taylor, 1992) after volcanism in the RA ceased.

In summary, although the VF has been active nearly continuously from the early-middle Eocene (except between 23-20 Ma), volcanism behind the VF (backarc spreading ~25-17 Ma, RA ~13-3 Ma, rift <3 Ma) has been nearly continuous since ~25 Ma.

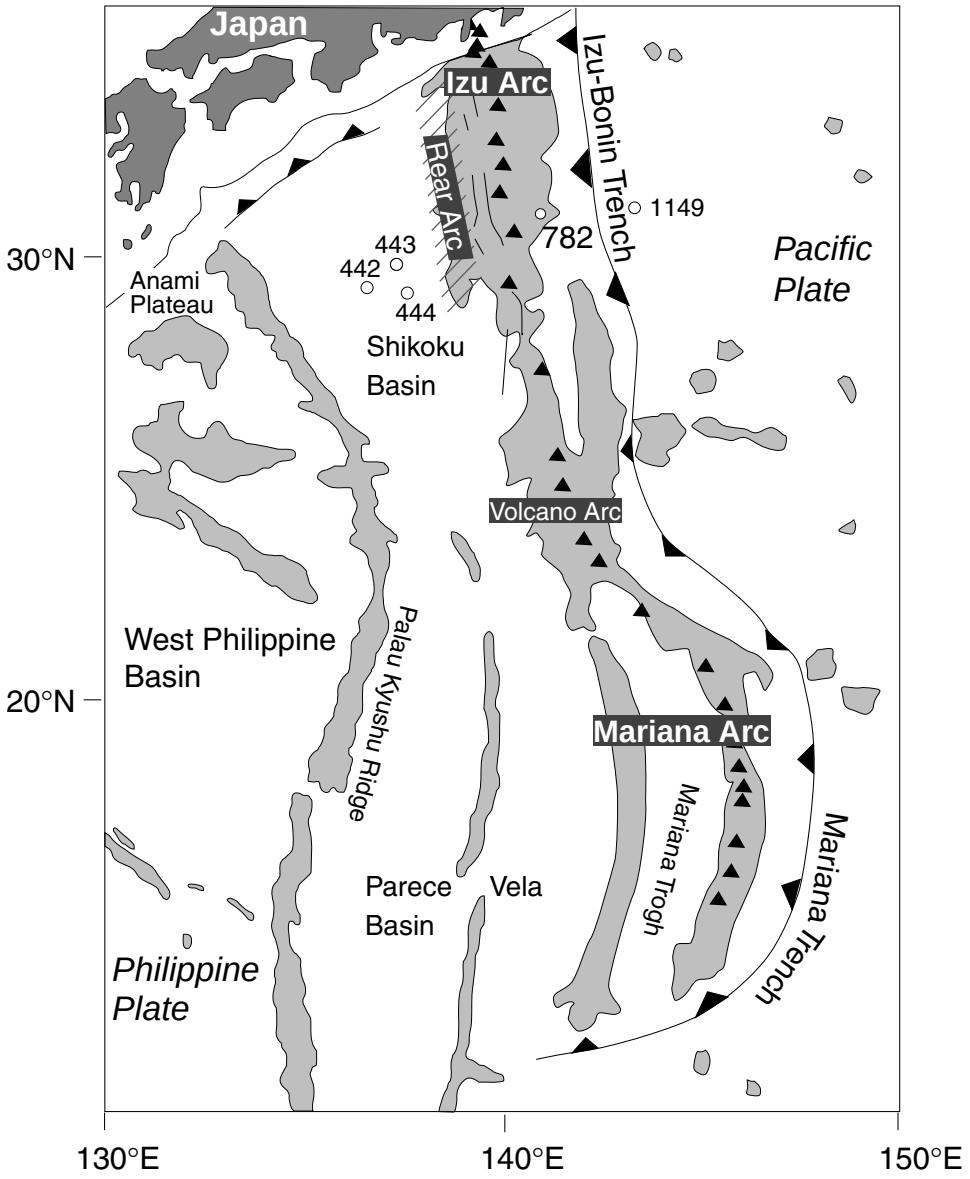

Figure 1: Active plate boundaries and geologic features in the Izu-Bonin-Mariana region. Black triangles denote volcanic front volcanoes, numbered open circles denote investigated ODP/DSDP drilling sites.

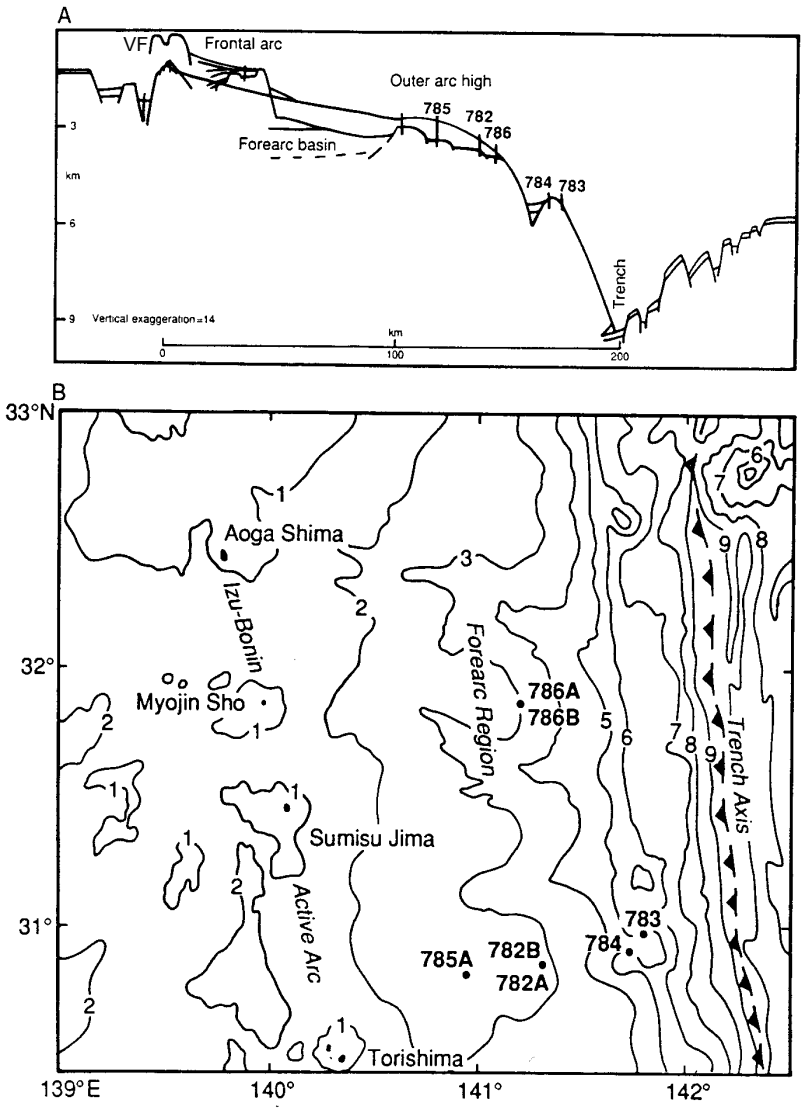

Figure 2: Schematic cross section of the morphology of the Izu forearc showing the locations of Sites 782-786 (A). Bathymetry (in 1000-m intervals) of the Izu forearc showing the Leg 125 drill sites (B). From Fryer and Pearce (1992).

3 Geology of Site 782

ODP Leg 125 Site 782 is situated on the Izu-Bonin forearc (Fig. 1, 2). The Izu forearc is interpreted to have experienced little deformation since subduction began (Honza and Tamaki, 1985). The forearc basin is thought to have developed behind an outer-arc high (Fig. 2A) that was uplifted in the early Eocene. The broad forearc basin is filled with several hundred meters of volcaniclastic and hemipelagic sediments. The basement of the basin presumably formed by volcanism in the initial stages of arc development in the Eocene and early Oligocene (Fryer and Pearce, 1992). Site 782 lies on the eastern margin of the Izu-Bonin forearc basin, about halfway between the active VF and the trench (Fig. 2B). Two lithostratigraphic units and 3 subunits (Fig. 3) were identified at Site 782 (Fryer et al., 1990):

- Subunit 1A (0-153.6 mbsf in 782A) is lower Pliocene to Holocene (?) gray to yellowish, homogeneous nannofossil marl.
- Subunit 1B (153.6-377.0 mbsf in 782A) is middle to upper Miocene light to dark gray, vitric nannofossil marl.
- Subunit 1C (377.0-409.2 mbsf) is middle Eocene to upper Oligocene vitric nannofossil chalk intercalated with tuffaceous sediment and pebble-rich sands and gravelly conglomerates.
- Unit 2 (409.2-476.8 mbsf in 782A and 459.3-468.9 mbsf in 782B) consists of angular to subrounded clasts of intermediate-acid lava.

Volcaniclastic layers and volcanic debris occur in each sedimentary subunit. Estimated sedimentation rates increased from the upper Oligocene section (about 5m/m.y.) through the upper Miocene and lower Pliocene sections (about 16.5 m/m.y.), to the upper Pliocene section (about 47 m/m.y.) with a possible decrease in the estimated sedimentation rate in the Pleistocene section. Two possible unconformities were identified in the succession: one between the lower Oligocene and upper Oligocene sections, the other between the uppermost Oligocene and middle Miocene sections, but these unconformities may simply reflect poor core recovery. The sediments exhibit common slump structures, burrows, and normal and inverse grading. More than 100 primary air-fall tephra layers and as many secondary volcaniclastic ash layers were identified in the cored section. The volcanogenic material in the primary tephra layers, in the secondary volcaniclastic layers and dispersed within the sediments include primary glass (obsidian), opaque minerals, feldspar, pyroxenes, and amphibole, together with alteration products such as chlorite, glauconite, zeolite, and epidote group minerals. The lavas of Unit 2 are glassy and fall into two geochemical groups, an andesite group and a dacite-rhyolite group.

During Leg 126 some volcaniclastic units were recovered that were interpreted to have been generated from sources to the west of the Izu arc (e.g. the Ryuku arc; Fujioka et al., 1992a; Fujioka et al., 1992b). We, however, interpret the volcaniclastic layers that we studied to be primary fallout ashes or proximal turbidites from the Izu arc.

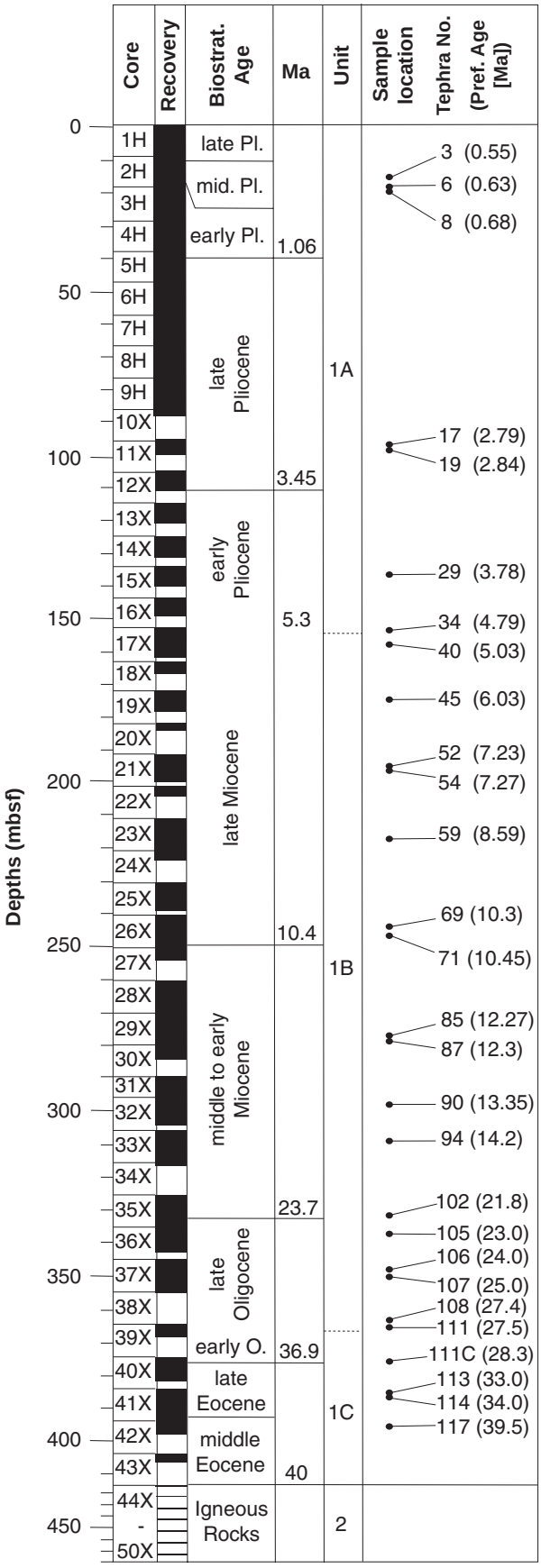

Figure 3: Sample location and biostratigraphic and assigned age (based on $^{40}Ar/^{39}Ar$ age data) of the volcaniclastic layers from Hole 782A. Modified after Fryer et al. (1990).

4 Sample Preparation and Analytical Procedures

Seven volcaniclastic layers from ODP Hole 782A were studied geochronologically and Sr, Nd and Pb isotope ratios were determined on twenty-five discrete volcaniclastic layers. The volcaniclastic rocks were deposited between 15 and 392 mbsf in Holocene to middle Eocene nannofossil marl and chalk (Fig. 3).

All samples from were freeze-dried and wet sieved with demineralized water to remove adhering clays and carbonate. The fraction <32-63 µm was rejected. After thorough washing in an ultrasonic bath the samples were hand-picked under a binocular microscope to obtain the freshest volcanic particles.

The $^{40}Ar/^{39}Ar$ laser dating was performed at the GEOMAR Geochronology Laboratory using a 25-W Spectra Physics Argon Laser and Mass Analyzer Product 260 noble gas mass spectrometer. Prior to irradiation, the mineral separates (plagioclase and hornblende) were etched in 5% HF acid and cleaned ultrasonically. The glass fragments were not etched but cleaned ultrasonically. All samples were irradiated in aluminium trays (with Cadmium shielding) at the Geesthacht Research Center (Germany) reactor position I-C6.

For the single-crystal and -particle analyses, between 6 and 33 single grains of each sample were evaporated in single fusion steps. Step-heating analyses were carried out with the laser as well, incrementally scanning samples with laser power increasing from ~100mW to 20W in 15 to 25 steps, but without temperature control. Procedural blanks at masses 36, 39, and 40 were determined as $6.5x10^{-14}$ ccSTP, $4.9x10^{-14}$ ccSTP, and $2.2x10^{-12}$ ccSTP during single-crystal analyses, and $1.1x10^{-13}$ ccSTP, $5.1x10^{-14}$ ccSTP, and $2.6x10^{-12}$ ccSTP during step-heating runs. Instrumental mass discrimination was determined by air pipette measurements (1.0108± 0.0005 per a.m.u.). Irradiation standard TC1 sanidine (27.92 Ma, Pringle et al., 1992) was used to monitor J values and gradients. Interfering neutron reactions on Ca and K were quantified based on co-irradiated pure CaF_2 and K_2SO_4 salt crystal analyses ($^{36}Ar/^{39}Ar_{Ca}$= 0.389± 0.006, $^{37}Ar/^{39}Ar_{Ca}$= 1104± 22, $^{40}Ar/^{39}Ar_{K}$= 0.0029± 0.0007). Raw data were corrected for mass discrimination, neutron fluence gradients, and interfering neutron reactions. Analytical error estimates include the uncertainties in the blanks and J values, and are quoted as 2 sigma throughout.

Pumice particles, glass and lithic whole rock particles from the volcaniclastic layers were analyzed for Sr, Nd and Pb isotope ratios. From some layers, more than one phase (e.g. lithic particles and pumice in sample 8, 90, 105 and 107) were analyzed to provide a test if the volcaniclastic layers preserve particles from a single volcanic event. The Sr, Nd and Pb isotope analyses were performed at the GEOMAR Finnigan MAT 262 Thermal Ion Mass Spectrometer (TIMS).

Prior to analyses all samples (hand-picked grains as well as powdered lava) were leached to remove possible surface contamination and to minimize the effects of alteration.

Detailed leaching experiments revealed that leaching for one hour with hot 6N HCl yields the best and reproducible results. The leaching residuum was dissolved in a mixture of hot concentrated HF and HNO_3. The ion exchange procedures have been discussed previously (Hoernle and Tilton, 1991). Total chemistry blanks for Sr, Nd and Pb were <300 pg and considered negligible.

Sr, Nd and Pb isotope ratios were measured on a Finnigan® MAT 262 thermal ionization mass spectrometer (TIMS) operating in the static mode at the GEOMAR Research Center in Kiel. Sr and Nd isotope ratios were normalized within run to $^{86}Sr/^{88}Sr$= 0.1194 and $^{146}Nd/^{144}Nd$= 0.7219. NBS 987 yielded $^{87}Sr/^{86}Sr$= 0.710243± 26 (2 sigma, N=25) and La Jolla $^{143}Nd/^{144}Nd$= 0.511843± 10 (2 sigma, N=21). The GEOMAR in house Nd Standard Nd-SPEX, calibrated against La Jolla gave $^{143}Nd/^{144}Nd$= 0.511704± 10 (2 sigma, N= 6) which corresponds to a La Jolla value of 0.511848. NBS 981 (N=20) gave $^{206}Pb/^{204}Pb$= 16.898± 10, $^{207}Pb/^{204}Pb$= 15.439± 11, $^{208}Pb/^{204}Pb$= 36.531± 35. The Pb isotope ratios of the samples were corrected for isotope fractionation to the values given in Todt et al. (1996). Replicate analyses yielded an external reproducibility better than 0.05% per a.m.u. (atomic mass unit) for Pb.

5 Results

5.1 Age Determination

The radiometric ages are presented in Table 1 and discussed in the following (all errors 2 sigma).

Sample	Phase	N	Type	Mean Apparent Age (Ma) or Plateau Age	2σ	MSWD	Isochron Age (Ma) or Integrated Age	2σ	Initial $^{40}Ar/^{39}Ar$	2σ	MSWD	Interpol. Age (Ma)
40	glass	19	sxx	**5.2**	**± 0.7**	1.44	4.5	± 0.8	296.6	± 1.0	1.17	5.03
40	glass	33	sth	6.8	± 1.6	1.95						5.03
94	glass	6	sxx	**13.3**	**± 1.0**	0.92	12.7	± 1.4	300.9	± 8.4	0.71	14.2
102	plag	25	sth	**23.5**	**± 0.9**	1.08						24.14
106	plag	13	sxx	24.6	± 0.5	0.84	24.7	± 3.0	291.7	± 74.9	0.91	26.64
106	hbl	9	sxx	21.9	± 1.2	2.40	21.9	± 3.2	299.5	±24.2	2.64	26.64
106	plag + hbl	23	sxx	**23.7**	**± 0.8**	2.40	24.7	± 1.0	281.7	± 11.8	2.02	26.64
111C	plag	30	sth	**28.3**	**±4.3**	1.28						32.19
117	plag	12	sxx	39.6	± 0.8	2.04	40.0	± 1.8	287.2	± 34.0	2.19	45.12
117	glass	4	sxx	38.4	± 3.0	2.82	40.1	± 8.2	291.4	± 18.2	3.86	45.12
117	plag + glass	16	sxx	**39.5**	**± 0.8**	2.18	39.8	± 1.0	291.7	± 6.4	2.13	45.12

Table 1: Results of the $^{40}Ar/^{39}Ar$ laser dating. MSWD= mean squared weighted deviates; sxx= single particle, sth= step-heating. N= number of single crystal analyses for sxx, number of heating steps for sth. Interpol. Age is based on biostratigraphy and sedimentation rates. Accepted ages in boldface.

40 (782A-17X4-0-2)

Nineteen obsidian glass fragments (0.1 to 0.76 mg) from fallout tephra sample 40 were analyzed by single-particle $^{40}Ar/^{39}Ar$ bulk fusion. Single-particle apparent ages ranging widely at generally high atmospheric ^{40}Ar contamination levels (88% to 99%), this data set yields a mean apparent age of 5.2± 0.7 Ma (MSWD= 1.44), an isochron age identical within error (4.5± 0.8 Ma; MSWD= 1.17, Fig. 4), and an initial $^{40}Ar/^{39}Ar$ ratio close to atmosphere 296.6± 1.0.

An incremental heating analysis of the available glass material remaining after single-particle fusion (2.891 mg), managed to preferentially drive off some of the atmospheric argon during low-temperature heating steps, and shows a largely undisturbed age spectrum with an integrated age of 7.4± 1.5 Ma, and a plateau region comprising 70% of the ^{39}Ar released (Fig. 5). Even the plateau step analyses, however, suffer from a high atmospheric contamination (63% to 98%), and thus yield a low-precision even on the plateau age estimate (6.6 ± 1.5 Ma; MSWD= 1.41).

94 (782A-33X5 36-39)

Six glass shards (0.07 to 0.2 mg) from volcaniclastic sample 94 range in apparent age from 11.6 to 14.9 Ma, and give a mean apparent age of 13.3± 1.0 Ma (MSWD= 0.92), identical within uncertainties to an isochron age of 12.7± 1.3 Ma at an initial $^{40}Ar/^{39}Ar$ ratio of 301± 8 (MSWD= 0.71). The argon isotope correlation diagram is depicted in Fig. 4.

102 (782A-35X6 142-144)

Laser step-heating analysis of a 2.942 mg plagioclase mineral separate from volcaniclastic sample 102 yields a flat age spectrum (Fig. 5), slightly disturbed only in the lowest-temperature ranges which comprise >60% of the bulk $^{40}Ar_{atm}$ released (but less than 2% of $^{39}Ar_K$), and an integrated age of 24.2± 1.2 Ma. Its step-heating plateau, comprising 98% of the $^{39}Ar_K$ released, gives an age of 23.5± 0.9 Ma (MSWD= 1.08).

106 (782A-37X4 43-45)

Single-crystal ages of 13 plagioclase and 9 hornblende crystals from this heterolithologic volcaniclastic layer have been determined. The plagioclase crystals give a mean apparent age of 24.6± 0.5 (MSWD= 0.84), an isochron age of 24.7± 2.9 Ma, and an initial of 292± 83 (MSWD= 0.91). The hornblende crystals give a mean apparent age of 21.9± 0.8 (MSWD= 1.16), an isochron age of 21.4± 1.0 Ma, initial 299± 15 (MSWD= 0.66). Combining plagioclase and hornblende data in a single isochron results in a mean apparent age of 23.7± 0.7 Ma (MSWD= 2.09), and an isochron age of 24.7± 0.8 Ma ($^{40}Ar/^{36}Ar_i$= 279± 10; MSWD= 1.48) for the eruption of the tephra material comprised by sample 106 (Fig. 4).

111C (782A-40X3 28-30)

Laser step-heating analysis of plagioclase mineral separate (1.738 mg) yields an age spectrum slightly disturbed in the low-temperature (high-atmos) region and an integrated age of 31.4± 7.6 Ma. The high-temperature plateau region comprises 94% of the $^{39}Ar_K$ released, and yields a plateau age of 28.3± 4.3 Ma (MSWD= 1.28, Fig. 5).

117 (782A-42X2 99-101)

Only four glass shards and twelve plagioclase crystals were recovered from sample 117 and analyzed by single-crystal fusion, yielding mean apparent ages of 39.6± 0.8 Ma (plagioclase; MSWD= 2.04) and 38.4± 3.0 Ma (glass; MSWD= 2.82) identical within uncertainties. Combining plagioclase and glass data into a single isochron gives a mean apparent age of 39.5± 0.8 Ma (MSWD= 2.18), and an isochron age of 39.8± 1.0 Ma ($^{40}Ar/^{36}Ar_i$= 292± 6; MSWD= 2.13) for the eruption of the tephra components in sample 117 (Fig. 4).

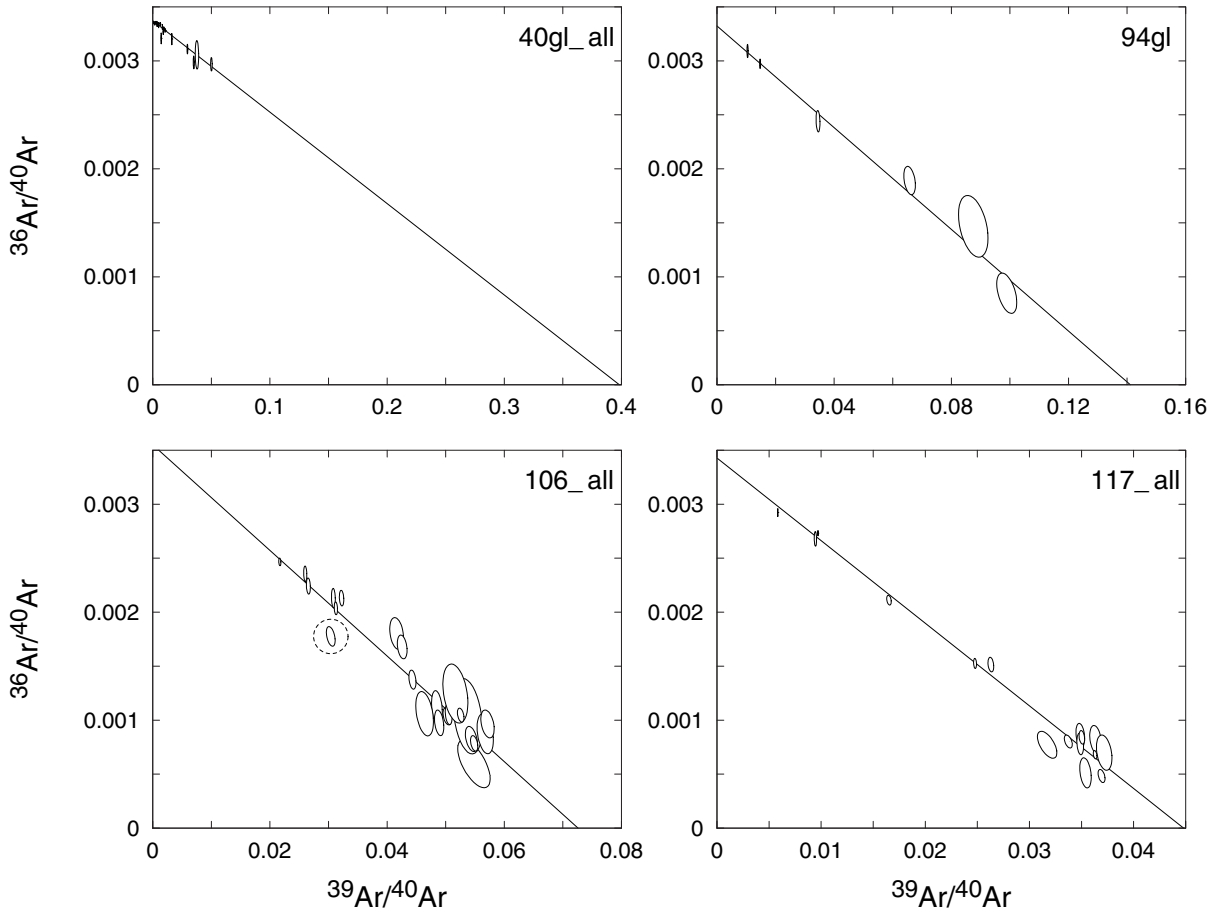

Figure 4: Argon isotope correlation diagrams of glass particles (sample 94), plagioclase and glass particles (sample 40 and 117), and plagioclase, hornblende and glass particles (sample 106). Regressions and isochrons were calculated after York (1969). All single crystal and particle analyses are shown with 1-σ error ellipses.

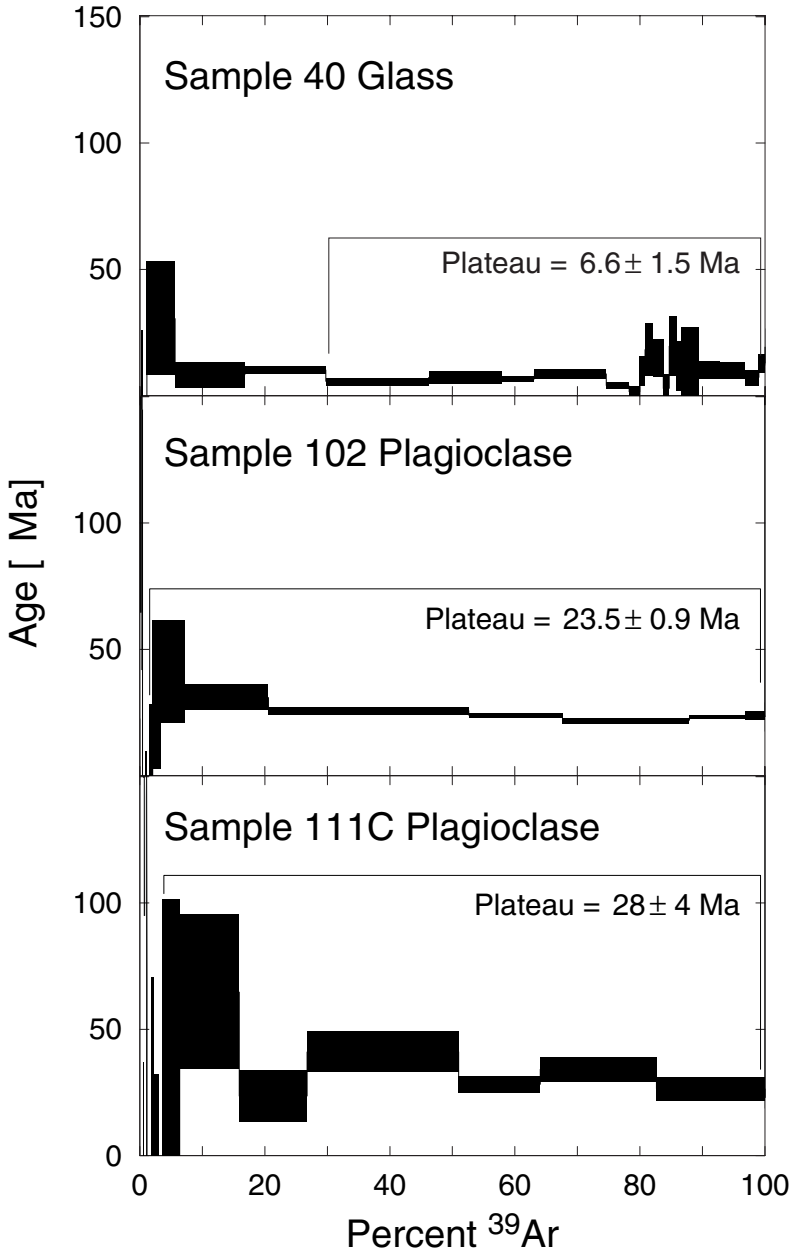

Figure 5: Age spectrum diagrams showing the results of laser step-heating analyses of glass particles (sample 40) and plagioclase crystals (sample 102 and 111C). Mean apparent ages of heating steps are shown with 1-σ error bars.

The ages of the tephra layers increase with increasing depths in the borehole and therefore stratigraphic depth correlates with increasing age. The $^{40}Ar/^{39}Ar$ ages show that the interpolated ages (interpolated based on biostratigraphic age and predicted sedimentation rates from Leg 125 Initial Report, Fryer et al., 1990) are often only slightly higher (especially at greater depths) than the $^{40}Ar/^{39}Ar$ ages. This may result from lower sedimentation rates than the estimated ones. Ages for units not dated here, are derived from interpolation. As we trust the independent age determination of the $^{40}Ar/^{39}Ar$ dating, we corrected the interpolated ages of volcaniclastic layers >23 Ma without $^{40}Ar/^{39}Ar$ age to slightly lower ages.

5.2 Sr-Nd-Pb Isotope Data

5.2.1 Variations in Measured Isotope Ratios

The radiogenic isotope results (measured and initial, age corrected) of the volcaniclastic deposits are presented in Table 2. The samples were divided into two age groups (<17 Ma and >23 Ma), separated by the gap in volcanic activity between 23-20 Ma during which backarc spreading occurred in the Shikoku Basin (~25-17 Ma; Shih, 1980). All samples studied are interpreted to have originated along the Izu VF. Isotope analyses of differing material (pumice and lithic particles) from the same volcaniclastic layer were performed on samples 8, 90, 105 and 107 (Table 2). The results are within 2-sigma error, consistent with delivering of different components within the volcaniclastic layers from the same magma source and from a single volcanic event. The Sr-Nd isotopic ratios of the volcaniclastic group <17 Ma ($^{87}Sr/^{86}Sr$= 0.70339-0.70360; $^{143}Nd/^{144}Nd$= 0.51307-0.51311) overlap almost complete with those of the VF lavas ($^{87}Sr/^{86}Sr$= 0.70331-0.70368; $^{143}Nd/^{144}Nd$= 0.51309-0.51311, Schmidt et al., in prep.). The $^{87}Sr/^{86}Sr$ ratios of the older volcaniclastic deposits (23-40 Ma) range between 0.70332-0.70413. If layer 117 is excluded, the variation is considerably smaller (0.70332-0.70368) and falls within the range of the younger VF samples. Sample 117 is the oldest sample studied, a highly vesicular pumice, thus alteration might have been more intense than in the younger samples. Therefore a possible reason for the more radiogenic Sr isotopic composition of sample 117 is that leaching may have failed to completely remove the effects of alteration. We, however, note that Oligocene basement samples recovered in ODP Hole 793B have similar $^{87}Sr/^{86}Sr$ ratios (Gill et al., 1994) and therefore the high Sr isotope ratio of sample 117 may reflect the composition of its source.

Table 2 (next two pages): Measured radiogenic isotope data ($_M$), mother/daughter isotope ratio and initial isotope ratio ($_i$) from Eocene to Pleistocene Izu volcaniclastic particles. Preferred age results from combination of $^{40}Ar/^{39}Ar$ ages and interpolated ages (based on sedimentation rates given in ODP Leg 125 Initial Report; Fryer et al., 1990). Trace elements of sample 3-94 are from Straub (in prep.). Mother/daughter isotope ratios of tephra 105-117 were interpolated based on the kind of volcanic particle (compare Appendix I, Table AI-1). $\varepsilon^t_{Nd} = (((^{143}Nd/^{144}Nd)_i / I^t_{CHUR}) - 1) \times 10^4$, $\varepsilon^0_{Nd} = (((^{143}Nd/^{144}Nd)_M / I^0_{CHUR}) - 1) \times 10^4$. P= pumice, G= glass, LP= lithic whole rock particle.

No.	3	6	8	8	17	19	29	34	40	45	52	54	59	69	71
sample	2H4-113-114	2H5-136-138	2H6-85-87	2H6-85-87	11X1-55-57	11X-3-0-1	15X3-9-10	17X1-56-58	17X4-0-2	19X-2-24-26	21X2-84-86	21X3-0-2	23X4-107-109	26X4-52-54	26X5-147-149
type	P	P	LP	P	LP	LP	LP	G	G	LP	LP	P	LP	P	P
pref. Age (Ma)	0.55	0.63	0.68	0.68	2.79	2.84	3.78	4.79	5.20	6.03	7.23	7.27	8.59	10.30	10.45
Rb	16.47	17.11	4.59	4.59	5.56	2.58	4.58	4.14	4.22	3.44	4.42	7.17	7.17	8.31	8.52
Sr	105.09	104.43	158.03	158.03	156.24	178.61	174.84	191.29	169.28	180.15	182.20	164.21	164.21	148.93	122.08
Rb/Sr	0.157	0.164	0.029	0.029	0.036	0.014	0.026	0.022	0.025	0.019	0.024	0.044	0.044	0.056	0.070
87Sr/86SrM	0.703565	0.703551	0.703548	0.703565	0.703504	0.703555	0.703565	0.703578	0.703534	0.703597	0.703553	0.703587	0.703528	0.703488	0.703507
2 s error	± 8	± 8	± 7	± 6	± 9	± 9	± 8	± 7	± 7	± 8	± 7	± 8	± 8	± 8	± 8
87Rb/86Sr	0.453	0.474	0.084	0.084	0.103	0.042	0.076	0.063	0.072	0.055	0.070	0.126	0.126	0.161	0.202
87Sr/86SrI	0.703562	0.703547	0.703547	0.703564	0.703500	0.703554	0.703561	0.703574	0.703529	0.703592	0.703546	0.703574	0.703513	0.703464	0.703477
Sm	3.63	3.79	1.70	1.70	2.23	2.39	2.01	2.36	2.66	1.64	2.00	3.12	3.12	4.31	3.90
Nd	10.59	11.96	4.78	4.78	5.81	5.94	5.34	6.18	7.19	4.08	4.90	8.62	8.62	12.30	11.42
Sm/Nd	0.343	0.317	0.356	0.356	0.384	0.402	0.376	0.382	0.370	0.401	0.407	0.362	0.362	0.351	0.342
143Nd/144NdM	0.513103	0.513091	0.513079	0.513073	0.513108	0.513087	0.513101	0.513084	0.513070	0.513078	0.513091	0.513093	0.513086	0.513081	0.513075
2 s error	± 8	± 9	± 9	± 9	± 9	± 9	± 8	± 8	± 7	± 8	± 6	± 9	± 8	± 8	± 9
147Sm/144NdM	0.206	0.191	0.214	0.214	0.231	0.242	0.226	0.230	0.223	0.241	0.245	0.218	0.218	0.211	0.206
143Nd/144Ndi	0.513103	0.513090	0.513078	0.513072	0.513104	0.513082	0.513095	0.513077	0.513062	0.513069	0.513080	0.513083	0.513074	0.513066	0.513061
etNd	9.08	8.84	8.60	8.48	9.16	8.74	9.02	8.68	8.41	8.56	8.80	8.86	8.71	8.62	8.51
e0Nd	9.08	8.84	8.61	8.48	9.17	8.75	9.03	8.70	8.43	8.59	8.84	8.88	8.74	8.64	8.52
Pb	6.30	6.53	2.80	2.80	5.92	2.50	5.20	2.34	2.86	2.72	2.77	4.23	2.81	4.63	5.20
U	0.400	0.481	0.129	0.129	0.190	0.100	0.100	0.120	0.120	0.090	0.100	0.200	0.100	0.300	0.260
Th	0.459	0.594	0.155	0.155	0.130	0.120	0.108	0.148	0.147	0.090	0.070	0.297	0.136	0.390	0.421
206Pb/204PbM	18.434	18.450	18.446	18.428	18.362	18.357	18.412	18.403	18.385	18.448	18.455	18.418	18.444	18.398	18.384
207Pb/204PbM	15.529	15.540	15.545	15.538	15.517	15.528	15.533	15.532	15.516	15.539	15.532	15.538	15.527	15.503	15.503
208Pb/204PbM	38.255	38.294	38.313	38.280	38.168	38.199	38.240	38.252	38.204	38.337	38.327	38.348	38.292	38.160	38.158
238U/204Pb	4.02	4.66	2.92	2.91	2.03	2.54	1.22	3.23	2.65	2.10	2.29	3.00	2.25	4.09	3.16
235U/204Pb	0.029	0.034	0.021	0.021	0.015	0.018	0.009	0.023	0.019	0.015	0.017	0.022	0.016	0.030	0.023
232Th/204Pb	4.77	5.95	3.62	3.62	1.43	3.14	1.36	4.13	3.35	2.17	1.65	4.60	3.16	5.50	5.28
232Th/238U	1.19	1.28	1.24	1.24	0.71	1.24	1.12	1.28	1.27	1.03	0.72	1.53	1.41	1.34	1.67
206Pb/204Pbi	18.433	18.449	18.446	18.428	18.361	18.356	18.411	18.400	18.383	18.446	18.452	18.414	18.441	18.391	18.379
207Pb/204Pbi	15.529	15.540	15.545	15.537	15.517	15.528	15.533	15.532	15.516	15.539	15.532	15.538	15.527	15.503	15.503
208Pb/204Pbi	38.255	38.294	38.313	38.280	38.168	38.199	38.240	38.251	38.203	38.336	38.326	38.347	38.290	38.157	38.155
SiO2	69.6	71.8	55.0	55.0	52.5	53.3	52.2	-	56.4	52.4	54.6	50.8	52.1	73.0	59.4
MgO	0.9	0.5	3.2	3.2	3.9	4.2	4.6	-	3.2	5.7	4.1	5.3	5.0	0.7	3.0

No.	85	90	90	94	105	105	106	107	107	108	111	113	114	117
sample	29X6-124-126	32X2-26-28	32X2-26-28	33X5-36-39	36X3-57-59	36X3-57-59	37X4-43-45	37X6-105-107	37X6-105-107	39X1-21-23	39X2-42-44	41X4-71-73	41X5-58-60	42X2-99-101
type	P	P	LP	LP	LP	P	P	LP	P	LP	P	LP	LP	P
pref. Age (Ma)	12.27	13.00	13.00	13.30	23.00	23.00	23.70	25.00	25.00	27.40	27.50	33.00	34.00	39.50
Rb	7.50	10.02	10.02	10.02	-	-	-	-	-	7.34	-	-	-	-
Sr	216.37	186.64	186.64	186.64	-	-	-	-	-	171.00	-	-	-	-
Rb/Sr	0.035	0.054	0.054	0.054	-	-	-	-	-	0.043	-	-	-	-
87Sr/86SrM	0.703394	0.703641	0.703640	0.703587	0.703335	0.703317	0.703514	0.703418	0.703423	0.703558	0.703383	0.703637	0.703675	0.704131
2 _ error	± 9	± 7	± 8	± 7	± 8	± 8	± 9	± 8	± 8	± 7	± 8	± 8	± 8	± 7
87Rb/86Sr	0.100	0.155	0.096	0.155	0.096	0.141	0.141	0.096	0.141	0.124	0.141	0.124	0.096	0.141
87Sr/86SrI	0.703377	0.703612	0.703622	0.703558	0.703305	0.703273	0.703467	0.703384	0.703373	0.703510	0.703328	0.703578	0.703629	0.704052
Sm	3.32	2.38	2.38	2.38	-	-	-	-	-	2.69	-	-	-	-
Nd	9.57	6.74	6.74	6.74	-	-	-	-	-	7.42	-	-	-	-
Sm/Nd	0.346	0.353	0.353	0.353	0.362	0.362	0.362	0.362	0.362	0.362	0.362	0.362	0.362	0.362
143Nd/144NdM	0.513084	0.513094	0.513099	0.513090	0.513023	0.513018	0.513064	0.513086	0.513079	0.513077	0.513026	0.513061	0.513080	0.512991
2 _ error	± 7	± 9	± 8	± 9	± 9	± 7	± 6	± 7	± 8	± 9	± 8	± 8	± 4	± 8
147Sm/144NdM	0.208	0.213	0.227	0.213	0.227	0.209	0.209	0.227	0.209	0.218	0.209	0.218	0.227	0.209
143Nd/144Ndi	0.513067	0.513076	0.513080	0.513071	0.512990	0.512988	0.513032	0.513049	0.513044	0.513037	0.512989	0.513014	0.513030	0.512937
_t Nd	8.68	8.88	8.95	8.79	7.42	7.38	8.28	8.65	8.55	8.48	7.53	8.16	8.49	6.83
__ Nd	8.70	8.90	9.00	8.82	7.51	7.42	8.31	8.75	8.59	8.55	7.57	8.25	8.62	6.89
Pb	5.87	7.22	7.22	3.47	-	-	-	-	-	4.00	-	-	-	-
U	0.210	0.300	0.300	0.200	-	-	-	-	-	0.190	-	-	-	-
Th	0.310	0.520	0.520	0.283	-	-	-	-	-	0.247	-	-	-	-
206Pb/204PbM	18.371	18.381	18.392	18.391	18.367	18.350	18.147	18.312		18.409	18.171	18.117	18.112	18.360
207Pb/204PbM	15.506	15.511	15.519	15.504	15.515	15.497	15.467	15.487		15.524	15.467	15.469	15.470	15.504
208Pb/204PbM	38.166	38.234	38.266	38.201	38.287	38.229	37.910	38.135		38.256	37.931	37.843	37.836	38.068
238U/204Pb	2.26	2.63	2.49	3.65	2.49	3.56	3.56	2.49	3.56	3.00	3.56	2.97	2.49	3.56
235U/204Pb	0.016	0.019	0.018	0.026	0.018	0.026	0.026	0.018	0.026	0.022	0.026	0.022	0.018	0.026
232Th/204Pb	3.44	4.70	3.05	5.33	3.05	4.83	4.83	3.05	4.83	4.04	4.83	4.00	3.05	4.83
232Th/238U	1.53	1.79	1.22	1.46	1.22	1.35	1.35	1.22	1.35	1.35	1.35	1.35	1.22	1.35
206Pb/204Pbi	18.366	18.376	18.387	18.383	18.359	18.338	18.133	18.302		18.396	18.155	18.102	18.099	18.339
207Pb/204Pbi	15.506	15.511	15.519	15.504	15.514	15.497	15.466	15.487		15.524	15.466	15.468	15.469	15.503
208Pb/204Pbi	38.164	38.230	38.264	38.197	38.284	38.224	37.904	38.131		38.250	37.924	37.837	37.830	38.059
SiO2	59.9	64.9	-	53.5	68.9	-	-	-	-	58.6	-	54.8	-	66.8
MgO	2.3	1.3	-	3.8	0.9	-	-	-	-	2.9	-	4.1	-	0.7

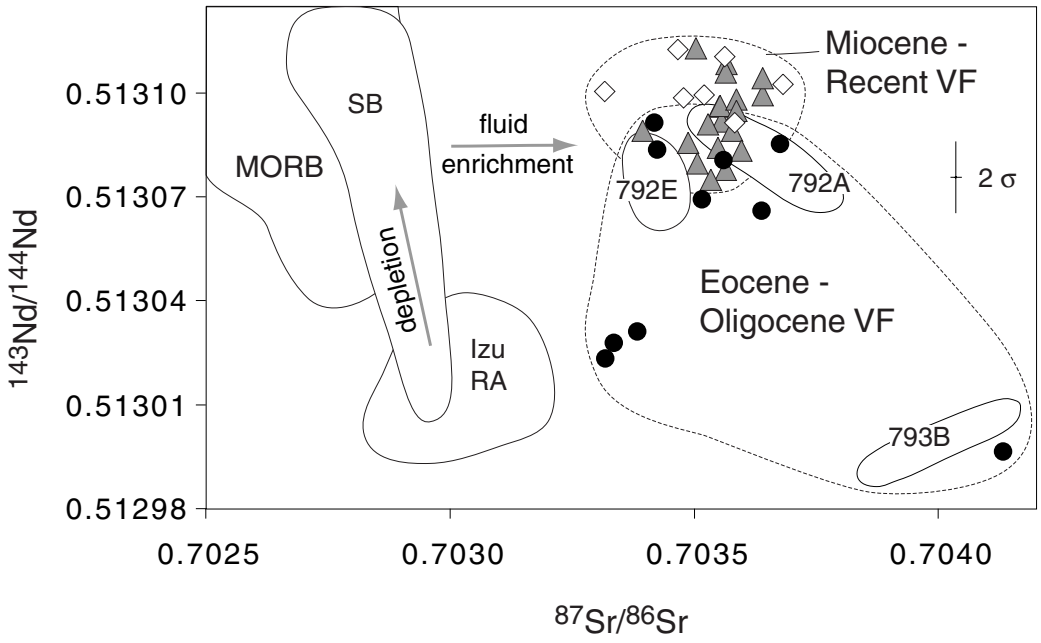

Figure 6: $^{87}Sr/^{86}Sr$ vs. $^{143}Nd/^{144}Nd$ isotope diagram showing <17 Ma volcaniclastic layers (triangles) and >23 Ma volcaniclastic layers (dots). Quaternary VF lava (diamonds), Izu RA (3-13 Ma) and SB (= Shikoku Basin; 25-17 Ma) from Schmidt et al. (in prep.); MORB (Indian and Pacific) from White et al. (1987); Hamelin and Allegre (1985) and Rehkämper and Hofmann (1997); Oligocene lavas (792A, 792E and 793B) from Gill et al. (1994) and Taylor and Nesbitt (1998): 792E= Oligocene arc volcano; 792A, 793B= Leg 126 Basement.

The measured $^{143}Nd/^{144}Nd$ ratios of the >23 Ma group range between 0.51299 (0.51302 excluding 117) - 0.51309 and are generally lower than those of the younger group (Fig. 6). The Eocene-Oligocene volcaniclastic samples display a similar range in Sr and Nd isotopic compositions to the Leg 126 basement (792A, 793B in Fig. 6) and arc volcano (792E in Fig. 6) samples (Gill et al., 1994; Taylor and Nesbitt, 1998). The older volcaniclastic samples have less radiogenic Sr but similar Nd isotope ratios to the RA lavas (13-3 Ma; Fig. 6).

The measured Pb isotope ratios of the 23-40 Ma volcaniclastic deposits ($^{206}Pb/^{204}Pb$= 18.11-18.41; $^{207}Pb/^{204}Pb$= 15.47-15.52; $^{208}Pb/^{204}Pb$= 37.29-38.84) are clearly lower than those of the <17 Ma volcaniclastic samples ($^{206}Pb/^{204}Pb$= 18.36-18.46; $^{207}Pb/^{204}Pb$= 15.50-15.55; $^{208}Pb/^{204}Pb$= 38.16-38.35), which in turn are lower than the Recent VF lavas ($^{206}Pb/^{204}Pb$= 18.42-18.56, $^{207}Pb/^{204}Pb$= 15.53-15.55, and $^{208}Pb/^{204}Pb$= 38.25-38.40; Schmidt et al., in prep.). The Pb isotope ratios thus increase with decreasing age (Fig. 7, 10). In $^{206}Pb/^{204}Pb$ vs. $^{207}Pb/^{204}Pb$ and $^{206}Pb/^{204}Pb$ vs. $^{208}Pb/^{204}Pb$ isotope variation diagrams (Fig. 7), the RA (13-3 Ma) and Oligocene lavas from Leg 126 (Gill et al., 1994; Taylor and Nesbitt, 1998) fall within the field for the Eocene-Oligocene volcaniclastic samples.

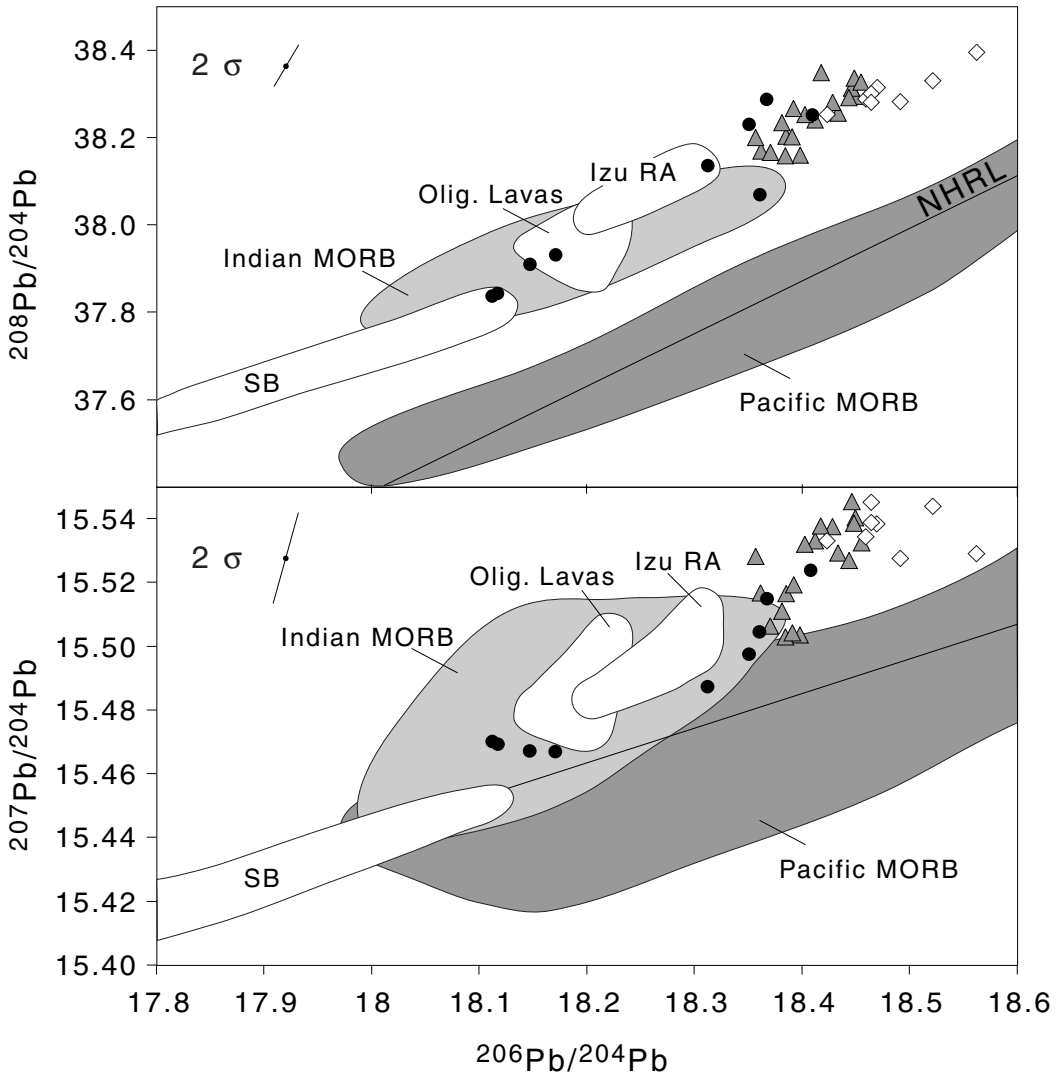

Figure 7: Pb isotope diagram of the studied volcaniclastic deposits and Recent VF lavas (Schmidt et al., in prep.). Symbols, abbreviations and references as in Fig. 6. Northern Hemisphere Reference Line (NHRL) after Hart (1984).

In summary, the Nd and Pb isotope ratios decrease with age from the old volcaniclastic deposits to the young volcaniclastic deposits to the Quaternary lavas. The old volcaniclastic samples overlap with the RA lavas (Fig. 8). Our Eocene and Oligocene samples correspond well with the Oligocene Lavas from Gill et al. (1994) and Taylor and Nesbitt (1998). Sr isotope ratios are similar in the old and young group and but are higher in both than in the RA lavas (Fig. 6). Finally the range in Sr-Nd-Pb isotope ratios is greatest in the old volcaniclastic deposits (Table 2, Fig. 10).

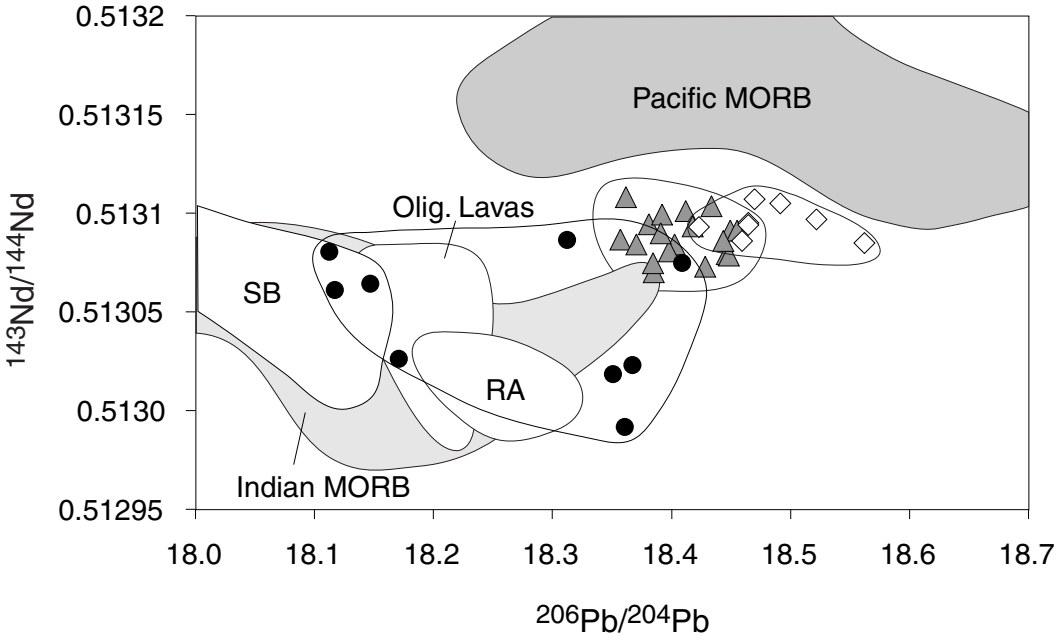

Figure 8: $^{206}Pb/^{204}Pb$ vs. $^{143}Nd/^{144}Nd$ of the studied samples. Symbols and references as in Fig. 6.

5.2.2 Effect of Age Correction on Isotope Data

Since the studied samples show a large range in SiO_2 and range from basalt to rhyolite (Table AI-1), differentiation processes such as fractional crystallization may affect the parent/daughter ratios of the different isotope systems ($^{87}Rb/^{86}Sr$, $^{147}Sm/^{144}Nd$, $^{238}U/^{204}Pb$, $^{235}U/^{204}Pb$, $^{232}Th/^{204}Pb$) and therefore could potentially affect the correction for in situ radioactive decay over the past 40 Ma. As is illustrated in Fig. 9, with the exception of the $^{87}Rb/^{86}Sr$ ratio in two young volcaniclastic layers (3 and 6) the parent/daughter ratios vary only slightly as a function of SiO_2. The effect of the differences in parent/daughter ratios as a result of differentiation on the initial isotope ratios is thus negligible. Considering the small parent/daughter ratios for $^{87}Rb/^{86}Sr$ (mean± 2-sigma standard deviation; range: 0.11± 0.04; 0.04-0.2), $^{238}U/^{204}Pb$ (2.87± 0.8; 1.22-4.66), $^{235}U/^{204}Pb$ (0.021± 0.006; 0.009-0.034), $^{232}Th/^{204}Pb$ (3.78± 1.35; 1.36-5.95), age corrections even for the 40 Ma sample will be negligible (e.g. Fig. 10). The $^{147}Sm/^{144}Nd$ (0.22± 0.01; 0.19-0.25) however, is large enough that the age correction over 40 Ma will be significant (Fig. 10).

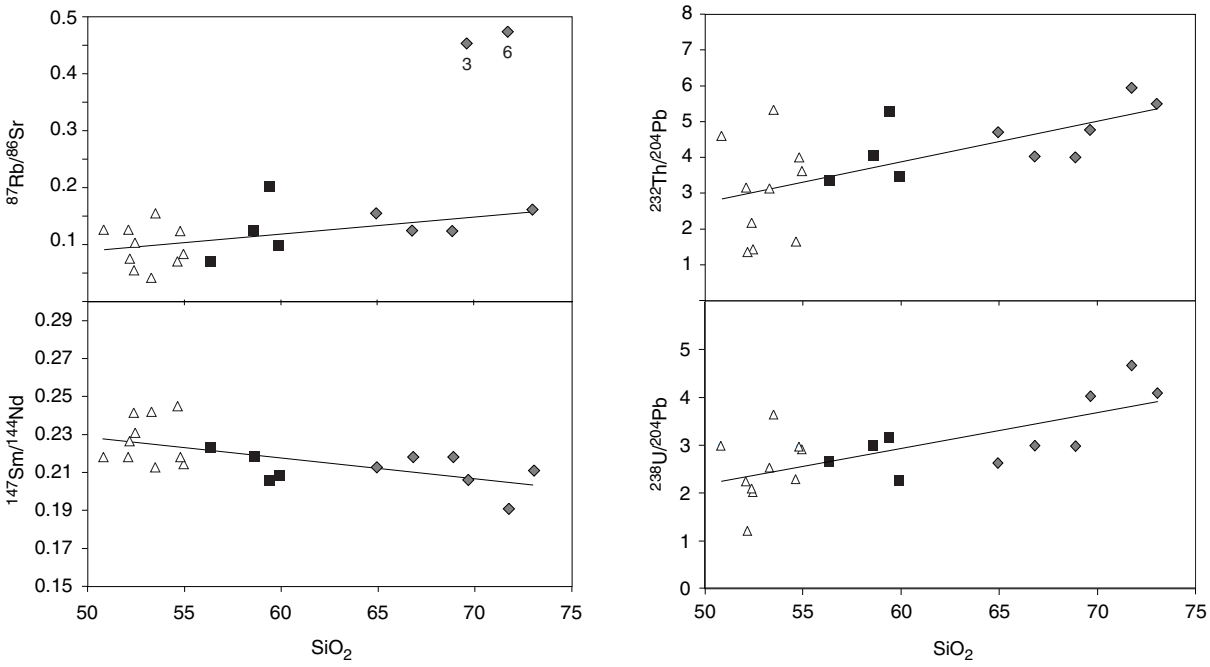

Figure 9: Parent/daughter isotope ratios as a subject of SiO_2 content (compare Appendix I, Table AI-1). Triangles denote basalts and basaltic andesites, squares denote andesites and diamonds denote dacites and rhyolites. $^{235}U/^{204}Pb$ behaves similar as $^{238}U/^{204}Pb$. Note that sample 3 and 6 have anomalously high $^{87}Rb/^{86}Sr$. Probably reflecting severe depletion in Sr as a result of extensive plagioclase fractionation, which did not significantly affect the Sm/Nd, U/Pb and Th/Pb ratios.

Considering the degrees of melting involved in generating arc basalts (~10-30%, e.g. Miller et al., 1992; Stolper and Newman, 1994; Vroon et al., 1995), parent/daughter ratios of the studied isotope systems will not be significantly fractionated from those of the source (Appendix I, Table AI-2). Therefore the measured isotope ratios are likely to reflect the composition of the sources at the present for all volcaniclastic deposits and will henceforth be used to compare the sources of the volcaniclastic samples.

6 Discussion: Causes of Temporal Variation in Isotopic Composition

The temporal evolution of the Izu VF as it arises from the studied volcaniclastic layers is depicted in Fig. 10. Despite the spiky lines, there is a general trend tending to lower $^{143}Nd/^{144}Nd$, $^{206}Pb/^{204}Pb$, $^{207}Pb/^{204}Pb$, and $^{208}Pb/^{204}Pb$ isotope ratios in the Oligocene and Eocene while the $^{87}Sr/^{86}Sr$ ratios stay almost constant over the last 40 million years. The temporal trends are visible in the measured isotope ratios as well as in the initial isotope ratios (Table 2, Fig. 10). In this section we are going to discuss the causes of the temporal variations in the isotope ratios of the Izu samples. The differing isotope systems help to distinguish between different causes of the temporal variations.

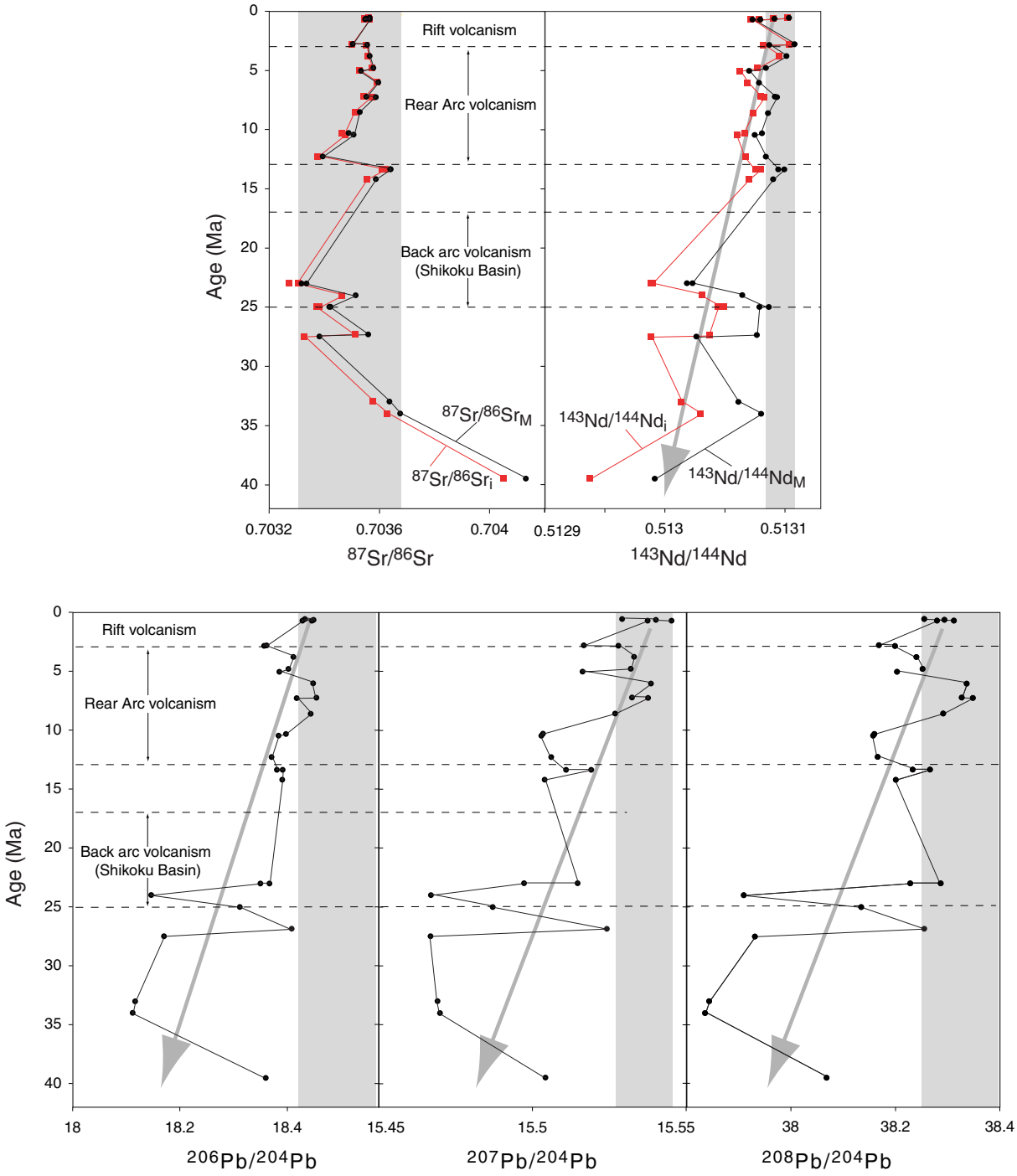

Figure 10: Temporal evolution of the studied volcaniclastic deposits from Hole 782A. For $^{87}Sr/^{86}Sr$ and $^{143}Nd/^{144}Nd$ the measured ($_M$) and initial ($_i$) isotope ratios are plotted. For the Pb isotope ratios only the measured isotope ratios are plotted as the initial and measured ratios do not differ at this scale. Gray area corresponds to Recent VF lavas.

As the Nd and Pb isotope ratios from the old group overlap with those of the Izu RA (Fig. 6-8), this may point to RA volcanism in the Eocene and Oligocene. The $^{87}Sr/^{86}Sr$ ratios, however, are higher than in the RA lavas and similar to those from the younger VF, which argues against the older samples to result from RA volcanism. As RA volcanism between 13-3 Ma seems to have been mainly submarine and not explosive and as there is no evidence

for RA volcanism before 13 Ma from age dating or morphology, we do not ascribe the older volcaniclastic deposits to RA volcanism but to be generated along the VF.

Previous investigations concerning the geochemistry of the early Izu arc revealed four different components (1: EM-II, 2: HIMU-OIB, 3: DMM with "EM-I" character and 4: a slab-derived fluid) to be present in the upper mantle beneath the Izu-Bonin arc (Gill et al., 1994; Hickey- Vargas, 1991). The proportions of these components, vary in space and time as a result of tectonics, thus leading to temporal changes of the geochemistry. The variable rates of the components have been interpreted to indicate a non-steady-state geochemical evolution of the Izu arc, that is more influenced by episodic events like e.g. backarc basin formation than uni-directional change. Periods of behind-the-front volcanism were suggested to deplete the magma source (which is the mantle wedge) beneath the VF in incompatible trace elements during rifting or backarc spreading, and becoming re-enriched after rifting or spreading stops in the basin (Gill et al., 1994).

A good indicator for the source region are $^{143}Nd/^{144}Nd$ isotope ratios, as Nd is more conservative than Pb and Sr (e.g. Pearce and Peate, 1995). Nd may not be transported or delivered in as great proportions as Sr and Pb from components other than the mantle wedge (e.g. subduction components) if recycling is restricted to fluids. The low $^{143}Nd/^{144}Nd$ isotope ratios of the older volcaniclastic rocks may thus be interpreted to point to a less depleted magma source (the mantle wedge) in the Eocene and Oligocene, which is consistent with the Pb isotope data. Recent investigations revealed that magmas from the rift and RA are less depleted than VF lavas (Hochstaedter et al., 2000; Hochstaedter et al., 1990; Ikeda and Yuasa, 1989; Schmidt et al., in prep). Across arc geochemical differences of the Izu arc can thus be attributed to melt extraction of fractional melts from the RA (and rift) that produce a residual, depleted magma source beneath the VF (Hochstaedter et al., 2000). Fundamental for this model is the flow direction of mantle material. The constancy of the isotope ratios (Fig. 10; Table 2) and trace element patterns (Straub, 1996) for 15 million years indicate that steady state processes continuously replenish the magma source in the rear of the arc, because otherwise the magmas along the VF should have become more and more depleted in the past 15 Ma. If we accept mantle flow from the rear of the arc beneath the VF magma source, the lower $^{143}Nd/^{144}Nd$ isotope ratios of the older volcaniclastic samples may denote the absence of volcanism behind the arc front. Indeed there are no evidences for magmatism behind the arc front earlier than the Shikoku Basin, we thus interpret the increase in Nd isotope ratios from the Eocene to Miocene to result from the onset of volcanism behind the arc front. Since then volcanism in the rear of the arc has been almost constant for the past 25 million years due to backarc spreading in the Shikoku Basin (25-17 Ma), RA volcanism (13-3 Ma), and rift volcanism (<3 Ma). It should be noted that the depleted character of the volcaniclastic VF samples starts a little later than spreading in the

Shikoku Basin starts. We ascribe this delay to the time that it takes the depleted mantle material to flow beneath the VF. The short term variations in $^{143}Nd/^{144}Nd$ isotope ratios in the Eocene and Oligocene samples may denote heterogeneity of the source region as e.g. samples 108, 111 and 117 seem to have been generated in more enriched source regions than the other layers.

The low Pb isotope ratios of their Oligocene samples led Taylor and Nesbitt (1998) to conclude that either less sediment was involved in magma production or the isotopic composition of one or more components (e.g. the mantle wedge, subducting crust or sediment) in the system was less radiogenic in the past. Taylor and Nesbitt (1998) noted that if the North New Guinea Plate was subducted in the Eocene and Oligocene along the Izu arc, it would have been very young and thus coated with a thinner carapace of sediment than the subducting plate today. As a result, the subducting basaltic oceanic crust may have dominated the Pb budget of the fluid. The increase in Pb isotopic composition with decreasing age thus correlates with thickness of the subducting sedimentary package. However, since the Pb isotope data point to Indian MORB rather than to Pacific MORB, we interpret the Pb to come from the mantle wedge and not from the subducting crust. The Pb isotope data can thus also be interpreted according to the Nd isotope ratios and point to a less depleted mantle wedge in Pb in the older group.

The $^{87}Sr/^{86}Sr$ ratios are quite similar in the older and younger group from the VF. These relatively constant Sr isotope ratios suggest that Sr is recycled from a component with constant $^{87}Sr/^{86}Sr$ ratios. As the sedimentary input may have varied since the Eocene (Taylor and Nesbitt, 1998), we suggest this component to be fluid from the altered oceanic crust, which will have the $^{87}Sr/^{86}Sr$ ratio of seawater. The $^{87}Sr/^{86}Sr$ ratio of seawater has changed only little over the past 40 million years ranging from 0.708 to 0.709 (Elderfield, 1986; Ingram, 1995).

Summarizing our new data suggest various effects to cause the temporal differences in the geochemistry of the VF. The decreasing Nd isotope ratios as well as the increasing Pb isotope ratios with age suggest that the mantle wedge has become more depleted with time which we trace back to mantle depletion in consequence of melt extraction in the backarc region (Fig. 11). The decrease of Nd isotope ratios is a direct result of mantle wedge depletion, whereas the increase of Pb isotope ratios correlates with a bigger influence of Pb-rich fluids on a depleted mantle wedge than on an enriched one. As the increase in Pb isotopic composition with decreasing age correlates with increasing age of the subducting crust and thickness of the sedimentary package being subducted into the trench, a variable subduction input into the trench might also influence the geochemistry (Fig. 11). The Sr isotope ratios seem to be relatively unaffected by the subduction input as well as the state of mantle enrichment. We interpret the relatively constant Sr isotope ratios to result from recycled fluids from the seawater altered subducted oceanic crust that has a relatively steady $^{87}Sr/^{86}Sr$ ratio due to the constant $^{87}Sr/^{86}Sr$ ratio of seawater.

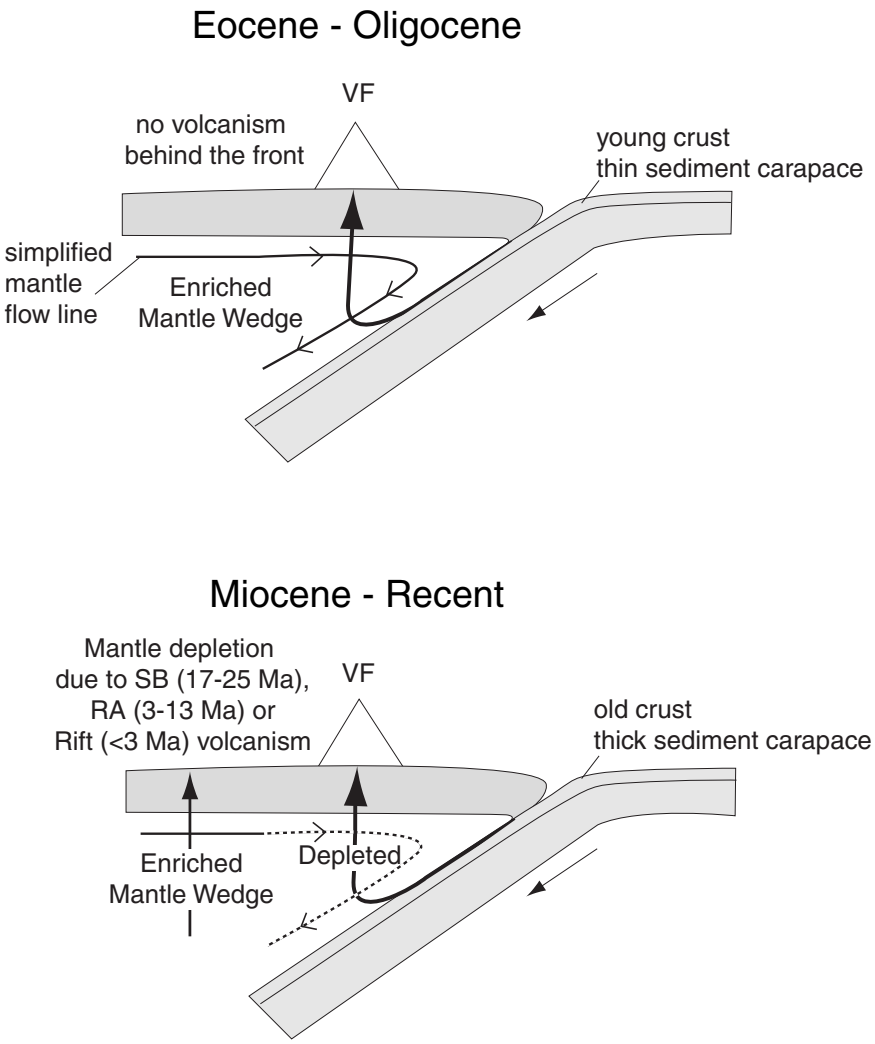

Figure 11: Schematic diagram showing direction of mantle flow in a subduction system assuming corner-flow of mantle material (simplified after Spiegelman and McKenzie, 1987). The upper diagram corresponds to VF volcanism in the Eocene and Oligocene Izu arc. Assuming a non-steady-state geochemical evolution of the island arc, the mantle wedge of the Miocene to Recent VF is depleted due to backarc spreading and RA and rift volcanism (lower diagram).

7 Summary and Conclusion

Sr, Nd and Pb isotopes of volcanic glasses, pumices and lithic whole rock particles of twenty-five volcaniclastic layers from ODP Leg 125 Hole 782A have been studied. All samples were generated along the VF of the Izu arc. Six of the volcaniclastic layers have been $^{40}Ar/^{39}Ar$ age dated to yield independent age determinations. Based on the $^{40}Ar/^{39}Ar$ age data and interpolated ages (using the sedimentation rates and biostratigraphic ages), preferred ages were assigned for each sample. The sample set comprises a chronology from the Eocene (sample 117= 40 Ma) to Pleistocene (sample 3= 0.55 Ma) to Recent (VF lavas) covering most of the ~48-49 Ma Izu arc history. Arc volcanism was at a minimum between 23-17 Ma in the Izu arc, with no volcanic ash record between 23-20 Ma (Taylor et al., 1990).

The deposits we studied can be divided in two age groups: 0-14 Ma and 23-40 Ma that are characterized by distinct Nd and Pb isotope compositions. The radiogenic isotope data of the <17 Ma group yield relatively limited Sr-, Nd- and Pb-isotope ratios while the ≥23 Ma group exhibit greater variability. Compared to the <17 Ma group, the ≥23 Ma group exhibits lower Pb and Nd isotope ratios, while the Sr isotope ratios are similar with one notable exception. We explain the lower $^{143}Nd/^{144}Nd$ ratios of the older samples to result from a less depleted mantle wedge in the beginning of the arc evolution. The lower Pb-isotope ratios are consistent with a greater contribution of Pb from the less depleted mantle wedge and a smaller contribution from the subducted plate 23-40 Ma ago. This reflects a greater Pb abundance in the older mantle wedge (more enriched source) and a lower sediment input and thus smaller Pb contribution from the subducted plate. The relatively constant Sr isotope ratios suggest that Sr is primarily transported in fluids from the altered oceanic crust, which will have the $^{87}Sr/^{86}Sr$ ratio of seawater. The $^{87}Sr/^{86}Sr$ ratio of seawater has changed little over the past 40 million years ranging from 0.708 to 0.709 at the present (Elderfield, 1986; Ingram, 1995).

Despite the general trends, the temporal isotope evolution exhibits excursions from the general trend that show that the system has been a dynamic system throughout its whole history. However, as the arc matured the system has become more steady state leading to a surprisingly uniform Sr-Nd-Pb isotopic composition of the volcaniclastic deposits over the past 10 million years (Fig. 10).

The arc evolution can be incorporated in a model in which depletion of the mantle wedge would have occurred as a result of melt extraction in the backarc region (Fig. 11). Many features of arc sources are consistent with them being residues of backarc basin genesis (e.g. McCulloch and Gamble, 1991). Assuming a corner flow-type model (Spiegelman and McKenzie, 1987) of mantle flow, depletion of the Indian MORB mantle beneath the Izu arc occurred in the Late Oligocene to Middle Miocene due to Shikoku backarc basin formation and during the Late Miocene to Recent as a result of melt extraction in the RA and rift. Therefore the material in the mantle wedge beneath the young VF is more depleted than beneath the old VF, which did not had a RA or backarc basin. The greater depletion in the young VF is reflected in the more radiogenic Nd. Since the mantle wedge beneath the young VF is more depleted, it will record a greater signal from the subducted plate (sediments and altered oceanic seafloor) in the isotope ratios of highly fluid mobile elements (such as Pb). In addition a thinner sediment cover, that supplied less sediment Pb to the older source, is likely to have been subducted beneath the older arc. The similar (with one exception) Sr isotope ratios of the samples suggest that Sr may primarily come from the seawater altered oceanic crust and not from the sediments, in contrast to Pb. The impressive geochemical constancy over the past 10 million years may be related to the constant RA volcanism that started to deplete the mantle wedge 13 m.y. ago.

References

Arculus, R.J., Pearce, J.A., Murton, B.J. and van der Laan, S.R., 1992. Igneous stratigraphy and major-element geochemistry of Holes 786A and 786B. In: P. Fryer, J.A. Pearce, L.B. Stokking and e. al. (Editors), Proceedings of the Ocean Drilling Program, Scientific Results. Ocean Drilling Program, College Station TX: 143-169.

Egeberg, P.C., Brunfelt, A.O. and Stabel, A.S., 1992. Characterization and correlation of megascopic tephras in site 792 core from the Izu-Ogasawara forearc basin (Japan) by trace elements and 87Sr/86Sr and 143Nd/144Nd isotopes. Proceedings of the Ocean Drilling Program, Scientific Results, 126: 457-465.

Elderfield, H., 1986. Strontium Isotope Stratigraphy. Paleogeography, Palaeoclimatology, Palaeoecology, 57: 71-90.

Fryer, P. and Pearce, J.A., 1992. Introduction to the scientific results of Leg 125. In: P. Fryer, Pearce, J.A., Stokking, L.B. et al. (Editors), Proceedings of the Ocean Drilling Program, Scientific Results. Ocean Drilling Program, College Station TX, 3-11.

Fryer, P., Pearce, J.A., Stokking, L.B. and al, e., 1990. Site 782. In: P. Fryer, Pearce, J.A., Stokking, L.B. et al. (Editor), Proc. of the ODP, Init. Rep. Ocean Drilling Program, College Station, TX, 197-252.

Fujioka, K., Matsuo, Y., Nishimura, A., Koyama, M. and Rodolfo, K.S., 1992a. Tephras of the Izu-Bonin Forearc (Sites 787, 792, and 793). In: B. Taylor, Fujioka, K. et al. (Editors), Proceedings of the Ocean Drilling Program, Scientific Results. Ocean Drilling Program, College Station TX: 47-74.

Fujioka, K., Nishimura, A., Matsuo, Y. and Rodolfo, K.S., 1992b. Correlation of the Quaternary tephras throughout the Izu-Bonin areas. In: B. Taylor, Fujioka, K. et al. (Editors), Proceedings of the Ocean Drilling Program, Scientific Results Leg 126. Ocean Drilling Program, College Station TX: 23-45.

Gill, J.B., Hiscott, R.N. and Vidal, P., 1994. Turbidite geochemistry and evolutions of the Izu-Bonin arc and continents. Lithos, 33: 135-168.

Hamelin, B. and Allegre, C.J., 1985. Large-scale regional units in the depleted upper mantle revealed by an isotope study of the south-west Indian ridge. Nature, 315: 196-199.

Hart, S.R., 1984. A large-scale isotope anomaly in the Southern Hemisphere mantle. Nature, 309: 753-757.

Hickey- Vargas, R., 1991. Isotope characteristics of submarine lavas from the Philippine Sea: implications for the origin of arc and basin magmas of the Philippine tectonic plate. Earth Planet. Sci. Lett., 107: 290-304.

Hochstaedter, A.G., Gill, J.B., Ishizuka, O., Yuasa, M. and Sumito, M., 2000. Across-arc geochemical trends in the Izu-Bonin arc: Constraints on source composition and mantle melting. J. Geophys. Res., 105 (B1): 495-512.

Hochstaedter, A.G., Gill, J.B. and Morris, J.D., 1990. Volcanism in the Sumisu Rift, II. Subduction and non-subduction related components. Earth Planet. Sci. Lett., 100: 195-209.

Hoernle, K.A. and Tilton, G.R., 1991. Sr-Nd-Pb isotope data for Fuerteventura (Canary Islands) basal complex and subaerial volcanics: application to magma genesis and evolution. Schweizerische Mineralogische und Petrographische Mitteilungen, 71: 3-18.

Honza, E. and Tamaki, K., 1985. The Bonin Arc. In: A.E.M. Nairn and S. Uyeda (Editors), The Ocean Basins and Margins. Plenum, New York: 459-487.

Ikeda, Y. and Yuasa, M., 1989. Volcanism in nascent back-arc basins behind the Shichito Ridge and adjacent areas in the Izu-Ogasawara arc, northwest Pacific: evidence for mixing between E-type MORB and island arc magmas at the initiation of back-arc rifting. Contributions to Mineralalogy and Petrology, 101: 377-393.

Ingram, B.L., 1995. Ichthyolith Strontium isotopic stratigraphy of deep-sea clays: sites 885 and 886 (North Pacific Transect). Proceedings of the Ocean Drilling Program, Scientific Results, 145: 399-406.

Ishizuka, O., Uto, K., Yuasa, M. and Hochstaedter, A.G., 1998. K-Ar ages from seamount chains in the back-arc region of the Izu-Ogasawara arc. The Island Arc, 7: 408-421.

Karig, D.E. and Moore, G.F., 1975. Tectonically controlled sedimentation in marginal basins. Earth Planet. Sci. Lett., 26: 233-238.

Kobayashi, K. and Nakada, M., 1979. Magnetic anomalies and tectonic evolution of the Shikoku inter-arc basin. In: S. Uyeda, R. Murphy and K. Kobayashi (Editors), Geodynamics of the Western Pacific. Advances Earth Planet Sci. Ser. Japanese Sci. Soc. Press., 391-402.

Lee, J.M., Stern, R.J. and Bloomer, S.H., 1995. Forty million years of magmatic evolution in the Mariana arc: the tephra record. J. Geophys. Res., 100 (B9): 17671-17687.

McCulloch, M.T. and Gamble, J.A., 1991. Geochemical and geodynamical constraints on subduction zone magmatism. Earth Planet. Sci. Lett., 102: 358-374.

Miller, D.M., Langmuir, C.H., Goldstein, S.L. and Franks, A.L., 1992. The importance of parental magma composition to calc-alkaline and tholeiitic evolution: evidence from Umnak Island in the Aleutians. J. Geophys. Res., 97 (B1): 321-343.

Pearce, J.A. and Peate, D.W., 1995. Tectonic implications of the composition of volcanic arc magmas. Ann. Rev. Earth Planet. Sci., 23: 251-285.

Pringle, M.S., McWilliams, M., Houghton, B.F., Lanphere, M.A., and Wilson, C.J.N. 1992. $^{40}Ar/^{39}Ar$ dating of Quaternary feldspar: Examples from the Taupo Volcanic Zone, New Zealand. Geology, 20: 531-534.

Rehkämper, M. and Hofmann, A.W., 1997. Recylced ocean crust and sediment in Indian Ocean MORB. Earth Planet. Sci. Lett., 147: 93-106.

Schmidt, A. et al., in prep. Across Arc variations in Trace Elements and Isotope Ratios in the Central Izu Arc, Japan

Shih, T.C., 1980. Magnetic lineations in the Shikoku Basin. In: G.d. Klein, K. Kobayashi and e. al. (Editors), Init. Rep. Deep-Sea Drill. Proj. U.S. Government Printing Office, Washington D.C.: 783-788.

Spiegelman, M. and McKenzie, D., 1987. Simple 2-D models for melt extraction at mid-ocean ridges and island arcs. Earth. Planet. Sci. Lett., 83: 137-152.

Stolper, E. and Newman, S., 1994. The role of water in the petrogenesis of mariana trough magmas. Earth Planet. Sci. Lett., 121: 293-325.

Straub, S.M. 1996. Miocene to Quarternary evolution of the Izu-Bonin island arc, EOS Trans., AGU 77 (46), Fall Meet. Suppl.: F842

Taylor, B., 1992. Rifting and the volcanic-tectonic evolution of the Izu-Bonin-Mariana Arc. In: B. Taylor, Fujioka, K. et al. (Editors), Proceedings of the Ocean Drilling Program, Scientific Results, College Station TX: 627-651.

Taylor, B., Fujioka, K. et al. (Editors), 1990. Proceedings of the Ocean Drilling Program, Initial Report 126, College Station TX (Ocean Drilling Program): 1002 pp.

Taylor, R.N. and Nesbitt, R.W., 1998. Isotopic characteristics of subduction fluids in an intra-oceanic setting, Izu-Bonin Arc, Japan. Earth Planet. Sci. Lett., 164: 79-98.

Todt, W., Cliff, R.A., Hanser, A. and Hofmann, A.W., 1996. Evaluation of a 202Pb-205Pb Double Spike for High-Precision Lead Isotope Analysis. In: A. Basu and S. Hart (Editors), Earth Processes: Reading the Isotopic Code. AGU, Washington: 429-437.

Vroon, P.Z., van Bergen, M.J., Klaver, G.J. and White, W.M., 1995. Strontium, neodymium, and lead isotopic and trace-element signatures of the East Indonesian sediments: Provenance and implications for Banda Arc magma genesis. Geochim. Cosmochim. Acta, 59: 2573-2598.

York, D. 1969. Least squares fitting of straight line with correlated errors. Earth Planet. Sci. Lett., 5, 320-324

White, W.M., Hofmann, A.W. and Puchelt, H., 1987. Isotope geochemistry of Pacific Mid-Ocean Ridge basalts. J. Geophys. Res., 92: 4881-4893

Appendix I

Table AI-1: Parent/daughter isotope ratios of different rock types. Note that dacites and rhyolites occur only as pumice (=P), while basalts and basaltic andesites occur as lithic particles (LP) in the volcaniclastic layers.

	Sample	SiO_2	MgO	type	$^{87}Rb/^{86}Sr$	$^{147}Sm/^{144}Nd$	$^{238}U/^{204}Pb$	$^{235}U/^{204}Pb$	$^{232}Th/^{204}Pb$
	6	71.8	0.49	P	*0.474*	0.191	4.663	0.034	5.948
	3	69.6	0.90	P	*0.453*	0.206	4.021	0.029	4.767
Dacite,	69	73.0	0.71	P	0.161	0.211	4.091	0.030	5.496
Rhyolite	106	68.9	0.85	P	0.124	0.218	2.977	0.022	4.005
	117	66.8	0.72	P	0.124	0.218	2.994	0.022	4.028
	90	64.9	1.29	P	0.155	0.213	2.628	0.019	4.707
	Ave	**68.4**	**0.9**		**0.141**	**0.215**	**3.172**	**0.023**	**4.559**
	85	59.9	2.29	P	0.100	0.208	2.258	0.016	3.445
	71	59.4	3.01	P	0.202	0.206	3.157	0.023	5.277
Andesites	108	58.6	2.90	LP	0.124	0.218	3.004	0.022	4.042
	40	56.4	3.24	G	0.072	0.223	2.649	0.019	3.353
	Ave	**58.6**	**2.9**		**0.125**	**0.214**	**2.767**	**0.020**	**4.029**
	8	55.0	3.24	LP	0.084	0.214	2.917	0.021	3.619
	113	54.8	4.10	LP	0.124	0.218	2.973	0.022	4.000
	52	54.6	4.11	LP	0.070	0.245	2.287	0.017	1.654
Basalts,	94	53.5	3.82	LP	0.155	0.213	3.645	0.026	5.330
basaltic	19	53.3	4.22	LP	0.042	0.242	2.536	0.018	3.135
Andesites	17	52.5	3.90	LP	0.103	0.231	2.026	0.015	1.432
	45	52.4	5.66	LP	0.055	0.241	2.097	0.015	2.167
	29	52.2	4.60	LP	0.076	0.226	1.216	0.009	1.357
	59	52.1	4.95	LP	0.126	0.218	2.250	0.016	3.162
	54	50.8	5.29	P	0.126	0.218	2.995	0.022	4.596
	Ave	**53.1**	**4.4**		**0.096**	**0.227**	**2.494**	**0.018**	**3.045**

Table AI-2: Trace element contents and calculated parent/daughter isotope ratios in the melt (C_L). F is the weight fraction of melt formed from the original solid (C_0) in the source region. The element concentrations of C_0 were calculated assuming 20% batch melting of the SiO_2-poorest volcaniclastic sample (54).

	F	Rb	Th	U	Pb	Sr	Nd	Sm	$^{87}Rb/^{86}Sr$	$^{147}Sm/^{144}Nd$	$^{238}U/^{204}Pb$	$^{235}U/^{204}Pb$	$^{232}Th/^{204}Pb$
Dbulk		0.01	0.005	0.008	0.02	0.03	0.04	0.05					
C_0	1	1.48	0.060	0.041	0.91	37.02	2.00	0.76	0.116	0.228	2.873	0.021	4.328
C_{L1}	0.9	1.64	0.067	0.046	1.01	40.98	2.21	0.84	0.116	0.227	2.876	0.021	4.335
C_{L2}	0.5	2.94	0.120	0.082	1.79	71.75	3.85	1.44	0.118	0.225	2.905	0.021	4.391
C_{L3}	*0.3*	4.84	0.199	0.135	2.91	114.9	6.10	2.24	0.122	0.221	2.946	0.021	4.474
C_{L4}	*0.1*	13.80	0.581	0.385	7.77	287.8	14.69	5.12	0.139	0.210	3.143	0.023	4.875
C_{L5}	0.05	25.67	1.114	0.717	13.36	461.5	22.68	7.53	0.161	0.200	3.404	0.025	5.435
C_{L6}	0.01	82.27	4.181	2.312	31.48	892.6	40.15	12.08	0.267	0.181	4.656	0.034	8.656

Across Arc variations in Trace Elements and Isotope Ratios in the Central Izu Arc, Japan

Schmidt, A.[1]*, Straub, S.M.[1], Hoernle, K.[1], Langmuir, C.H.[2], Gill, J.B.[3] and Hochstaedter, A.G.[3]

1 GEOMAR Research Center, Wischhofstr. 1-3, 24148 Kiel, Germany
2 Lamont Doherty Earth Observatory of Columbia University, Palisades, New York 10964
3 Earth Sciences Department, University of California, Santa Cruz, CA 95064

Keywords: Izu arc, Subduction, Sr-Nd-Pb Isotopes

*corresponding author
Tel. (49) 431-600-2644
Fax (49) 431-600-2978

(For Submission to International Journal of Earth Sciences)

Abstract

Volcanism in the Izu arc occurs over a broad area at various depths above the Benioff zone. The Izu arc is thus ideally suited to study changes in element recycling as a function of depth to the subducting plate. We present a comprehensive Sr-Nd-Pb isotopic data set from a trench perpendicular profile through the Izu volcanic front, rift and rear arc to the Miocene Shikoku backarc basin. The isotopes can be explained by mixing between a variously depleted Indian MORB component in the mantle wedge and a variously depleted slab component from subducted sediments and altered oceanic crust. Element and Sr-Nd isotopic ratios require that recycling across the arc changes from subduction component dominated in the volcanic front region to mantle dominated in the rear of the arc. Comparison of the Izu arc with the adjacent Mariana arc reveals that the Mariana volcanic front lavas require sediment-melt contributions while the Izu volcanic front is fluid-dominated, which may reflect the differences in the angle of incidence of the subducting slab (60-70° in the Izu arc, 80-90° in the Marianas). The differences in Pb isotope ratios between the two arc segments are interpreted to reflect in particular the presence of an OIB component in the subducted sediments as well as in the subducted oceanic crust beneath the Marianas.

1 Introduction

The distinct geochemical signatures of island arcs provide a key to magma genesis and recycling processes. The enrichment of fluid-mobile large ion lithophile (LIL) elements (e.g. Li, Sr, K, Rb, Ba) as well as the depletion of fluid-immobile high field strength (HFS) elements (Nb, Ta, Zr, Hf) points to a hydrous fluid as important transport medium for elements in island arcs (Pearce, 1982; Weaver, 1991). Hydrous fluids are also believed to be directly responsible for triggering melting in the mantle wedge by lowering the solidus temperature (e.g. Gill, 1981; Tatsumi and Eggins, 1995). However, studies of trace elements and stable and radiogenic isotopes suggested the incorporation of the following components in island arcs:

- fluids from subducted sediments (Ishikawa and Tera, 1999; Morris et al., 1990; Pearce et al., 1999; Taylor and Nesbitt, 1998);
- fluids from subducted altered oceanic crust (=AOC; Class et al., 2000; Elburg and Foden, 1998; Elliott et al., 1997; Ishikawa and Nakamura, 1994; Ishikawa and Tera, 1997; Ishikawa and Tera, 1999; Miller et al., 1994; Moriguti and Nakamura, 1998; Turner et al., 1997);
- melts from subducted sediments (Class et al., 2000; Elburg and Foden, 1998; Elliott et al., 1997; Hoogewerff et al., 1997; Turner et al., 1997; Vroon et al., 1993);

- melts from subducted slabs (Yogodzinski and Kelemen, 1998; Defant and Kepezhinskas, 2001; Peacock et al., 1994)
- depleted MORB-type mantle in the wedge (Gribble et al., 1996; Pearce et al., 1999; Ishikawa and Tera, 1999; McCulloch and Gamble, 1991; Volpe et al., 1987; Woodhead et al., 1993);
- enriched OIB-type mantle in the wedge (Hochstaedter et al., 2000; Hochstaedter et al., 1990b; Ikeda and Yuasa, 1989) and
- subarc crust (Vroon et al., 1993).

The physical conditions under which these different components are involved in arc magmatism are poorly constrained, as is the relationship between the chemistry of arc magmas and the structure (for example the dip of the subducting slab) of the arc and the relationship between the input into the arc and the chemistry of the arc volcanic rocks.

Here we investigate trace elements and Sr-, Nd-, Pb- isotopic variations across the central (29-32°N) Izu arc/backarc system in order to evaluate the endmember compositions and recycling in the different parts of the arc. The broad area over which subduction zone volcanism and thus element recycling occurs in the Izu arc provides the opportunity to detect detailed variations in geochemistry across the arc. We also compare the chemistry of the Izu VF to those from the Marianas in order to evaluate the relationship between arc structure, arc input and the chemistry of the arc lavas.

2 Tectonic Setting

The intraoceanic Izu arc is located in the western Pacific, south of Honshu, Japan (Fig. 1). It is part of the ~2500-km long N-S trending Izu-Bonin-Mariana (IBM) arc/backarc system. Volcanism results from subduction of the Pacific Plate beneath the Philippine Sea Plate. Presently subduction below the Izu and Mariana trench is occurring at a rate of 8-10 cm per year to the northwest (Fryer and Pearce, 1992) with a subduction angle of 57-70° at 29-32°N beneath the Izu arc and an angle of 80-90° at 17-19°N beneath the Marianas (Van der Hilst and Seno, 1993). The IBM island arc evolved through alternating phases of arc front volcanism, rifting and back arc spreading. A detailed summary is given by Taylor (1992). Subduction in the IBM system started in the middle Eocene when young hot oceanic crust was moved adjacent to old (Cretaceous-Jurassic) cold crust along a transform fault (Clague & Dalrymple, 1987). Near the Oligocene-Miocene boundary, backarc spreading formed the Shikoku back arc basin and volcanic activity in the Izu arc was at a minimum. Volcanism forming the active Izu arc started 17 m.y. ago (Taylor, 1992). The 250-km broad recent Izu arc (illustrated schematically in Fig. 2 and 3) is composed from east to west of an active volcanic front (VF; 0-17 Ma), a zone of incipient rifting (0-3 Ma), a zone of inactive N-E to S-

W trending seamount chains (active between 3-13 Ma, Ishizuka et al., 1998) that is denoted as Rear arc (RA) and the Miocene extinct Shikoku backarc Basin (SB; 17-25 Ma). The recent Mariana arc in contrast consists of a VF, a minor RA, an active spreading back arc basin (the Mariana Trough) and the Parece Vela backarc basin (18-31 Ma) that is the equivalent to the SB (17-25 Ma) in the Izu area. The western border of the IBM is the Palau-Kyushu Ridge, an Eocene to Oligocene arc segment that was rifted apart when the Parece Vela and SB opened.

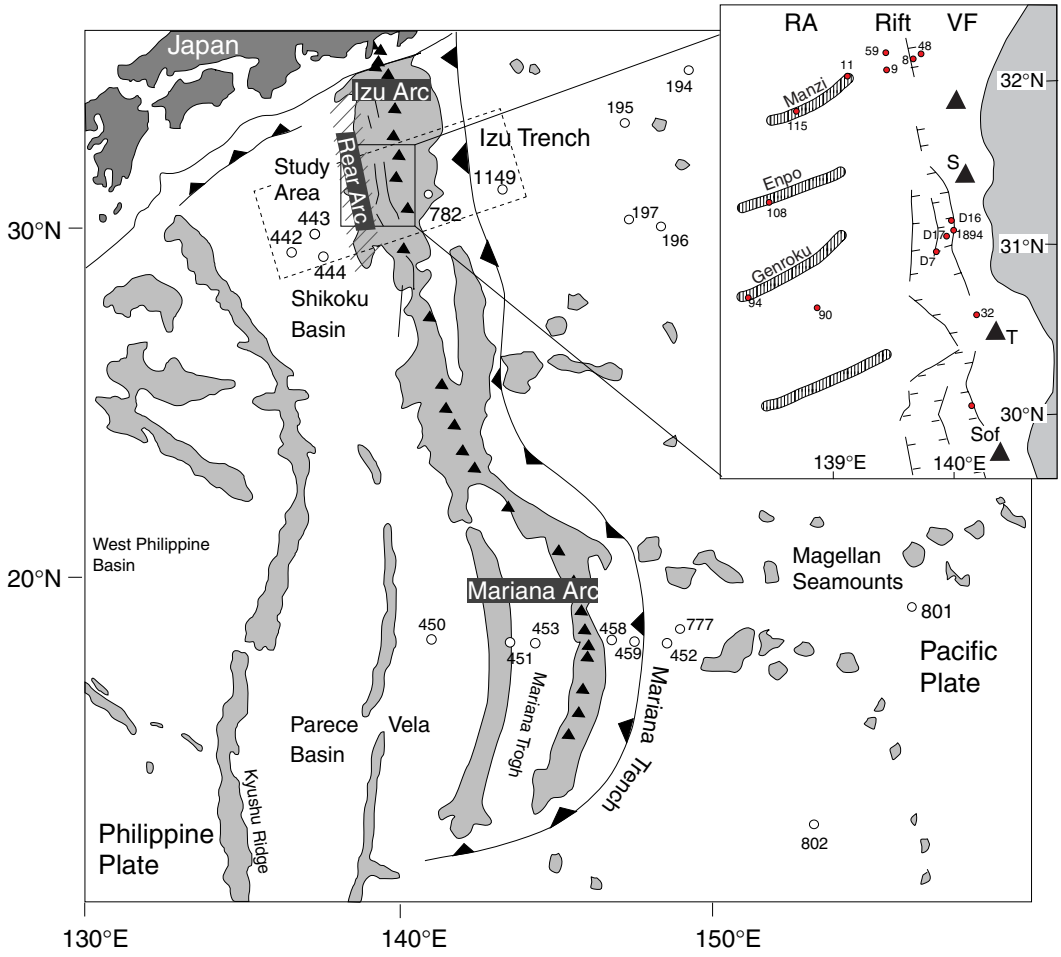

Figure 1: Map showing the Izu-Bonin-Mariana subduction system. Black triangles denote volcanic front volcanoes, numbers denote ODP/DSDP drilling sites. Inset to the right: enlargement of the marked area showing the sample locations. S= Sumisujima, T= Torishima, Sof= Sofugan.

3 Previous Investigations Concerning Across Arc Geochemical Differences in the Izu Arc

The Izu arc is a relatively well sampled and studied arc due to several subaerial outcropping VF volcanoes as well as repeated dredging activities and DSDP/ODP drilling campaigns in the forearc (Legs 125, 126), backarc (Legs 31, 58) and subducting plate (Legs 20, 32, 129, 185). Numerous geochemical studies of the Izu arc revealed across arc geochemical differences in major elements, trace elements and isotope ratios (e.g. (Hochstaedter et al., 2000; Hochstaedter et al., 1990a; Hochstaedter et al., 1990b; Ikeda and Yuasa, 1989; Notsu et al., 1983; Tatsumi et al., 1992; Taylor and Nesbitt, 1998).

Across arc isotopical differences in the northern part of the Izu arc were detected relatively early by Notsu et al. (1983). They ascribed the higher $^{87}Sr/^{86}Sr$ ratios and lower $^{87}Sr/^{86}Sr$ ratios in the RA region to a smaller contribution of subducted sediment, altered basalt or seawater as the distance from the VF increases. Sediments and altered basalt or seawater (henceforth referred to as subduction component) were suggested to accompany the subducting slab to the source magma, which they interpreted to have originated from a partially melted upper mantle wedge. The lower contribution of subduction components in the backarc region compared to the VF was confirmed by later investigations of differing isotope systems (e.g. Li, B, Pb; Ishikawa and Nakamura, 1994; Moriguti and Nakamura, 1998). Notwithstanding the consensus about the decrease in subduction component contribution with increasing distance from the VF, the details (e.g. source, composition and recycling process) are still controversial discussed. Fluids were suggested to be the recycling agent (e.g. Brenan et al., 1995b; Morris et al., 1990; Saunders et al., 1991; Tatsumi, 1989) as well as melts (e.g. Morris and Tera, 1989; Plank and Langmuir, 1993; Schmidt et al., 2000). The source of the subduction component is discussed as controversial. The compositional differences of the subduction component were attributed to a variable composition beneath the VF and RA that can be explained to result either from different hydrous phases, that decompose beneath different parts of the arc (Tatsumi et al., 1992) or from depletion of the fluid in incompatible elements with continuing subduction deeper into the mantle due to progressive loss of fluid phases in the slab as a function of depth (Ishikawa and Nakamura, 1994; Moriguti and Nakamura, 1998). Also the composition of the subduction component is ambiguous and divers components (compare Introduction) have been detected in the arc sources of various arcs, however, the exact composition even in the Izu arc stays a matter of debate.

In addition to the variable subduction component, across arc geochemical variations in the Izu area were suggested to result from enriched mantle material in the backarc region (active rift, RA and SB) and accordingly a heterogeneous mantle in the Izu arc. The enriched

material was interpreted to either represent blobs of enriched material in a depleted matrix, that are preferentially tapped by the backarc, RA and rift lavas or an enriched source, that was injected beneath the backarc region (Hochstaedter et al., 1990a; Hochstaedter et al., 1990b; Ikeda and Yuasa, 1989). Thus the mantle wedge heterogeneity, might either be ancient, with behind-the-front magmatism trapping a different, isotopically distinct mantle than beneath the VF (e.g. Shibata and Nakamura, 1997), or recent, with melt extraction beneath the backarc region causing the differences (e.g. Woodhead et al., 1993).

The combination of a variable subduction component and a variable depleted mantle wedge was presented by Taylor and Nesbitt (1998) as well as in the successive investigations of Hochstaedter et al. (Hochstaedter et al., 1990a; Hochstaedter et al., 1990b; Hochstaedter et al., 2000; Hochstaedter et al., in press.) The results of our study confirm the recent models and can be explained by a combination of (1) increasing depletion of the mantle wedge due to e.g. magma extraction in the backarc region that is accompanied by (2) increasing depletion of the subduction component due to loss of incompatible elements e.g. resulting from prograde dehydration (Fig. 2). It should be noted that this model is dependent on the mantle streamlines and requires corner flow. In this study, we present quantitative modeling that show that the across arc geochemical differences can be explained with two component mixture between 1) a variable depleted mantle wedge beneath the different areas of the Izu arc; and 2) a subduction component being a mixed fluid from AOC and sediment, that is continuously depleted with increasing depths of the subducted plate and yield a contribution to decipher the Izu across arc geochemical differences.

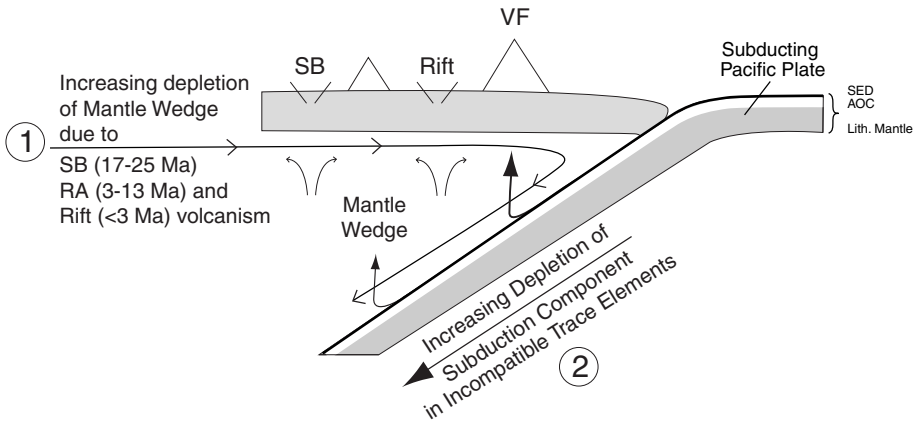

Figure 2: Simplified cartoon of a possible physical model, discussed in the text that can account for the key geochemical features observed in the Izu arc.

4 Samples and Analytical Techniques

The samples from the central Izu VF comprise subaerial lavas from Sumisujima (acronym S), Torishima (T) and Sofugan (Sof) and dredged submarine samples from R/V Moana Wave cruise in 1995 close to Torishima (32) and Myojin Knoll (49) (Hochstaedter et al., 2000; Langmuir et al., in press.). For comparison volcaniclastic samples (0.5-14 Ma) from the VF are also included (Schmidt et al., in prep). The rift samples consist of one sample from the Atlantis II cruise in 1987 (Hochstaedter et al., 1990a), three samples from the R/V Moana Wave cruise in 1995 (Hochstaedter et al., 2000) and several samples from the Kana Keoki cruise (Fryer et al., 1990). Some of our rift samples are denoted as Enpo-rift interaction samples by Hochstaedter et al. (2000) The RA samples were dredged during the R/V Moana Wave cruise in 1995. Our term for the RA is consistent with the western and eastern seamounts of Hochstaedter et al. (2000). We also denote the back-arc knolls and Enpo-rift interaction samples of Hochstaedter et al. (2000) that are located on seamounts in extension of the western seamount chains, as RA. The samples from the Shikoku back arc basin consist of DSDP Leg 58 (site 442-444) basalts (Fig. 1, 3).

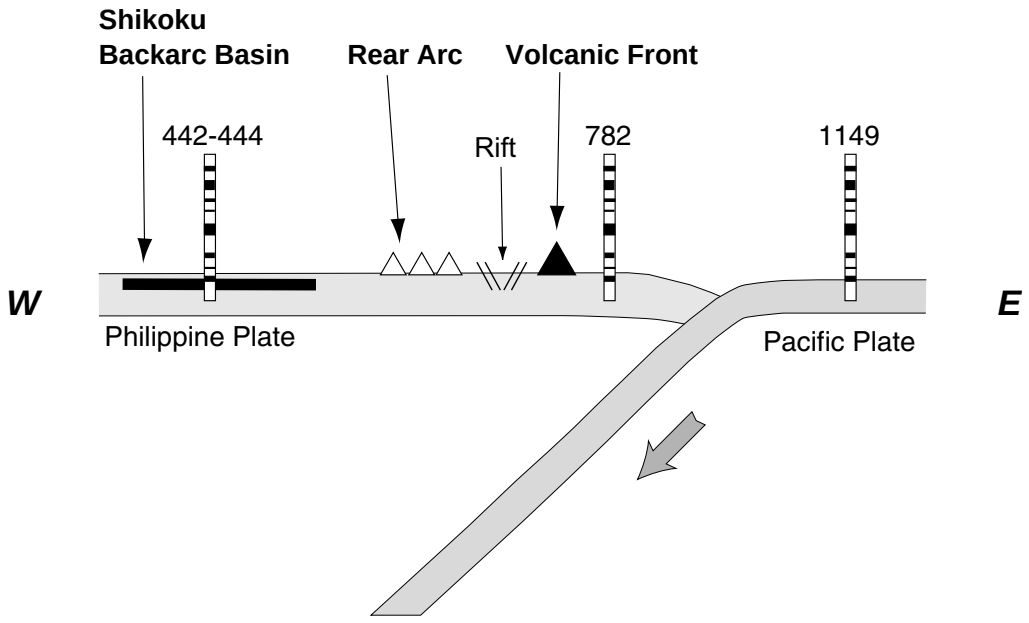

Figure 3: Schematic structure of the Izu arc. Numbers denote ODP/DSDP drilling sites studied.

The samples from the Pacific plate are derived from ODP site 1149 (Fig. 1, 3). From the drilled sedimentary section, clay from the top and from the bottom of the ~120 m long ash and biogenic silica-bearing clay section (unit 1, Plank et al., 2000) were studied (Fig. 4). The basement studied contains variously altered basaltic samples from Hole 1149 B, C and D

(Fig. 4). All samples from site 1149 belong to a subset of priority common samples chosen by the Leg 185 scientific party.

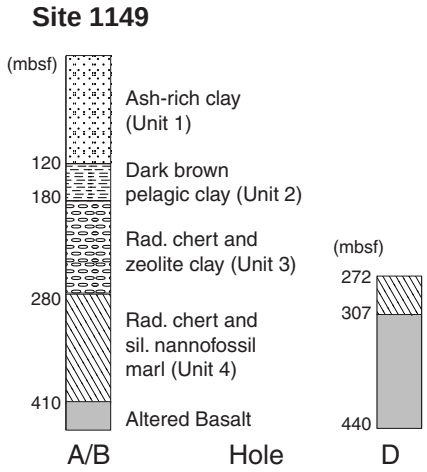

Figure 4: Simplified stratigraphic sections of Site 1149, Hole A, B and D. Modified from Plank et al. (2000).

Li, Rb, Sr, Y, Zr, Nb, Cs, Ba, Ta, Hf, U, Th, Pb, and the rare earth elements (REE) of a subset of the studied samples were determined with a VG-Plasmaquad PQ1 inductively coupled plasma-mass spectrometer (ICP-MS) at the Geological Institute of the University of Kiel. Two preparation methods were carried out to resolve the sample: 1) the methods of Garbe-Schönberg (1993) with $HClO_4$ and 2) the methods of (Garbe-Schönberg, 1993) without $HClO_4$. No systematic variations, however, were detected between the two methods (Table 1). Replicate analysis show that within-run precision is generally better than ±2% and blank levels are negligible. Analytical accuracy and precision were monitored with international standard reference material BHVO-1 and JB-2. Significant variations occur but the analytical accuracy for the REE is within ±10%.

Whole rock powders from the freshest portion of the lavas were analyzed for Sr, Nd and Pb isotopic composition (IC) and Pb concentration by isotope dilution (ID). The SB basalts were crushed and then hand-picked. The samples consist of fresh unaltered glass rims (Site 442 and 443) and whole rock pieces (Site 444). Because alteration can significantly affect the Sr-Nd-Pb isotopic composition, the “output” samples from the Izu VF, rift, RA and SB were leached for 1 hour in hot (70-100°C) 6N HCl to remove the products of alteration. The samples from the Pacific plate in contrast were not leached in order to properly assess the “input” into the subduction zone. The samples were dissolved in a mixture of hot concentrated HF and HNO_3. The ion exchange procedures have been discussed in Hoernle and Tilton (1991). Total chemistry blanks for Sr, Nd and Pb were <300 pg and considered negligible.

Sr, Nd and Pb isotope ratios and Pb concentrations by isotope dilution analyses were carried out on a Finnigan® MAT 262 thermal ionization mass spectrometer (TIMS) operating in static mode at the GEOMAR Research Center in Kiel. Sr and Nd isotope ratios were normalized within run to $^{86}Sr/^{88}Sr$= 0.1194 and $^{146}Nd/^{144}Nd$= 0.7219. NBS 987 yielded $^{87}Sr/^{86}Sr$= 0.710243± 26 (N=25; all error values are reported at the 2-σ confidence level) and La Jolla $^{143}Nd/^{144}Nd$= 0.511843± 10 (N=21). The GEOMAR in house Nd Standard Nd-SPEX, calibrated against La Jolla gave $^{143}Nd/^{144}Nd$= 0.511704± 10 (N=6) which corresponds to a La Jolla value of 0.511848. NBS 981 (N=20) gave $^{206}Pb/^{204}Pb$= 16.898± 10, $^{207}Pb/^{204}Pb$= 15.439± 11, $^{208}Pb/^{204}Pb$= 36.531± 35. The Pb isotope ratios of the samples were corrected for isotope fractionation to the values given in Todt et al. (1996). Replicate analyses yielded an external reproducibility better than 0.05% per a.m.u. (atomic mass unit) for most samples for Pb.

$\partial^{18}O$ was measured on whole rock powders on a Finnigan MAT 251 SIRMS at the University of Göttingen by J. Hoefs and colleagues who estimated the analytical error to be max. 0.2 ‰. Replicate analyses yield that the external reproducibility is better than 5%. The analytical procedure is described in Mengel and Hoefs (1990).

5 Trace Element Results

The trace element analyses from the Izu VF, rift, RA and SB are presented in Table 1. The samples all show arc-type trace element patterns, with enrichments of LIL elements (e.g. Cs, Rb, Ba, Th, LREE and Pb) compared to HFS elements (e.g. Nb, Zr, Hf) and HREE (Fig. 5). Rb, Th and the light and medium REE are more enriched in the RA than in the VF and rift region, whereas Pb decreases from the VF to the SB. Altogether the patterns become flatter in the direction VF -> Rift -> RA -> SB and element ratios like Th/U and Ce/Pb increase systematically from the VF to the SB. The SB sample from Hole 444A is clearly more enriched than the samples from Holes 442B and 443A. The extremely high U and slightly anomalous Rb and Pb in the sample from Hole 444A are likely to reflect the effects of alteration. This result is consistent with the findings of Hickey-Vargas (1998), who interpreted the enrichment to result from E-MORB influence.

Table 1 (next two pages): ICP-MS analyses from different regions of the Izu arc. VF= Volcanic front, RA= Rear Arc, SB= Shikoku Basin. * denotes dissolution method with $HClO_4$ as described in Garbe-Schönberg (1993). Samples without * have been dissolved like * but without $HClO_4$. The factor F denotes the difference between the dissolution methods. F is for most elements close to 1. Systematic variations between the dissolution methods could not be detected. Note that Ta is in all but the ODP samples (volcaniclastic sample 34 and SB samples) to high, probably due to sample preparation using tungsten carbide grinders (compare Hochstaedter et al., 2000).

Region	VF			VF			VF			VF					Rift			Rift		
Sample	32-3 *	32-3	F	32 - 1*	32 - 1	F	tephra 34*	tephra 34	F	49-2-D*	49-2-D	49-2-D	F1	F2	41-1*	41-1	F	59 - 7*	59 - 7	F
Rb	1.61	1.79	0.90	2.63	3.01	0.87	3.73	4.14	0.90	11.27	11.10	10.89	1.03	1.02	1.93	2.01	0.96	1.22	1.17	1.04
Sr	197.7	205.0	0.96	209.8	230.8	0.91	178.1	191.3	0.93	125.2	125.6	122.6	1.02	1.02	179.0	181.1	0.99	250.3	282.2	0.89
Y	13.02	12.82	1.02	13.95	14.69	0.95	22.49	23.15	0.97	31.67	31.74	31.23	1.01	1.02	13.99	13.68	1.02	17.17	15.42	1.11
Zr	20.53	20.27	1.01	21.60	22.40	0.96	38.10	38.83	0.98	125.32	125.97	122.92	1.02	1.02	27.64	26.60	1.04	30.61	29.47	1.04
Nb	0.68	0.72	0.94	0.72	0.76	0.95	0.37	0.42	0.88	1.41	1.02	1.93	0.73	0.53	0.68	0.73	0.94	0.96	0.98	0.98
Cs	0.17	0.15	1.12	0.09	0.09	0.93	0.36	0.38	0.96	0.67	0.61	0.71	0.95	0.86	0.13	0.10	1.27	0.04	0.02	1.93
Ba	34.51	32.71	1.05	46.89	48.37	0.97	64.26	65.36	0.98	180.26	180.12	171.87	1.05	1.05	36.37	34.68	1.05	14.28	13.16	1.09
La	1.12	1.05	1.07	2.29	2.31	0.99	1.96	1.98	0.99	6.06	6.08	5.87	1.03	1.04	1.47	1.39	1.06	2.70	2.47	1.09
Ce	3.37	3.26	1.03	5.78	5.89	0.98	5.79	6.00	0.97	16.55	16.62	16.21	1.02	1.03	4.39	4.21	1.04	7.71	7.22	1.07
Pr	0.62	0.61	1.02	0.96	0.98	0.98	1.05	1.09	0.97	2.55	2.56	2.51	1.02	1.02	0.79	0.76	1.04	1.40	1.31	1.07
Nd	3.54	3.47	1.02	5.12	5.27	0.97	5.97	6.18	0.97	12.27	12.30	12.15	1.01	1.01	4.41	4.26	1.03	7.67	7.21	1.06
Sm	1.38	1.34	1.03	1.68	1.72	0.98	2.25	2.36	0.95	3.69	3.75	3.70	1.00	1.01	1.61	1.58	1.02	2.43	2.31	1.05
Eu	0.61	0.60	1.02	0.63	0.65	0.97	0.84	0.90	0.94	1.03	1.04	1.03	1.00	1.01	0.67	0.65	1.02	0.98	0.92	1.07
Gd	1.95	1.90	1.02	2.12	2.20	0.96	3.19	3.26	0.98	4.55	4.59	4.45	1.02	1.03	2.16	2.10	1.03	3.04	2.77	1.10
Tb	0.35	0.35	1.01	0.36	0.37	0.96	0.58	0.61	0.96	0.80	0.81	0.81	1.00	1.01	0.39	0.38	1.02	0.51	0.47	1.09
Dy	2.49	2.45	1.02	2.41	2.48	0.97	4.14	4.27	0.97	5.54	5.57	5.55	1.00	1.00	2.71	2.61	1.04	3.36	3.12	1.08
Ho	0.53	0.53	1.02	0.51	0.53	0.97	0.89	0.93	0.96	1.20	1.20	1.20	1.00	1.00	0.57	0.55	1.03	0.70	0.64	1.09
Er	1.57	1.54	1.02	1.50	1.55	0.97	2.65	2.75	0.96	3.60	3.66	3.64	0.99	1.00	1.65	1.59	1.04	1.98	1.81	1.09
Tm	0.24	0.23	1.03	0.22	0.23	0.97	0.39	0.41	0.95	0.57	0.57	0.57	1.00	1.01	0.24	0.23	1.01	0.28	0.26	1.10
Yb	1.60	1.54	1.04	1.48	1.54	0.96	2.70	2.81	0.96	3.95	4.00	3.98	0.99	1.01	1.58	1.54	1.03	1.83	1.65	1.11
Lu	0.24	0.23	1.02	0.23	0.23	0.97	0.41	0.43	0.96	0.60	0.61	0.61	0.99	0.99	0.23	0.23	1.02	0.27	0.24	1.11
Hf	0.74	0.72	1.03	0.78	0.80	0.98	1.39	1.50	0.93	3.72	3.77	3.81	0.98	0.99	0.89	0.87	1.03	1.04	0.99	1.05
Ta	0.79	0.82	0.95	0.71	0.74	0.96	0.03	0.04	0.84	0.47	0.26	1.13	0.41	0.23	0.68	0.69	0.97	0.61	0.59	1.03
Pb	1.13	1.10	1.03	1.02	1.09	0.94	2.31	2.37	0.98	3.51	3.51	3.57	0.98	0.98	0.84	0.84	0.99	0.70	0.47	1.50
Th	0.05	0.05	0.98	0.22	0.24	0.95	0.14	0.16	0.90	0.72	0.73	0.75	0.96	0.98	0.09	0.10	0.94	0.12	0.11	1.04
U	0.04	0.04	0.99	0.19	0.20	0.96	0.12	0.13	0.90	0.35	0.35	0.37	0.95	0.96	0.06	0.06	0.97	0.12	0.12	0.99

Region	Rift			Rift			Rift			Rift					RA			SB			SB	SB
Sample	9 - 6 *	9 - 6	F	1891 - 7*	1891 - 7	F	1894 - 9*	1894 - 9	F	48-4-R*	48-4-R	48-4-R C	F1	F2	11-3-A1*	11-3-A1	F	444A*	444A	F	442B	443A
Rb	1.99	1.97	1.01	6.57	6.52	1.01	3.48	3.66	0.95	9.52	10.21	9.88	0.93	0.96	16.54	17.13	0.97	3.36	3.85	0.87	2.31	2.01
Sr	341.5	266.4	1.28	207.7	216.0	0.96	186.8	185.6	1.01	125.1	131.8	129.4	0.95	0.97	280.8	280.3	1.00	142.4	160.3	0.89	156.0	152.8
Y	19.12	15.18	1.26	15.77	15.60	1.01	14.90	14.92	1.00	28.27	29.47	29.04	0.96	0.97	37.47	35.77	1.05	26.84	28.44	0.94	33.05	26.69
Zr	38.71	31.31	1.24	44.36	44.66	0.99	37.69	37.51	1.00	117.57	123.11	121.82	0.95	0.97	138.25	132.31	1.04	94.29	101.95	0.92	102.35	76.31
Nb	1.00	0.91	1.11	0.77	0.79	0.97	0.64	0.68	0.95	1.44	2.05	2.00	0.70	0.72	5.17	5.39	0.96	4.88	5.39	0.90	2.24	1.65
Cs	0.06	0.04	1.62	0.43	0.29	1.48	0.13	0.10	1.29	0.62	0.70	0.68	0.88	0.91	0.42	0.42	1.01	0.11	0.10	1.10	0.06	0.05
Ba	17.43	14.32	1.22	31.62	31.03	1.02	27.04	26.23	1.03	168.32	167.99	166.83	1.00	1.01	180.09	168.27	1.07	42.18	45.15	0.93	16.95	15.41
La	3.17	2.52	1.26	3.64	3.52	1.03	2.32	2.21	1.05	5.50	5.58	5.60	0.99	0.98	13.01	11.98	1.09	5.39	5.55	0.97	4.32	3.30
Ce	9.48	7.63	1.24	9.76	9.57	1.02	6.60	6.37	1.04	15.13	15.56	15.60	0.97	0.97	31.40	29.00	1.08	14.46	15.04	0.96	12.82	10.19
Pr	1.68	1.36	1.24	1.59	1.56	1.02	1.15	1.12	1.03	2.35	2.41	2.41	0.98	0.97	4.59	4.27	1.07	2.25	2.37	0.95	2.11	1.69
Nd	9.01	7.36	1.22	8.00	7.87	1.02	6.19	6.10	1.01	11.27	11.63	11.77	0.97	0.96	21.63	20.15	1.07	11.40	12.09	0.94	11.37	9.42
Sm	2.83	2.32	1.22	2.39	2.37	1.01	2.10	2.06	1.02	3.37	3.50	3.53	0.96	0.95	6.06	5.63	1.08	3.64	3.90	0.94	3.71	3.11
Eu	1.11	0.92	1.20	0.87	0.84	1.03	0.82	0.79	1.04	0.96	0.98	0.99	0.97	0.96	1.98	1.84	1.08	1.26	1.37	0.92	1.32	1.18
Gd	3.36	2.76	1.22	2.84	2.78	1.02	2.66	2.52	1.06	4.13	4.24	4.24	0.97	0.97	6.95	6.30	1.10	4.54	4.83	0.94	4.82	4.17
Tb	0.57	0.47	1.22	0.48	0.46	1.03	0.45	0.44	1.02	0.73	0.75	0.76	0.97	0.96	1.14	1.06	1.08	0.79	0.84	0.93	0.82	0.71
Dy	3.80	3.10	1.23	3.09	3.05	1.01	2.93	2.88	1.02	4.95	5.15	5.21	0.96	0.95	7.40	6.88	1.08	5.21	5.60	0.93	5.88	5.04
Ho	0.78	0.64	1.21	0.64	0.63	1.02	0.60	0.60	1.01	1.06	1.11	1.13	0.96	0.94	1.55	1.43	1.08	1.08	1.16	0.93	1.23	1.04
Er	2.22	1.81	1.22	1.81	1.80	1.01	1.71	1.69	1.01	3.19	3.37	3.41	0.94	0.93	4.49	4.15	1.08	3.07	3.30	0.93	3.52	3.02
Tm	0.31	0.26	1.22	0.27	0.26	1.01	0.25	0.24	1.04	0.50	0.52	0.53	0.96	0.95	0.67	0.61	1.09	0.44	0.47	0.93	0.53	0.44
Yb	2.05	1.67	1.23	1.74	1.71	1.02	1.64	1.58	1.04	3.48	3.61	3.67	0.96	0.95	4.49	4.13	1.09	2.87	3.09	0.93	3.54	2.97
Lu	0.30	0.24	1.22	0.25	0.25	1.02	0.24	0.23	1.02	0.53	0.56	0.56	0.95	0.94	0.67	0.62	1.07	0.41	0.45	0.92	0.53	0.45
Hf	1.22	1.02	1.20	1.32	1.33	1.00	1.23	1.20	1.02	3.44	3.68	3.74	0.93	0.92	4.09	3.80	1.07	2.67	2.92	0.92	2.70	2.24
Ta	0.48	0.40	1.19	0.19	0.17	1.13	0.40	0.41	0.99	0.67	1.42	1.44	0.47	0.46	0.99	1.12	0.88	0.32	0.36	0.89	0.16	0.13
Pb	0.62	0.52	1.20	0.82	0.82	1.01	0.61	0.61	1.01	3.03	3.20	3.26	0.94	0.93	2.86	2.61	1.10	0.32	0.38	0.85	0.76	0.72
Th	0.15	0.14	1.13	0.52	0.48	1.09	0.20	0.20	1.00	0.54	0.58	0.59	0.94	0.92	1.56	1.42	1.10	0.44	0.43	1.02	0.22	0.20
U	0.07	0.06	1.15	0.20	0.20	0.96	0.14	0.15	0.98	0.29	0.31	0.32	0.92	0.89	0.54	0.50	1.08	0.89	1.02	0.88	0.09	0.07

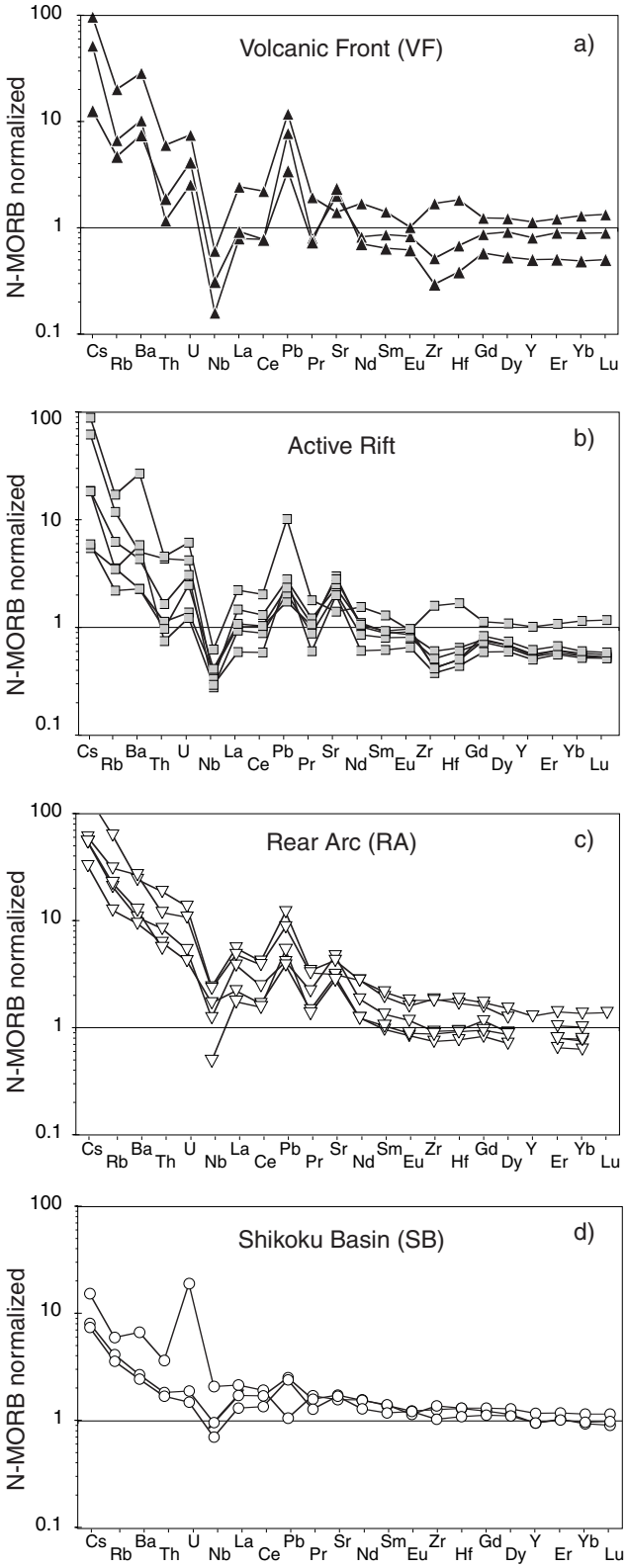

Figure 5: MORB-normalized trace element diagrams of the Izu samples. (a) Volcanic front (32-1, volcaniclastic layer 34, 49-2-d); (b) Active rift (9-6-6, 48-4, 41-1, 59-7, 1891-7, 1894-9); (c) Rear Arc (11-3-a); for comparison samples 90-1, 94-1, 108-6 and 115-2 from Hochstaedter et al. (2001), for which a complete data set was not available, are also shown; (d) Shikoku Basin (442A, 443B, 444A). Average MORB from Sun and McDonough (1989).

5 O-Sr-Nd-Pb Isotope Results

The analytical results are presented in Table 2. The $\delta^{18}O$ data range between 5 and 13‰ and span a significantly wider range than Mariana and Volcano arc lavas (5.5- 6.8 ‰, Ito and Stern, 1985/1986; Woodhead, 1989; Woodhead et al., 1987). Apart from one bims sample (No. 69) all VF samples fall within the range of the Mariana samples and correlate well with SiO_2 (Fig. 6) as expected (e.g. Epstein and Taylor, 1967). The rift samples show the same features as the VF and $\delta^{18}O$ values rise with SiO_2 as well. Except in samples 9-6-6 and 11-3-a the $\delta^{18}O$ values of the RA are higher than the VF and rift rocks. This may result from the higher age (>3 Ma vs. <2 Ma for VF and rift) and resulting higher alteration. A combination of "crustal contamination" and "source contamination" as described by (Ellam and Harmon, 1990) is unlikely because the $\delta^{18}O$ variations of the unaltered rocks are interpreted to result from closed system fractionation. Notwithstanding the alteration of the RA rocks, the radiogenic isotope ratios are regarded precise because all samples were leached prior to analyses very carefully. Further all radiogenic isotope ratios of the RA lie within a restricted range together with the samples that show the lowest $\delta^{18}O$ values (Table 2).

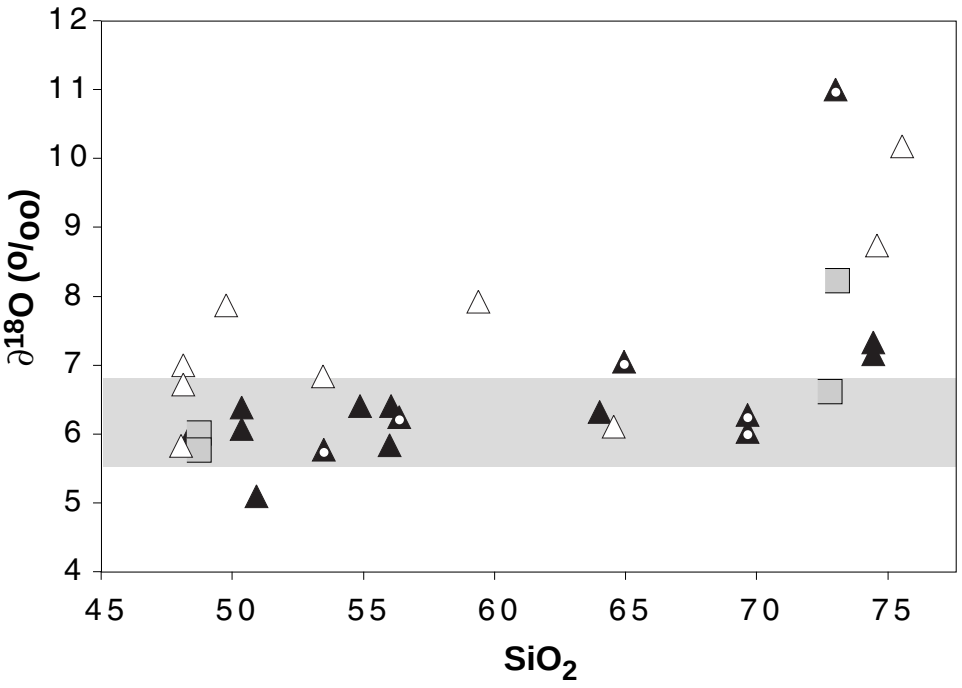

Figure 6: $\partial^{18}O$ composition of the Izu arc rocks shown against SiO_2 content. Symbols as in Fig. 5. Volcaniclastic samples are marked with a white circle. SiO_2 data from Straub (unpublished data) and Hochstaedter et al. (2000). Gray area in the background: Mariana and Volcano island arcs (Ito and Stern, 1985/1986; Woodhead, 1989; Woodhead et al., 1987).

Sample	$^{87}Sr/^{86}Sr$	$^{143}Nd/^{144}Nd$	$^{206}Pb/^{204}Pb$	$^{207}Pb/^{204}Pb$	$^{208}Pb/^{204}Pb$	Pb (ppm)	Age (Ma)	type	$\delta^{18}O$	data source
S-10	0.703327 ±8	0.513085 ±8	18.564	15.531	38.399	1.56	recent	WR	5.1	1
T-10	-	-	-	-	-	1.59	recent	WR	6.4	1
T-60	0.703576 ±8	0.513086 ±7	18.459	15.534	38.288	-	recent	WR	6.32	1
T-65	0.703460 ±8	0.513107 ±9	18.470	15.538	38.314	1	recent	WR	6	1
T-88	0.703513 ±7	0.513094 ±9	18.464	15.539	38.300	-	recent	WR	-	1
Sof 1A	0.703556 ±7	0.513105 ±8	18.491	15.527	38.281	-	recent	WR	6.4	1
Sof-3	0.703675 ±9	0.513097 ±10	18.522	15.544	38.330	-	recent	WR	5.84	1
32-3	0.703471±6	0.513093 ±8	18.423	15.533	38.253	-	recent	WR	-	1
32-1	0.703310 ±10	0.513095 ±8	18.464	15.545	38.281	1.12	recent	WR	-	1
782A-2H4-113-114 (3)	0.703565 ±8	0.513103 ±8	18.434	15.529	38.255	-	0.5	P	6.16	2
782A-2H5-136-138 (6)	0.703551 ±8	0.513091 ±9	18.450	15.540	38.294	-	0.6	P	-	2
782A-2H6-85-87 (8)	0.703565 ±6	0.513073 ±9	18.428	15.538	38.280	-	0.7	P	-	2
782A-2H6-85-87 (8)	0.703548 ±7	0.513079 ±9	18.446	15.545	38.313	-	0.7	LP	-	2
782A-11X-1-55-57 (17)	0.703504 ±9	0.513108 ±9	18.362	15.517	38.168	-	2.8	LP	-	2
782A-11X-3-0-1 (19)	0.703555 ±9	0.513087 ±9	18.357	15.528	38.199	-	2.8	LP	-	2
782A-15X3-9-10 (29)	0.703565 ±8	0.513101 ±8	18.412	15.533	38.240	-	3.8	LP	-	2
782A-17X1-56-58 (34)	0.703578 ±7	0.513084 ±8	18.403	15.532	38.252	-	4.8	G	-	2
782A-17X4-0-2 (40)	0.703534 ±7	0.513070 ±7	18.385	15.516	38.204	-	5.0	G	6.24	2
782A-19X-2-24-26 (45)	0.703597 ±8	0.513078 ±8	18.448	15.539	38.337	-	6.0	LP	-	2
782A-21X2-84-86 (52)	0.703553 ±7	0.513091 ±6	18.455	15.532	38.327	-	7.2	LP	-	2
782A-21X3-0-2 (54)	0.703587 ±9	0.513093 ±9	18.418	15.538	38.348	-	7.3	P	-	2
782A-23X4-107-109 (59)	0.703528 ±8	0.513086 ±8	18.444	15.527	38.292	-	8.6	LP	-	2
782A-26X4-52-54 (69)	0.703488 ±8	0.513081 ±8	18.398	15.503	38.160	-	10.3	P	13.31	2
782A-26X5-147-149 (71)	0.703507 ±8	0.513075 ±9	18.384	15.503	38.158	-	10.4	P	-	2
782A-29X6-124-126 (85)	0.703394 ±9	0.513084 ±7	18.371	15.506	38.166	-	12.3	P	-	2
782A-32X2-26-28 (90)	0.703641 ±7	0.513094 ±9	18.381	15.511	38.234	-	13.3	P		2
782A-32X2-26-28 (90)	0.703640 ±8	0.513099 ±8	18.392	15.519	38.266	-	13.3	LP	7.05	2
782A-33X5-36-39 (94)	0.703587 ±7	0.513090 ±9	18.391	15.504	38.201	-	14.2	LP	5.77	2
8-3	0.70 3068 ±10	0.51 3054 ±8	18. 303	15. 503	38. 132	·	(-2	- R		
39-5B	-	-	-	-	-	-	0-2	WR	8.22	1
41-1	-	-	-	-	-	-	0-2	WR	5.88	1
48-4-r	0.703366 ±8	0.513077 ±10	18.443	15.553	38.393	-	0-2	WR	6.61	1
59-7	0.702822 ±8	0.513053 ±8	18.163	15.464	37.878	-	0-2	WR	-	1
840604	0.703175 ±8	0.513118 ±8	18.176	15.484	37.939	-	0-2	WR	-	1
1604	0.703280 ±7	0.513071 ±9	18.359	15.513	38.147	-	0-2	WR	-	1
RD 7-3	0.702962 ±6	0.513060 ±10	18.208	15.494	38.008	-	0-2	WR	-	1
KK 811 D16-12	0.703279 ±6	0.513072 ±8	18.373	15.509	38.161	-	0-2	WR	-	1
KK 84 D6-1	0.702896 ±8	0.513110 ±8	18.034	15.453	37.752	-	0-2	WR	-	1
KK 84 D17-x	0.703008 ±7	0.513060 ±8	18.267	15.514	38.105	-	0-2	WR	-	1
1891-7	-	-	-	-	-	-	0-2	WR	5.75	1
1894-9	0.702911 ±7	0.513072 ±8	18.253	15.482	38.002	-	0-2	WR	-	1
9-6	0.702816 ±8	0.513024 ±6	18.158	15.469	37.887	0.5	3	WR	5.83	1
11-3-a-1	0.703063 ±8	0.513017 ±7	18.287	15.491	38.086	-	3	WR	6.11	1
12-2d	-	-	-	-	-	-		WR	10.17	1
13-10 d1	-	-	-	-	-	-		WR	8.74	1
90-1	0.703146 ±7	0.512996 ±8	18.290	15.497	38.099	1.87	12.4	WR	6.83	1
94-1	0.702873 ±6	0.512996 ±8	18.250	15.495	38.088	1.53	4.8	WR	7.87	1
108-6	0.702919 ±7	0.513014 ±9	18.251	15.493	38.119	1.15	3.6	WR	6.86	1
115-2	0.702994 ±7	0.513002 ±6	18.254	15.499	38.100	-	8.8	WR	7.92	1
782A-29X-CC-5-7 (87)	0.702943 ±6	0.513020 ±8	18.181	15.481	37.991	-	12.3	P	-	1
442B-19R2-59-63	0.702780 ±7	0.513082 ±4	17.767	15.413	37.485	0.69	17-25	G	-	1
443-62R3-71-74	0.702678 ±9	0.513091 ±8	17.806	15.416	37.550	0.52	17-25	G	-	1
444A-26R1-9-13	0.702890 ±8	0.513042 ±8	18.075	15.449	37.773		17-25	LP	-	1
1149C 10R2 47-51	-	-	17.888	15.473	37.270	-	>160	basalt	-	1
1149D 7R1 37-42	-	-	18.766	15.482	37.885	-	>160	basalt	-	1
1149D 16R3 2-8	-	-	18.959	15.470	38.109	-	>160	basalt	-	1
1149D 17R1 92-98	-	-	18.773	15.481	38.033	-	>160	basalt	-	1
1149D 19R1 85-89	-	-	18.136	15.454	37.695	-	>160	basalt	-	1
1149A 4H2 140-150	-	-	18.632	15.623	38.761	-	<5	clay	-	1
1149A 14H2 140-150	-	-	18.627	15.623	38.775	-	15-20	clay	-	1

Table 2: Radiogenic and stable isotope ratios of the Izu arc/ backarc system, Japan. Abbreviations in column "type" denote material used for Sr-, Nd-, and Pb- isotope analyses; G= glas, LP= lithic particles, P= pumice, WR= whole rock powder. Numbers in parenthesis of 782A samples denote working numbers. Data sources for radiogenic isotope ratios: 1= this study; 2=Schmidt et al. (in prep.). SB= Shikoku Basin, AOC= altered oceanic crust, SED= subducted sediment.

As found previously (e.g. Hochstaedter et al., 2000; Pearce et al., 1999; Taylor and Nesbitt, 1998), the VF, rift, RA and back arc samples from the Izu arc exhibit different ranges in Sr, Nd- and Pb- isotope ratios (Table 2).

The Sr and Nd isotope ratios of each zone of the volcanic arc are distinct (Table 2, Fig. 7). VF samples (this study and Schmidt et al., in prep.) exhibit the highest $^{87}Sr/^{86}Sr$ isotope ratios (0.7033-0.7037) and moderate to high $^{143}Nd/^{144}Nd$ isotope ratios (0.51306-0.51311). The active rift zone shows slightly less radiogenic $^{87}Sr/^{86}Sr$ ratios (0.7028-0.7034) but similar $^{143}Nd/^{144}Nd$ ratios (0.51305-0.51312) to the VF. The RA has similar $^{87}Sr/^{86}Sr$ (0.7028-0.7032) to the rift but lower $^{143}Nd/^{144}Nd$ ratios (0.51300-0.51302). The Shikoku back arc basin exhibits the lowest $^{87}Sr/^{86}Sr$ ratios (0.7027-0.7029) but similar $^{143}Nd/^{144}Nd$ ratios (0.51304-0.51309) to the VF and rift. On a plot of $^{87}Sr/^{86}Sr$ vs. $^{143}Nd/^{144}Nd$ (Fig. 7), the data do not form a single array. Instead the SB, VF and rift samples lie on an array with constant Nd isotope ratios and with Sr isotope ratios increasing from the SB to the VF. The RA samples form a negative correlation with the Shikoku basalts (Fig. 7).

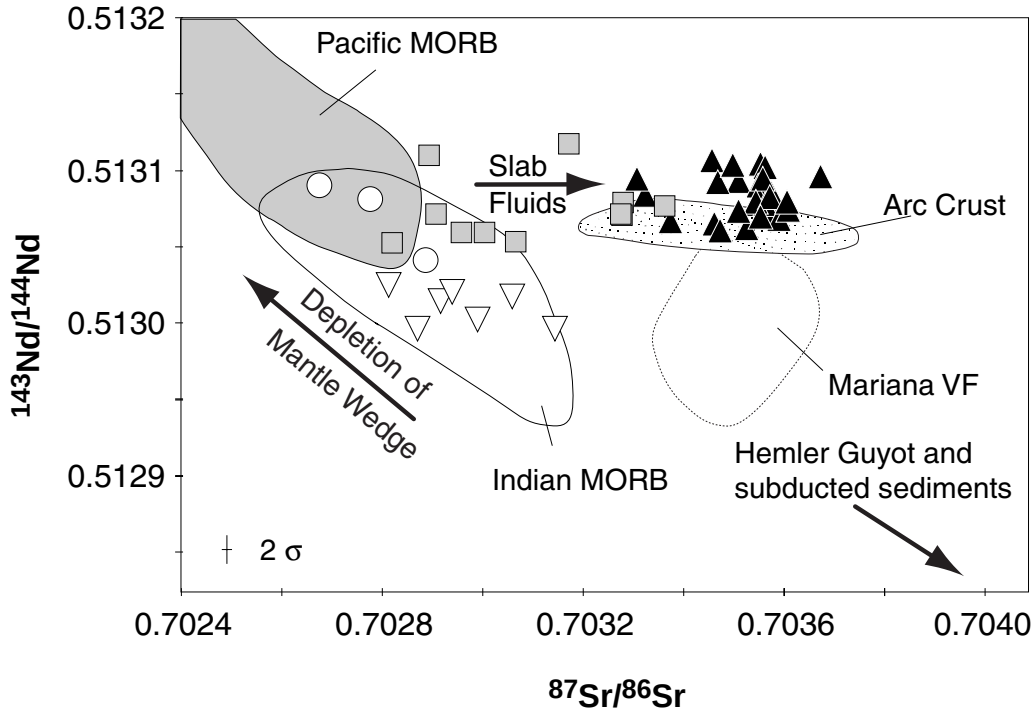

Figure 7: $^{87}Sr/^{86}Sr$ vs. $^{143}Nd/^{144}Nd$ isotope variation diagram for the Izu VF lavas and volcaniclastic samples (Schmidt et al., in prep.; black triangles), rift (gray squares), RA (white triangles) and SB (white circles). Mariana VF from Elliott et al. (1997); Arc Crust from DeBari et al. (1999); Pacific MORB from White et al. (1987); and Indian MORB from Hamelin and Allegre (1985) and Rehkämper and Hofmann (1997).

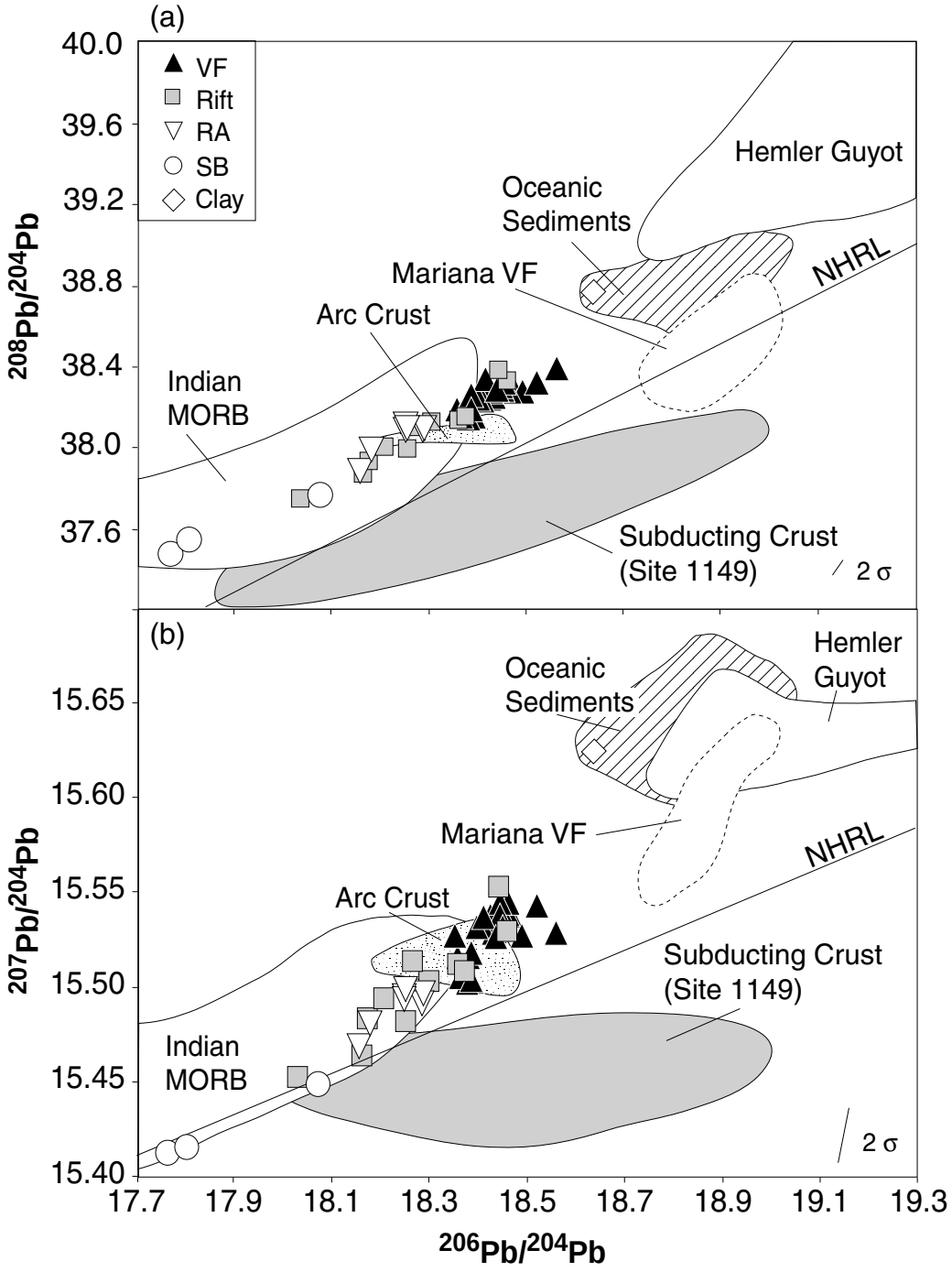

Figure 8: Pb isotope variation diagrams for the Izu samples. Sediment field from this study, Elliott et al. (1997) and Pearce et al. (1999); Mariana field from Elliott et al. (1997); Hemler Guyot from Staudigel et al. (1991); Arc Crust from DeBari et al. (1999); Subducting Crust from this study; and Indian MORB from Hamelin and Allegre (1985) and Rehkämper and Hofmann (1997). Northern Hemisphere Reference Line (NHRL) from Hart (1984).

The VF lavas (this study and Schmidt et al.; in prep.) have the most radiogenic Pb isotope ratios in the Izu arc ($^{206}Pb/^{204}Pb$= 18.36-18.56, $^{207}Pb/^{204}Pb$= 15.50-15.55, and $^{208}Pb/^{204}Pb$= 38.16-38.40, the RA samples have less radiogenic Pb ($^{206}Pb/^{204}Pb$= 18.16-18.29, $^{207}Pb/^{204}Pb$= 15.47-15.50, and $^{208}Pb/^{204}Pb$= 37.89-38.12) and the rift samples span the widest range in Pb isotopic composition ($^{206}Pb/^{204}Pb$= 18.03-18.46; $^{207}Pb/^{204}Pb$= 15.45-15.55 and $^{208}Pb/^{204}Pb$= 37.75-38.39) overlapping the VF and RA (Fig. 8). The Shikoku back arc basin samples have the least radiogenic Pb isotope ratios ($^{206}Pb/^{204}Pb$= 17.77-18.08, $^{207}Pb/^{204}Pb$= 15.41-15.45, and $^{208}Pb/^{204}Pb$= 37.49-37.77). The Pb isotope data for the VF, rift and RA lie above the Northern Hemisphere Reference Line (NHRL; Hart, 1984) in both Pb isotope diagrams and form linear arrays. The Shikoku back arc basin field plot along the NHRL in the uranogenic Pb isotope diagram and above the NHRL on the thorogenic Pb isotope diagram (Fig. 8).

The basement samples from the subducting Pacific plate show a wide range in $^{206}Pb/^{204}Pb$ (17.89-18.96) and a smaller range in $^{208}Pb/^{204}Pb$ (37.27-38.11). The range in $^{207}Pb/^{204}Pb$ (15.45-15.48) is within the analytical precision.

The sediments have $^{206}Pb/^{204}Pb$ ratios >18.6 and the highest $^{207}Pb/^{204}Pb$ (>15.62) and $^{208}Pb/^{204}Pb$ ratios (>38.7) of the samples studied.

On a $^{206}Pb/^{204}Pb$ vs. $^{87}Sr/^{86}Sr$ plot (Fig. 9a) the samples lie on a single trend, whereas on the $^{206}Pb/^{204}Pb$ vs. $^{143}Nd/^{144}Nd$ plot two trends are formed (Fig. 9b), similar to the Sr versus Nd isotope diagram.

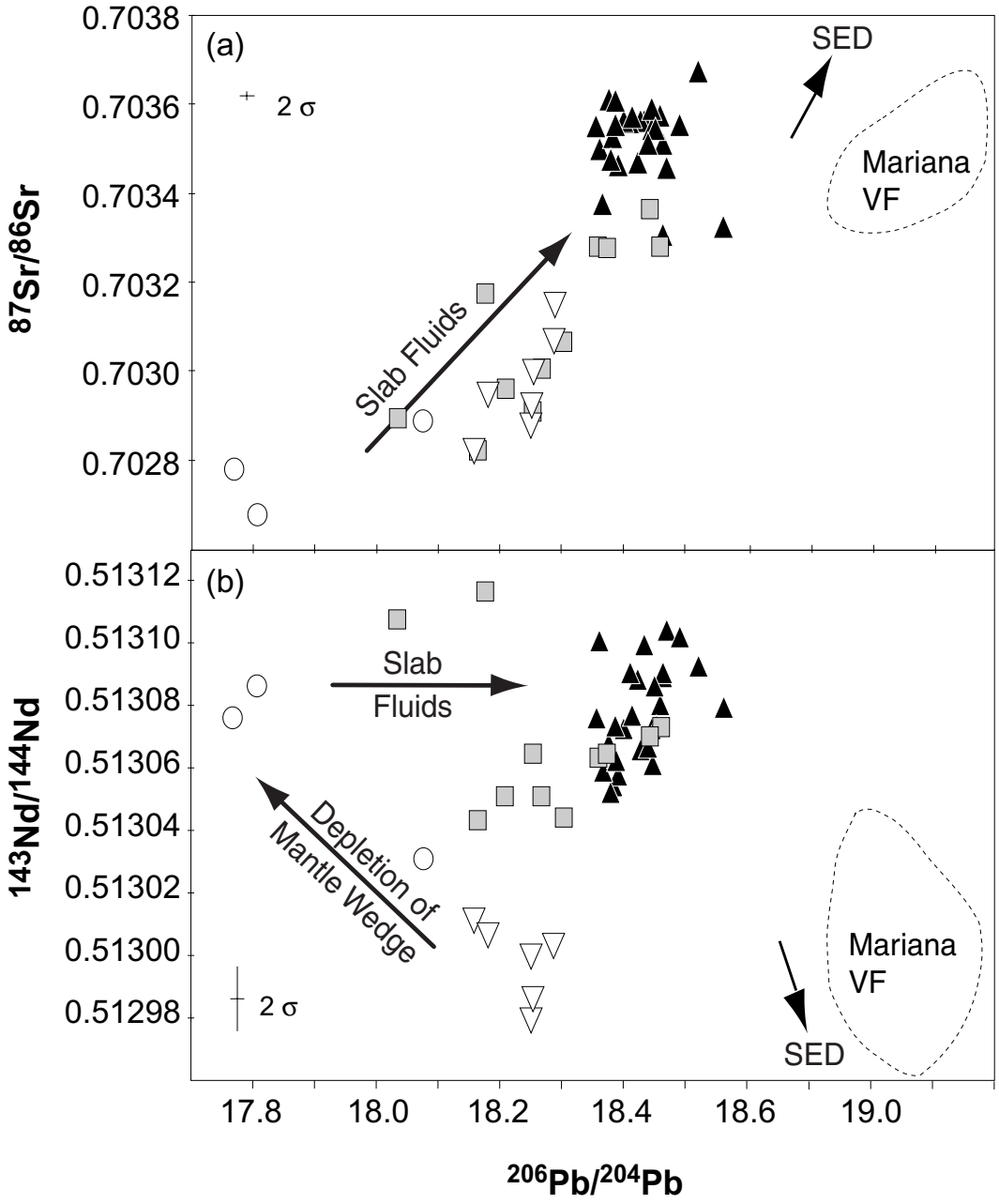

Figure 9: $^{206}Pb/^{204}Pb$ vs. $^{87}/Sr/^{86}Sr$ (a) and $^{206}Pb/^{204}Pb$ vs. $^{143}Nd/^{144}Nd$ (b) isotope diagrams of the Izu samples. Arrows denote direction of local sediments. Field denotes Mariana VF. Symbols as in Fig 3.

6 Discussion

As noted above, the VF, rift, RA and SB of the Izu arc display differences in trace element contents (Fig. 5) as well as in radiogenic isotope composition (Table 2, Fig. 7-9). Below we discuss possible models for explaining these variations and what they imply about magma genesis in volcanic arcs.

6.1 Two Component Mixing?

Considering the large number of possible components involved in the genesis of arc magmas (fluids from subducted sediments, fluids from subducted altered oceanic crust, melts from subducted sediments, melts from subducted slabs, depleted MORB-type mantle in the wedge, enriched OIB-type mantle in the wedge, subarc crust), there is not likely to be a unique explanation of these variations. Our goal is to present the simplest model for explaining these variations and therefore we begin with a two component mixing model as is suggested by the linear array on the Pb-isotope diagram.

Assuming two-component mixing, one endmember must be unradiogenic in Pb and Sr and radiogenic in Nd isotopic ratios similar to MORB (henceforth referred to as component A). On the thorogenic Pb isotope diagram (Fig. 8b), this endmember falls in the field for Indian MORB and above the field for recent and Mesozoic Pacific MORB. Basalts recovered from spreading centers, basins and ridges from the Philippine Sea Plate reveal Indian MORB-type isotopic signatures (this study, Hickey- Vargas, 1991; Hickey- Vargas, 1992; Hickey-Vargas, 1998; Hickey-Vargas et al., 1995; Pearce et al., 1999). Hence the Philippine Sea plate has been interpreted to have originated over an Indian Ocean upper mantle domain (Hickey-Vargas, 1998). The oceanic crust subducted along the Izu-Mariana margin, however, is Mesozoic Pacific MORB. The endmember component unradiogenic in Pb and Sr must therefore represent the mantle wedge.

Characterizing the second endmember (called hereafter endmember B) is not straightforward, since there are several possibilities.

(1.) OIB-type seamounts with isotopic signature similar to e.g. Hemler Guyot (Staudigel et al., 1991) east of the Marianas are a likely candidate for endmember B (e.g. Fig. 8). However, considering the restricted occurrence of OIB-type seamounts on the Pacific plate outboard the Izu arc, it is unlikely that they were a major component in the Izu arc, since the analyzed volcaniclastic layers have had very homogeneous isotopic signatures over the past 15 million years (Table 2; Schmidt et al., in prep.).

(2.) Another possibility for endmember B has recently been recovered along the central inner trench slopes of the central Izu-Bonin. The samples are N-MORB-type diabase and basalt with Mesozoic Pacific MORB and West Philippine Basin resembling trace element patterns (DeBari et al., 1999). Based on the limited available isotopic data they exhibit Sr, Nd and Pb isotope ratios similar to the VF samples of the Izu arc (Fig. 7, 8). Because the trace element contents and isotope ratios of the samples are very similar to those recovered e.g. in DSDP Site 447 in the West Philippine Basin (Hickey- Vargas, 1991), they are interpreted to have originated from the Philippine Sea plate. Similar rocks with unknown extent may occur elsewhere below the Izu arc and might be a source of radiogenic Pb for the Izu arc lavas.

However, since subduction erosion is unlikely to transport enough of this material into the source region of the Izu magmas and 2.) crustal assimilation by ascending magmas is unlikely to generate the homogeneous isotope ratios observed in the VF, we also exclude arc crust to be endmember B.

(3.) Subducted AOC has been suggested to dehydrate beneath island arcs (e.g. Class et al., 2000; Elliott et al., 1997; Ishikawa and Tera, 1999; Pawley and Holloway, 1993; Peacock, 1990; Poli and Schmidt, 1995). However, the altered Mesozoic Pacific Crust outboard the Izu arc doesn't have the appropriate isotopic composition (e.g. Fig. 8).

(4.) Subducted sediments have the appropriate isotopic composition to account for endmember B in Pb (Fig. 8) and Pb-Sr (Fig. 9a) isotope space. Although the Sr and Pb isotope arrays suggest mixing between the mantle wedge and subducted sediments, diagrams of $^{87}Sr/^{86}Sr$ vs. $^{143}Nd/^{144}Nd$ (Fig. 7) and $^{206}Pb/^{204}Pb$ vs. $^{143}Nd/^{144}Nd$ isotope ratios (Fig. 9b), do not form linear arrays. As Pb and Sr are fluid-mobile elements and Nd is generally considered to be relatively immobile in arc fluids (e.g. Pearce and Peate, 1995), the decoupling of the Nd isotope ratios from the Pb and Sr ratios (Fig. 7, 9b) may reflect differences in the geochemical behavior of these elements. It has been suggested that differing recycling media (fluids vs. melts) from subducted sediments may account for these differences (e.g. Schmidt et al., 2000). Nevertheless, if subducted sediments can melt beneath island arcs is still a matter of debate (see discussion in Johnson and Plank, 1999) and thermal models predict slab temperatures more than 100°C lower than sediment solidi (e.g. Peacock, 1996).

Considering the element contents (e.g. Pb) of VF, rift and RA, even more problems arise with two-component mixing between sediment and the mantle wedge. Sediments contain much higher Pb concentrations than the mantle wedge (e.g. clay (Site 801)= 46.4 ppm Pb; chert (Site 801)= 4.2 ppm Pb; Plank and Langmuir (1998); N-MORB= 0.3 ppm Pb; Sun and McDonough (1989)). If only the mantle wedge and subducted sediments contribute to the Izu volcanic rocks, the VF should be more enriched in Pb than the RA because the VF is shifted towards sediments in the Pb isotope diagrams (Fig. 8). The VF (1-1.59 ppm Pb, Table 2) however, contains similar Pb concentrations as the RA (1.15-1.87 ppm Pb, Table 2), despite the overall greater degree of differentiation of the VF samples.

The last argument against simple sediment- mantle wedge mixing is provided by Fig. 10. On Nd/Pb vs. Pb-isotope plots, the mixing lines between a mantle wedge (1) with Nd/Pb= 25-30 similar to N-MORB and isotopic composition of the SB and either sediment-fluid (2a) with Nd/Pb≈ 0 or bulk sediment (2b) with Nd/Pb= 10-12 fail to intersect most of the samples (Fig. 10a).

Two component mixing between a mantle wedge with uniform Pb-concentration and (1.) OIB-type seamounts; (2.) arc crust; (3.) subducted Pacific crust; or (4.) subducted

sediments is thus not consistent with the Pb-contents and Pb-isotopic ratios of the samples despite the binary trend in Pb isotope diagrams.

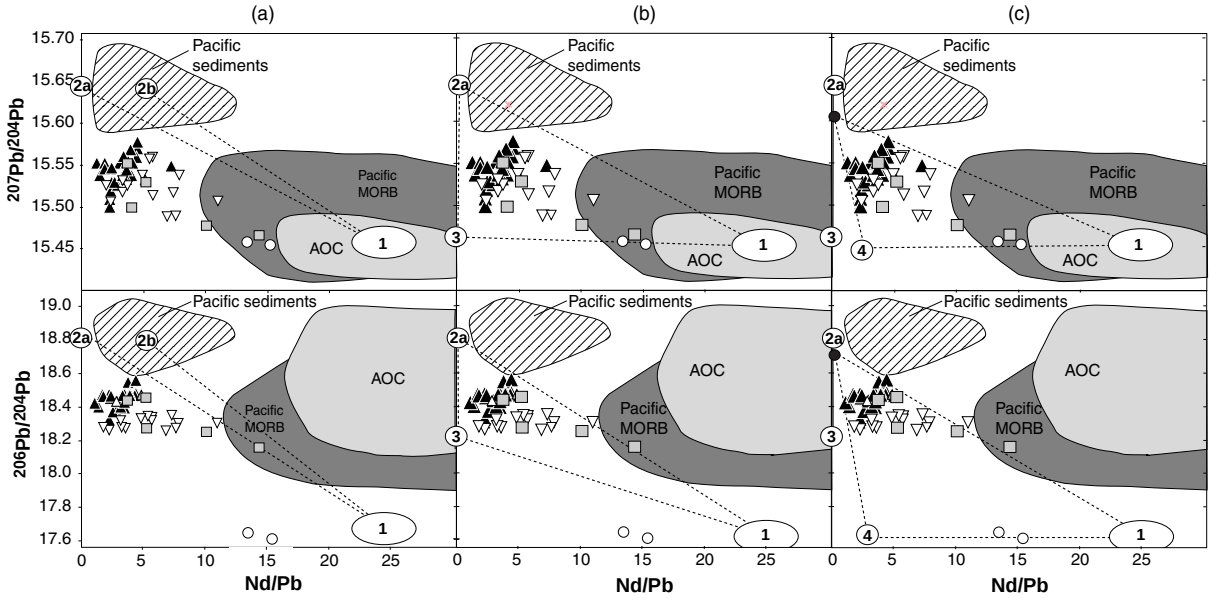

Figure 10: Nd/Pb vs. Pb-isotope plot of the Izu samples. (a): two component mixing between the mantle wedge (1) and sediment-fluid (2a) as well as bulk sediment (2b); (b): mixing between the mantle wedge (1), sediment-fluid (2a) and AOC-fluid (3); and (c): mixing between the mantle wedge (1), a subduction component (black circle) resulting from mixture of sediment-fluid (2a) and AOC-fluid (3), and fluid with the isotopic signature from the mantle wedge (4). Symbols as in Fig. 5. Data are from this study; Hochstaedter et al. (in press.); Janney and Castillo (1997); Pearce et al. (1999); Plank and Langmuir (1998) and Taylor and Nesbitt (1998).

A solution of the “Pb-problem” was suggested by Miller et al. (1994) who proposed the mixing of MORB-derived fluid with sediment for the Aleutians where similar mixing problems as in the Izu arc arose in Nd/Pb vs. Pb-isotope plots. Class et al. (2000) in an expanded study of the same samples studied by Miller et al. (1994), identified three different subduction components that must be added to the mantle wedge in Umnak island, Aleutians: a hydrous fluid from the AOC with MORB-like isotopic composition; a sediment-fluid and a sediment-melt. Ishikawa and Nakamura (1994) and Taylor and Nesbitt (1998) provided evidence for the involvement of AOC in addition to sediment and the mantle wedge in the Izu arc as well. Mixing of the mantle wedge (1), fluid from subducted sediments (2a) and fluid from the subducted Pacific oceanic crust (3) is illustrated in Fig. 10b. Since these components are capable to explain the VF, rift and RA samples, we conclude that fluid from the AOC is also in the Izu arc a dominant fluid source although this is not obvious from the isotope data. As the binary mixing trend in the Pb-isotopes is so clear, we suggest that the dehydration fluids from sediments are mixed with those from the AOC and work as a single subduction component. The composition of this subduction component seems to be remarkably

homogeneous across the arc, since the VF, rift and RA trends are so similar in the Pb isotopes.

What we cannot explain, however, with mixture of components (1) - (3) is the SB (Fig. 10b). As the Pb isotope ratios of the endmembers are fixed (Fig. 8), only the Nd/Pb ratios may vary. We thus need in addition to components (1) - (3) a fluid with mantle wedge Pb isotope ratios ((4) Fig. 10c). The presence of sediment-melts or AOC-fluids in the backarc (RA and SB) cannot be ruled out but are not necessary to explain the Pb isotope ratios. Therefore it seems likely that there are still fluids coming off the subducting slab behind the arc front, but either they are no longer transferring Pb from the slab or the Pb has been exchanged with Pb from the mantle wedge. A mechanism to enrich the mantle in elements like Pb was described by Stolper and Newman (1994). If the mantle wedge reacts similar to a chromatographic column, fluids from the slab may interact with sufficient mantle to loose their slab signature. The loss of the slab signature is clearly dependant on the element compatibility (with respect to fluid-mantle interaction) and the length and state of enrichment or depletion of the mantle column. In longer, enriched mantle columns (e.g. beneath the RA) the slab signature will thus be removed much more complete than in shorter, depleted mantle columns (e.g. beneath the VF). Alternatively the fluids may come from the breakdown of amphibole or phlogopite from mantle wedge material being dragged to depth with corner flow of the plate. We do not favor either of these models, but the mantle wedge seems to dominate the Pb in the RA and SB area (Fig. 10c).

6.2 Causes of Across Arc Variations

Hochstaedter et al. (2000) showed that the across arc increase from the VF to the RA in incompatible element concentration does not result from a reduction in the degree of melting of a homogeneous source. To the contrary, there are clear hints that the mantle wedge below the Izu arc is heterogeneous (e.g. Fig. 5). A good indicator for the extent of enrichment or depletion of a sample are HFSE ratios like Nb/Ta or Zr/Hf. HFSE in general are presumed to reflect mantle compositions because they are least mobile during slab-fluxing processes (McCulloch and Gamble, 1991; Woodhead et al., 1993). While the Izu RA shows MORB-like Zr/Hf ratios, the Izu VF exhibits lower, more depleted Zr/Hf ratios (Table 2). Low Zr/Hf ratios can be attributed to prior melt extraction in the backarc region (e.g. Hochstaedter et al., 2000), that happened in the Izu arc by SB (25-17 Ma), RA (13-3 Ma) and rift (2-0 Ma) volcanism. The depletion of the mantle wedge beneath the VF is also depicted in Nb content. Nb of primitive samples from the Izu VF ranges between 0.14 and 0.28 while Nb contents of primitive samples from the RA have clearly higher values between 1.16 and 3.94 (Hochstaedter et al., 2000; Taylor and Nesbitt, 1998, Table 2).

sample	region	SiO_2	MgO	Nb (ppm)	Zr (ppm)	Hf (ppm)	Zr/Hf	source
781/4	VF	49.55	5.2	0.19	17.8	0.58	30.69	T+N
781/5b	VF	49.58	5.52	0.19	18	0.58	31.03	T+N
MY 17	VF	49.44	5.79	0.28	29.5	0.94	31.38	T+N
HJ 01	VF	47.84	8.23	0.14	14.3	0.5	28.60	T+N
TR 03D	VF	48.43	5.54	0.18	17.1	0.63	27.14	T+N
TRS 13	VF	48.16	6.30	0.15	14	0.56	25.00	T+N
ave	*VF*	*48.83*	*6.10*	*0.19*	*18.45*	*0.63*	*28.97*	-
NJ 06	RA	49.84	5.229	1.16	49.4	1.27	38.90	T+N
92-7	RA	49.69	5.82	2.18	63.3	1.87	33.87	H
94-1	RA	49.75	6.15	2.87	68.0	1.92	35.36	H
108-6	RA	48.14	12.25	3.94	54.7	1.57	34.89	H
118-2	RA	48.89	10.08	1.39	47.8	1.40	34.22	H
ave	*RA*	*49.26*	*7.91*	*2.31*	*56.64*	*1.61*	*35.45*	-
N*MORB	-	-	-	2.33	74	2.05	36.1	S+M
OIB	-	-	-	48	280	7.8	35.9	S+M

Table 2: Compilation of HFSE contents in the Izu VF and RA. For comparison N-MORB and OIB values are also given. T+N= Taylor and Nesbitt (1998), H= Hochstaedter et al. (2000), S+M= Sun and McDonough (1989).

A depleted mantle wedge beneath the VF is sometimes correlated with E-MORB influence behind the VF (Hochstaedter et al., 2000; Hochstaedter et al., 1990b; Ikeda and Yuasa, 1989; Taylor and Nesbitt, 1998). If enriched 'blobs' in the mantle wedge are melted in the RA and rift and are consumed beneath the VF, these heterogeneities could create the observed geochemical differences by progressive melt extraction. However, if there are enriched blobs or not, the mantle wedge is clearly more depleted beneath the VF than beneath the rear of the arc which is likely to result from backarc spreading in the Miocene, RA volcanism between 13-3 Ma and rift volcanism for 3 million years.

An effect that is opposite to depletion of the mantle wedge is the continuing depletion of the subducted slab in fluid mobile elements with deeper subduction into the mantle (Tatsumi and Kosigo, 1997). A consequence of the combined lower fluid flux and less depleted mantle wedge beneath the RA (and rift) is that the isotope ratios are dominated by the mantle wedge instead of being dominated by subduction fluids. This is exactly what we observe in the Pb isotopes of the Izu arc (Fig. 8): the VF is dominated by the subduction component, which we ascribe to the greater influence from the subduction component on a depleted mantle wedge. The RA on the other hand is dominated by the mantle wedge, which may result from a less depleted mantle wedge as well as a more depleted subduction component.

The Sr-Nd isotope ratios (Fig. 7) are explainable in the same manner. Under the VF, the mantle wedge probably exhibits $^{143}Nd/^{144}Nd$ ratios similar to the depleted SB that is shifted to more radiogenic $^{87}Sr/^{86}Sr$ ratios due to addition of subduction fluids. The less depleted mantle wedge beneath the RA exhibits lower $^{143}Nd/^{144}Nd$ ratios.

6.3 Mixing Models

Mixing models are presented in Fig. 11. As we assume only fluid addition in the VF region and Nd is thought to be immobile in fluids, Nd must be derived solely from the mantle wedge. The Nd content of the mantle wedge was calculated assuming 20% batch melting of primitive average VF lavas. To determine the Pb and Sr contents of the mantle wedge, we interpolated the element contents using MORB-normalized multi-element diagrams of primitive VF lavas and assumed that the enrichment of Pb and Sr was generated solely from addition of subduction fluids (see Appendix II for method). The Pb and Sr contents of the unmodified mantle wedge should correspond then to that of the fluid-immobile elements of comparable incompatibility with respect to normal mantle minerals (e.g. Ce, Pr, Nd). For the AOC composition we adopted 0.25% fluid release, an eclogitic composition (garnet:clinopyroxene= 60:40) of the AOC and used the partition coefficients of (Brenan et al., 1995a; Brenan et al., 1995b). The sediment-fluid was assumed to consist of 25% clay and 75% chert. As the partition coefficients for sediment/fluid are not as well constrained as for eclogite/fluid, we assumed the partition coefficients for sediment/fluid to be equal to that for eclogite/fluid and predicted 1% fluid release. It must be noted that the partition coefficients of Sr must be lower than those derived experimentally by Brenan et al. (1995b). To fit the mixing proportions we thus choose different values. The mixing relation between the sediment-fluid and the AOC-fluid that generates the subduction component was calculated to be on average 96% AOC and 4% sediment. Mixtures of about 0.5-2% from this subduction component and 98-99.5% MW is needed to generate the VF magmas. The model endmembers are summarized in Table 3.

		$^{87}Sr/^{86}Sr$	$^{143}Nd/^{144}Nd$	$^{206}Pb/^{204}Pb$	$^{207}Pb/^{204}Pb$	$^{208}Pb/^{204}Pb$	Sr	Nd	Pb
VF	Mantle wedge	0.702700	0.513087	17.800	15.420	37.500	7.2	0.6	0.02
	Sub. Comp.	0.704129	0.513016	18.450	15.540	38.270	1008	0.29	18.04
	AOC-Fluid	0.704000	0.513100	18.200	15.450	37.700	1000	0.26	9.05
	SED-Fluid	0.707116	0.512490	18.680	15.622	38.793	1200	1	235
RA	Mantle wedge	0.702700	0.513000	17.900	15.430	37.600	20.3	1.66	0.07
	Sub. Comp.	0.704131	0.512997	18.377	15.513	38.102	595	0.29	13.598
	AOC-Fluid	0.704000	0.513100	18.200	15.450	37.700	600	0.26	9.05
	SED-Fluid	0.707116	0.512490	18.680	15.622	38.793	500	1	100

Table 3: Endmember compositions used for modeling.

We used the same approach as for the VF to calculate the mantle wedge composition beneath the RA. As we assume fluids with mantle wedge signatures to be added to the mantle wedge, the calculated scenario is an endmember that allows calculating the

maximum slab component. In reality the amount of slab component is likely to be less than our calculations show. However, compared to the interpolated Sr, Nd and Pb contents of the VF (Sr= 7.2 ppm, Nd= 0.6 ppm, Pb= 0.02 ppm), the interpolated mantle wedge beneath the RA is more enriched (Sr= 20.3 ppm, Nd= 1.66 ppm, Pb= 0.07 ppm) which approaches the variable depletion model of Hochstaedter et al. (2000). We assumed the sediment and AOC component to be depleted in Sr beneath the RA, the sediment component to be depleted in Pb and everything else to be equal. The mixing relation between AOC-fluid and the sediment was calculated to be 95% AOC-fluid and 5% sediment. Less than 1-3% from this subduction component mixed with the mantle wedge are needed to generate the RA lavas. The mixing models are presented in Fig. 11.

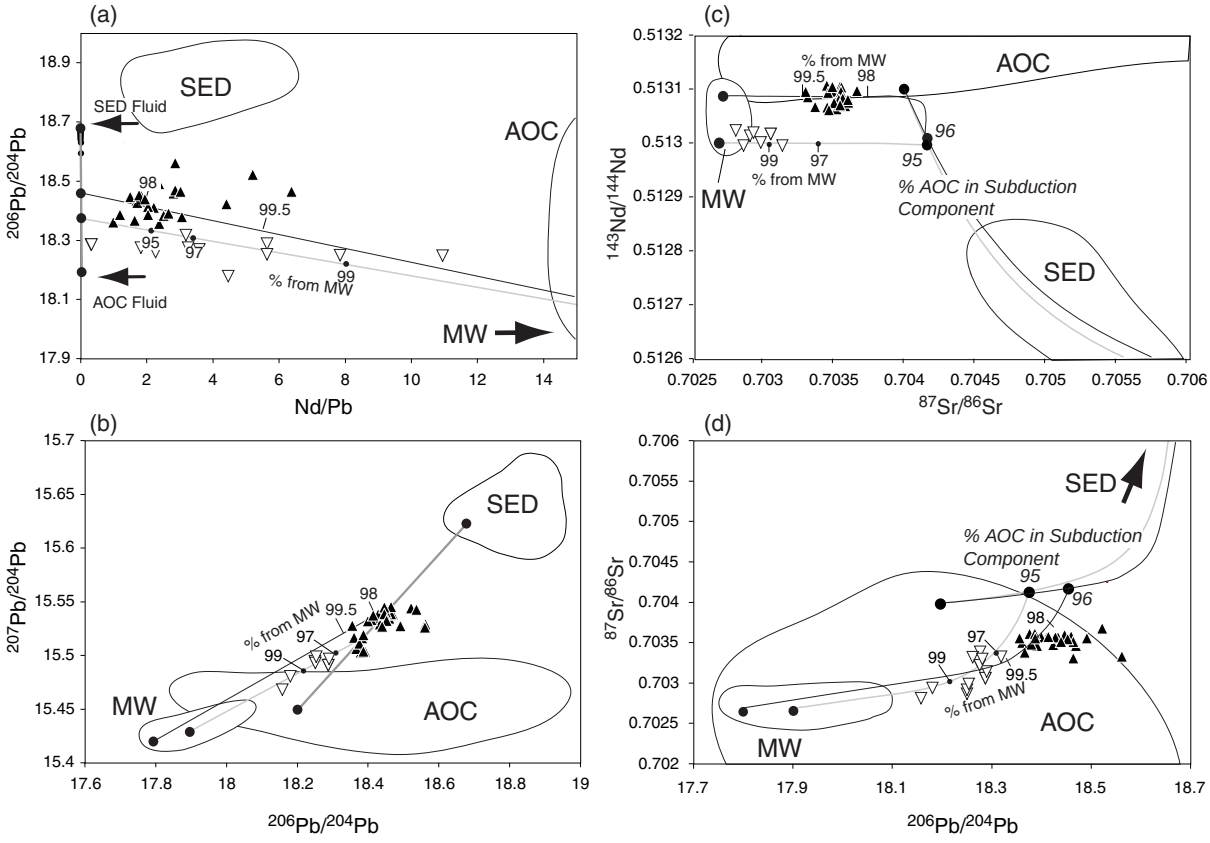

Figure 11: (a) Nd/Pb-$^{206}Pb/^{204}Pb$; (b) $^{206}Pb/^{204}Pb$-$^{207}Pb/^{204}Pb$; (c) $^{87}Sr/^{86}Sr$-$^{143}Nd/^{144}Nd$; and (d) $^{206}Pb/^{204}Pb$-$^{87}Sr/^{86}Sr$ diagrams showing VF (black symbols) and RA samples (open symbols) from this study and Taylor and Nesbitt (1998). Mixing models assume two-component mixing between a variable depleted mantle wedge and a variable enriched subduction component. Sediment field from Hochstaedter et al. (2000); Pearce et al. (1999); Plank and Langmuir (1998) and this study; AOC from Janney and Castillo (1997) and this study; mantle wedge contains SB field. See text for details.

6.4 Mass Balance for the Recycled Sr, Nd and Pb Contents

The amount of recycled elements can be estimated by mass-balance (see Appendix II for method). Mass balancing Pb yields that 5-18% of the Pb from the VF lavas are derived from the mantle wedge, and that 72-95% are derived from the subduction component. The Pb in the subduction component is derived from AOC and sediment with about the same proportions each (Fig. 12). For the RA the Pb mass balance yields that 14-34% are derived from the mantle wedge, 24-32% are derived from sediments and 42-54%, and therewith as much as in the VF, are derived from AOC-fluids (Fig. 12).

Mass balancing Sr yields that 30-64% of the Sr at the VF stem from the mantle wedge, 1-3% are derived from sediments and 35-67% are derived from the AOC (Fig. 12). In the RA region the mantle wedge contribution to the Sr budget increases to 53-77%. The AOC is with 22-46% contribution to the RA magma source still a big source for Sr and the sediment contribution is with 1-2% neglectable (Table 6). The AOC is thus a dominant source for Sr across the whole Izu arc. The mantle wedge's contribution increases across the arc. Subducted sediments contribute almost no Sr to the arc magmas.

Nd per definition is derived almost solely from the mantle wedge. Thus more than 99% of the Nd are derived from the mantle wedge.

The mass balance results clearly reflect the model (depleted mantle wedge beneath the VF; depleted subduction component beneath the RA) and partition coefficients. The results however show that the contribution of each endmember must change across the arc. The relative constancy of AOC contribution is interesting and can be explained with the huge reservoir of AOC (4-5 km) subducted into the trench in contrast to subducted sediments (300-400 m).

	SC added to mantle wedge	Sr (%)	Nd (%)	Pb (%)
Volcanic Front				
Mantle wedge	0.5%	64	100	18
AOC-fluid	0.5%	35	0	39
Sediment-fluid	0.5%	1	0	43
Mantle wedge	2%	30	99	5
AOC-fluid	2%	67	1	45
Sediment-fluid	2%	3	0	50
Rear Arc				
Mantle wedge	1%	77	100	34
AOC-fluid	1%	22	0	42
Sediment-fluid	1%	1	0	24
Mantle wedge	3%	52	99.5	14
AOC-fluid	3%	46	0.5	54
Sediment-fluid	3%	2	0	32

Table 4: Element budget for the endmembers. SC= subduction component, AOC= altered oceanic crust.

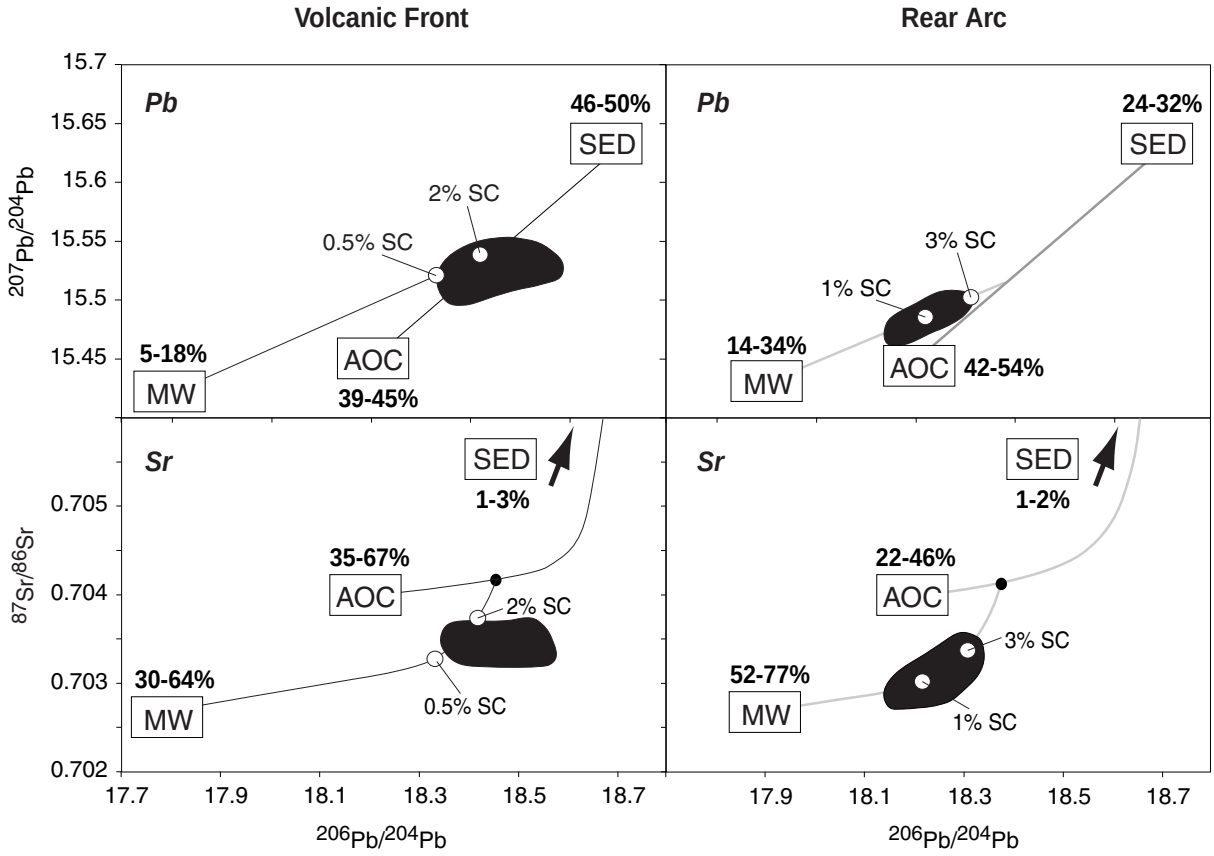

Figure 12: Mixing lines and mass balance for Pb (above) and Sr (below) for the Izu Volcanic front (left) and Rear arc (right). Percent range result from different amounts of subduction component (= AOC + sediment). Compare Table 4. MW= mantle wedge, AOC= altered oceanic crust, SED= subducted sediments.

6.5 Comparison of the Izu and Mariana Volcanic Fronts

The Mariana island arc is located south and adjacent to the Izu arc (Fig. 1). Subduction at both arcs started in the middle Eocene and continued until the present with a similar subduction rate and orientation of the subducting plate (e.g. Taylor et al., 1992). Despite these similarities, striking differences exist in the geochemistry of each arc's volcanic output. The Izu arc is less radiogenic in Pb (Fig. 8), more radiogenic in Nd (Fig. 7) and less enriched in incompatible trace elements (e.g. Rb, Ba, K, Nb) than the Mariana arc (Fig. 13). The Pb isotope arrays are linear in both arcs but point towards distinct radiogenic and unradiogenic endmembers (Fig. 8).

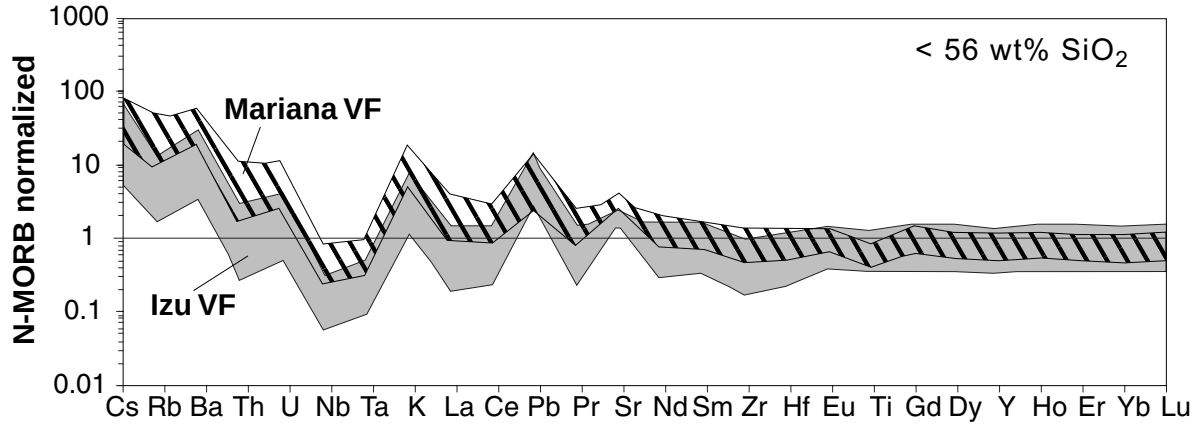

Figure 13: Comparison of MORB-normalized Izu and Mariana VF samples. Data sources Mariana Arc: Elliott et al. (1997), Izu Arc: Taylor & Nesbitt (1998), N-MORB: Sun & McDonough (1989).

The differing radiogenic endmembers can be attributed to the differing sedimentary input into each arc: pelagic sediments are recycled into the Izu arc in contrast to a mixture of pelagic sediments and intraplate volcaniclastic rocks with higher radiogenic Pb ratios recycled in the Mariana arc (e.g. Plank et al., 2000). The unradiogenic endmember of the Izu VF is explained as a mixture of the mantle wedge and fluids from the subducted AOC. Compared to the unradiogenic Izu endmember, the unradiogenic Mariana endmember points towards more radiogenic AOC compositions (Fig. 8). We propose that this may be due to OIB components in the AOC. Thus ultimately the difference in Pb between the Marianas and the Izu reflects the presence of OIB in the subducting assemblage beneath the Marianas, both in the ocean crust (most likely as intrusions and lavas) and the sediments (volcaniclastica).

The Mariana VF was studied extensively by Elliott et al. (1997) who interpret the Mariana VF to result from mixing of a sediment-melt with an AOC-fluid. As described in detail above, the Izu VF is interpreted to result from mixing of fluids derived from the subducted AOC and subducted sediments. The mantle wedge of both arcs is assumed to be depleted, so that the element contribution from the mantle wedge is minor for fluid-mobile elements like Pb and Sr. Sediment recycling thus apparently happens by differing recycling processes at both arcs (via fluids in the Izu VF and via melt and fluids in the Mariana VF).

We propose that the differing recycling processes along the VF reflect the differing subduction angles (80-90° beneath the Marianas compared to 50-70° in the central Izu arc). Fluids are also recycled beneath the Mariana VF, but the steeper subduction angle introduces a higher P-T regime in the area of recycling beneath the Mariana VF, so that differing recycling processes are mixed, leading to the observed geochemical signatures (e.g. Fig. 8). The flatter subduction angle and thus lower P-T conditions beneath the Izu arc on the other hand seem to be unable to produce a sediment-melt in the VF area.

Summarizing we propose that the differing geochemistry of the Izu and Mariana VF result from (1) differing recycling processes in the Mariana and Izu arcs (slab fluids versus slab fluids and melts respectively) and (2) a differing input into both subduction zones.

7 Conclusions

Two end-members contribute to the geochemistry of the central Izu arc/backarc lavas: 1) the mantle wedge (± a fluid with the isotopic signatures of the mantle wedge), and 2) a subduction component consisting of fluids from subducted sediments and subducted AOC. The mantle wedge and subduction component are not homogeneous across the arc. Qualitative findings indicate that across arc geochemical differences in the Izu arc result from 1) the depletion of the mantle wedge beneath the VF due to magma extraction in the RA and rift, and 2) from the depletion of the subduction component in fluid-mobile elements in the RA, due to element loss beneath the VF and forearc regions.

Assuming this model, the Sr, Nd and Pb isotopic compositions and element contents were modeled. The results are in accordance with the qualitative findings and indicate that 80-95% of the Pb of the VF is derived from the subducting plate and only 5-20% are derived from the mantle wedge. In the RA 14-34% of the Pb is derived from the less depleted mantle wedge. Sediments with a 24-32% contribution to the Pb budget are a less significant source of Pb than beneath the VF, while the AOC contribution to the arc Pb budget is almost the same beneath the VF and the RA. Sr modeling shows that the mantle wedge and AOC are the dominant sources for Sr in both the VF and RA. The sediment delivers almost no Sr while the mantle wedge contribution increases from 30-64% in the VF region to 52-77% in the RA region. It is assumed that Nd comes only from the mantle wedge beneath both the VF and RA.

A comparison with the geochemistry and structure of the adjacent Mariana VF suggests that differing recycling processes occur in the arc front regions that might be related to differing depths of the Benioff zone. The geochemistry of the Mariana VF is interpreted to result from a mixture of sediment-melt and AOC-fluid recycling, while we interpret the geochemistry of the Izu VF to result from recycling of fluids from both sediments and AOC. We suggest that the differing recycling processes result from different P-T conditions as the subduction angle and hence the Wadati-Benioff zone is steeper beneath the Marianas than beneath the Izu arc. In addition to the differing structure of the Izu and Mariana arc, that determines differing recycling processes, the differing input into the trenches also cause geochemical differences. The subducted sediments as well as the AOC in the Mariana region are OIB influenced, while the Izu subduction input is not. The differing input is most obvious in the Pb isotope composition of the VF lavas.

References

Brenan JM, Shaw HF and Ryerson FJ (1995a) Experimental evidence for the origin of lead enrichment in convergent-margin magmas. Nature, 378: 54-56.

Brenan JM, Shaw HF, Ryerson FJ and Phinney DL (1995b) Mineral-aqueous fluid partitioning of trace elements at 900°C and 2.0 GPa: Constraints on the trace element chemistry of mantle and deep crustal fluids. Geochim Cosmochim Acta, 59 (16): 3331-3350.

Class C, Miller DM, Goldstein SL and Langmuir CH (2000) Distinguishing melt and fluid subduction components in Umnak volcanics, Aleutian arc. Geochem. Geophys. Geosyst., 1: Paper number 1999GC000010.

Clague DA and Dalrymple GB (1987) The Haxaiian-Emperor Seamount Chain, Part I, Geologic evolution. US Geol Surv Professional Paper 1350: 5-54

DeBari SM, Taylor B, Spencer K and Fujioka K (1999) A trapped Philippine Sea plate origin for MORB from the inner slope of the Izu-Bonin trench. Earth Planet Sci Lett, 174: 183-197.

Defant, MJ and Kepezhinskas, P (2001) Evidence Suggests Slab Melting in Arc Magmas. EOS Trans, 82 (6): 65-69.

Elburg M and Foden J (1998) Temporal changes in arc magma geochemistry, northern sulawesi, Indonesia. Earth Planet. Sci. Lett., 163: 381-398.

Ellam RM and Harmon RS (1990) Oxygen isotope constraints on the crustal contribution to the subduction-related magmatism of the Aeolian Islands, southern Italy. J Volcanol Geotherm Res, 44: 105-122.

Elliott T, Plank T, Zindler A, White W and Bourdon B (1997) Element transport from slap to volcanic front at the Mariana arc. J Geophys Res, 102 (B7): 14991-15019.

Epstein S and Taylor HP Jr (1967) Variation of $^{18}O/^{16}O$ in minerals and rocks. In P.H. Abelson (Editor) Researches in Geochemistry Vol. 2, John Wiley, New York, 29-62

Fryer, P and Pearce, JA (1992) Introduction to the scientific results of Leg 125. In: P. Fryer, Pearce, J.A., Stokking, L.B. et al. (Editor), Proceedings of the Ocean Drilling Program, Scientific Results. Ocean Drilling Program, College Station TX, pp. 3-11.

Fryer, P, Taylor, B, Langmuir, CH and Hochstaedter, AG 1990. Petrology and geochemistry of lavas from the Sumisu and Torishima backarc rifts. Earth Planet Sci Lett, 100: 161-178.

Garbe-Schönberg, CD (1993) Simultaneous determination of thirthy-seven trace elements in twenty-eight international rock standards by ICP-MS. Geostandards Newslett, 17 (1): 81-97.

Gribble RF, Stern RJ, Bloomer SH, Stüben D, O'Hearn T and Newman S (1996) MORB mantle and subduction components interact to generate basalts in the Southern Mariana Trough back-arc basin. Geochim Cosmochim Acta, 60 (12): 2153-2166.

Hamelin B and Allegre CJ. (1985) Large-scale regional units in the depleted upper mantle revealed by an isotope study of the south-west Indian ridge. Nature, 315: 196-199.

Hart SR (1984) A large-scale isotope anomaly in the Southern Hemisphere mantle. Nature, 309: 753-757.

Hickey-Vargas R (1991) Isotope characteristics of submarine lavas from the Philippine Sea: implications for the origin of arc and basin magmas of the Philippine tectonic plate. Earth Planet Sci Lett, 107: 290-304.

Hickey-Vargas R (1992) A refractory HIMU component in the sources of island-arc magma. Nature, 360: 57-59.

Hickey-Vargas R, Hergt JM and Spadea P (1995) The Indian Ocean-Type Isotopic Signature in Western Pacific Marginal Basins: Origin and Significance. In: B. Taylor and J. Natland (Editors), Active Margins and Marginal Basins of the Western Pacific. Geophys Monogr Ser. Am Geophys Union, Washington D.C.: 175-197.

Hickey-Vargas R (1998) Origin of the Indian Ocean-type isotopic signature in basalts from the Phillipine Sea plate spreading centers: An assasment of local versus large-scale processes. J Geophys Res, 103 (B9): 20963-20979.

Hochstaedter A, Gill J, Peters R, Broughton P, Holden P and Taylor B (in press) Across-Arc Geochemical Trends in the Izu-Bonin Arc: Contributions from the Subducting Slab. Geochem Geophys Geosyst

Hochstaedter A, Gill JB, Ishizuka O, Yuasa M and Sumito M (2000) Across-arc geochemical trends in the Izu-Bonin arc: Constraints on source composition and mantle melting. J Geophys Res, 105 (B1): 495-512.

Hochstaedter AG, Gill JB, Kusakabe M, Newman S, Pringle M, Taylor B and Fryer P.(1990a) Volcanism in the Sumisu Rift, I. Major element, volatile, and stable isotope geochemistry. Earth Planet Sci Lett, 100: 179-194.

Hochstaedter AG, Gill JB and Morris JD (1990b) Volcanism in the Sumisu Rift, II. Subduction and non-subduction related components. Earth Planet Sci Lett, 100: 195-209.

Hoernle KA and Tilton GR (1991) Sr-Nd-Pb isotope data for Fuerteventura (Canary Islands) basal complex and subaerial volcanics: application to magma genesis and evolution. Schweizerische Mineral Petrogr Mitt, 71: 3-18.

Hoogewerff JA, van Bergen MJ, Vroon PZ, Hertogen J, Wordel R, Sneyers A, Nasution A, Varekamp JC, Moens HLE and Mouchel D (1997) U-series, Sr-Nd-Pb isotope and trace-element systematics across an island arc-continent collision zone: Implications for element transfer at the slap-wedge interface. Geochim Cosmochim Acta, 61 (5): 1057-1072.

Ikeda Y and Yuasa, M (1989) Volcanism in nascent back-arc basins behind the Shichito Ridge and adjacent areas in the Izu-Ogasawara arc, northwest Pacific: evidence for mixing between E-type MORB and island arc magmas at the initiation of back-arc rifting. Contrib Mineral Petrol, 101: 377-393.

Ishikawa T and Nakamur E (1994) Origin of the slap component in arc lavas from across-arc variation of B and Pb isotopes. Nature, 370: 205-208.

Ishikawa T and Tera F (1997) Source, composition and distribution of the fluid in the Kurile mantle wedge: Constraints from across-arc variations of B/Nb and B isotopes. Earth Planet Sci Lett, 152: 123-138.

Ishikawa T and Tera F (1999) Two isotopically distinct fluid components involved in the Mariana arc: Evidence from Nb/B ratios and B, Sr, Nd and Pb isotope systematics. Geology, 27: 83-86.

Ito E and Stern RJ. (1985/1986) Oxygen- and strontium-isotopic investigations of subduction zone volcanism: the case of the Volcano Arc and the Marianas Island Arc. Earth Planet Sci Lett, 76: 312-320.

Janney P. and Castillo PR (1997) Geochemistry of Mesozoic Pacific mid-ocean ridge basalt: Constraints on melt generation and the evolution of the Pacific upper mantle. J Geophys Res, 102 (B3): 5207-5229.

Johnson MC and Plank T (1999) Dehydration and Melting Experiments Constrain the Fate of Subducted Sediments. Geochem Geophys Geosyst, 1: 1999GC000014.

Langmuir CH, Zhang Y, Taylor B, Plank T, Rubenstone J and Schmidt A (in press) Petrogenesis of Torishima and adjacent volcanos of the Izu-Bonin arc: one end member of the global spectrum of arc basalt compositions. Contrib Mineralal Petrol

McCulloch MT and Gamble JA (1991) Geochemical and geodynamical constraints on subduction zone magmatism. Earth Planet Sci Lett, 102: 358-374.

Mengel K and Hoefs J (1990) Li-δ^{18}O-SiO_2 systematics in volcanic rocks and mafic lower crustal granulite xenoliths. Earth Planet Sci Lett, 101: 42-53.

Miller DM, Goldstein SL and Langmuir CH (1994) Cerium/ lead and lead isotope ratios in arc magmas and the enrichment of lead in the continents. Nature, 368: 514-520.

Moriguti T and Nakamura E (1998) Across-arc variation of Li isotopes in lavas and implications for crust/mantle recycling at subduction zones. Earth Planet Sci Lett, 163: 167-174.

Morris J and Tera F (1989) ^{10}Be and ^{9}Be in mineral separates and whole rocks from volcanic arcs: Implication for sediment subduction. Geochim Cosmochim Acta, 53: 3197-3206.

Morris JD, Leeman WP and Tera F (1990) The subducted component in island arc lavas: constraints from Be isotopes and B-Be systematics. Nature, 344: 31-36.

Notsu K, Isshiki N and Hirano M (1983) Comprehensive strontium isotope study of Quarternary volcanic rocks from the Izu-Ogasawara arc. Geochem J, 17: 289-302.

Pawley AR and Holloway JR (1993) Water Sources for Subduction Zone Volcanism: New Experimental Constraints. Science, 260: 664-667.

Peacock SM (1990) Fluid Processes in Subduction Zones. Science, 248: 329-337.

Peacock SM (1996) Thermal and petrologic structure of subduction zones. In: G.E. Bebout (Editor), Subduction Top to Bottom. Geophys Monogr Ser AGU, Washington, D.C., pp. 119-133.

Peacock SM, Rusher T and Thompson AB (1994) Partial melting of subducting oceanic crust. Earth Planet Sci Lett, 121: 227-244.

Pearce JA, Kempton PD, Nowell GM and Noble SR (1999) Hf-Nd Element and Isotope Perspective on the Nature and Provenance of Mantle and Subduction Components in Western Pacific Arc-Basin Systems. J Petrol, 40 (11): 1579-1611.

Pearce JA and Peate DW (1995) Tectonic implications of the composition of volcanic arc magmas. Ann Rev Earth Planet Sci, 23: 251-285.

Plank T and Langmuir CH (1993) Tracing trace elements from sediment input to volcanic output at subduction zones. Nature, 362: 739-743.

Plank T and Langmuir CH (1998) The geochemical compostion of subducting sediment and its consequences for the crust and the mantle. Chem Geol, 145: 325-394.

Plank T, Ludden JN, Escutia C et al (2000) Proc ODP, Init Repts, 185 [Online]. Available from World Wide Web: <http://www-odp.tamu.edu/publications/185_IR/185ir.htm>.

Poli S and Schmidt MW (1995) H2O transport and release in subduction zones: Experimental constraints on basaltic and andesitic systems. J Geophys Res, 100: 22299-22314.

Rehkämper M and Hofmann AW (1997) Recylced ocean crust and sediment in Indian Ocean MORB. Earth Planet Sci Lett, 147: 93-106.

Saunders AD, Norry MJ and Tarney J (1991) Fluid influence on the trace element compositions of subduction zone magmas. Philosophical Transactions of the Royal Society of London, 335: 377-392.

Schmidt A, Hoernle KA, Straub SM and van den Bogaard P (in prep) Eocene to Recent Evolution of the Izu arc, Japan.

Schmidt A, Straub SM, Hoernle K, Langmuir CH, Gill JB and Hochstaedter AG (2000) Causes of geochemical differences between the adjacent Izu and Mariana arcs, West Pacific, International Association of Volcanology and Chemistry of the Earth's Interior (IAVCEI), General Assembly, Bali, Indonesia, pp 20.

Shibata T and Nakamura E (1997) Across-arc variations of isotope and trace element compositions from Quarternary basaltic volcanic rocks in northeastern Japan: Implications for interaction between subducted oceanic slab and mantle wedge. J Geophys Res, 102 (B4): 8051-8064.

Staudigel H, Park KH, Pringel M, Rubenstone JL, Smith WHF and Zindler A (1991) The longevity of the South Pacific isotopic and thermal anomaly. Earth Planet Sci Lett, 102: 24-44.

Stolper E and Newman S (1994) The role of water in the petrogenesis of mariana trough magmas. Earth Planet Sci Lett, 121: 293-325.

Sun SS and McDonough WF (1989) Chemical and isotopic systematics of oceanic basalts: implications for mantle composition and processes. In: A.D.N. Saunders, M.J. (Editor), Magmatism in the Ocean Basins. Geological Special Publication, pp 313-345.

Tatsumi Y (1989) Migration of fluid phases and the genesis of basalt magmas in subduction zones. J Geophys Res, 94 (B4): 4697-4707.

Tatsumi Y and Kosigo T (1997) Trace element transport during dehydration processes in the subducted oceanic crust: 2. Origin of chemical and physical characteristics in arc magmatism. Earth Planet Sci Lett, 148: 207-221.

Tatsumi Y, Murasaki M and Nohda S (1992) Across-arc variation of lava chemistry in the Izu-Bonin arc: identification of subduction components. Journal of Volcanology and Geotherm Res, 49: 179-190.

Taylor B (1992) Rifting and the volcanic-tectonic evolution of the Izu-Bonin-Mariana Arc. In: B. Taylor, Fujioka, K. et al. (Editors), Proc of the Ocean Drilling Program, Sci Res, College Station TX: 627-651.

Taylor RN and Nesbitt RW (1998) Isotopic characteristics of subduction fluids in an intra-oceanic setting, Izu-Bonin Arc, Japan. Earth Planet Sci Lett, 164: 79-98.

Todt W, Cliff RA, Hanser A and Hofmann AW (1996) Evaluation of a ^{202}Pb-^{205}Pb Double Spike for High-Precision Lead Isotope Analysis. In: A. Basu and S. Hart (Editors), Earth Processes: Reading the Isotopic Code. AGU, Washington, pp 429-437.

Turner S, Hawkesworth C, Rogers N, Bartlett J, Worthington T, Hergt J, Pearce J and Smith, I. (1997) ^{238}U-^{230}Th disequilibria, magma petrogenesis, and flux rates beneath the depleted Tonga-Kermadec island arc. Geochim Cosmochim Acta, 61: 4855-4884.

Van der Hilst R and Seno T (1993) Effects of relative plate motion on the deep structure and penetration depth of slabs below the Izu-Bonin and Mariana island arcs. Earth Planet Sci Lett, 120: 395-407.

Volpe AM, Macdougall JD and Hawkins JW (1987) Mariana trough basalts (MTB): trace element and Sr-Nd isotopic evidence for mixing between MORB-like and arc-like melts. Earth Planet Sci Lett, 82: 241-254.

Vroon PZ, van Bergen MJ, White WM and Varekamp JC (1993) Sr-Nd-Pb Isotope Systematics of the Banda Arc, Indonesia: Combined Subduction and Assimilation of Continental Material. J Geophys Res, 98: 22349-22366.

White WM, Hofmann AW and Puchelt H (1987) Isotope geochemistry of Pacific Mid-Ocean Ridge basalts. J Geophys Res, 92, 4881-4893.

Woodhead J, Eggins S and Gamble J (1993) High field strength and transition element systematics in island arc and back-arc basin basalts: evidence for multi-phase melt extraction and a depleted mantle wedge. Earth Planet Sci Lett, 114: 491-504.

Woodhead JD (1989) Geochemistry of the Mariana arc (western Pacific): Source composition and processes. Chem Geol, 76: 1-24.

Woodhead JD, Harmon RS and Fraser DG (1987) O, S, Sr and Pb isotope variations in volcanic rocks from the Northern Mariana islands: implications for crustal recycling in intra-oceanic arcs. Earth Planet Sci Lett, 83: 39-52.

Yogodzinski GM and Kelemen PB (1998) Slab melting in the Aleutians: Implications of an ion probe study of clinopyroxene in primitive adakite and basalt. Earth Planet Sci Lett, 158: 53-63.

Appendix II

Mantle Wedge Interpolations

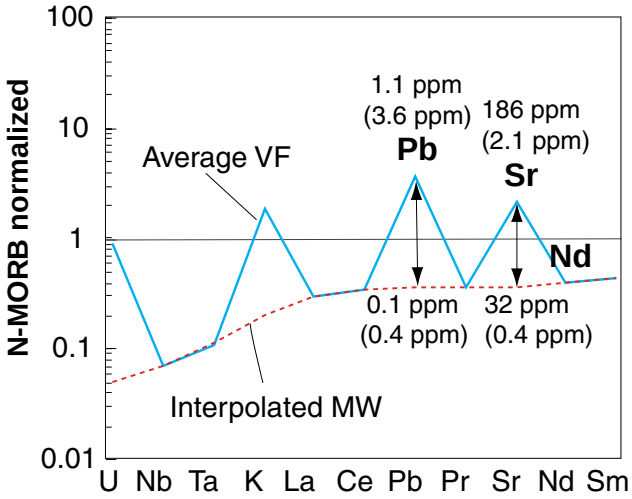

The sketch shows how we interpolated the Sr and Pb contents of the mantle wedge beneath the VF. The bold line shows the averade composition of the primitive VF samples HJ 01, TRS 13, Tr03D and 32-2 from Taylor and Nesbitt (1998) and Hochstaedter et al. (in prep.). The strippled line shows the interpolated mantle wedge. The upper numbers correspond to the measured element contents, the lower numbers are the interpolated element contents (normalized values in parentheses).

Mass balance

Mass balancing calculations were performed by multiplying the amount of the component with the concentration. Via the rule of three the percent of the component was calculated. An example for Pb recycling beneath the VF is given below. For estimation of mixtures (0.5-2% subduction component, 98-99.5% mantle wedge) see text, element concentrations are given in Table 3.

	Mantle Wedge	Subduction Component
Pb concentration	0.02 ppm	18.04 ppm
fraction (%)	98 (99.5)	2 (0.5)
Pb from component	0.02 ppm x 0.98	18.04 ppm x 0.02
	= 0.0196 ppm	= 0.361 ppm

100% = 0.0196 ppm + 0.361 ppm = 0.3804 ppm

rule of three: 100% = 0.3804 ppm
X% = 0.0196 ppm

→ Mantle Wedge = 5.2%; Subduction Component = 94.8%

For the mixture of 98% mantle wedge with a Pb concentration of 0.02 ppm and 2% subduction component with a Pb concentration of 18.04 ppm
~5% from the Pb recycled along the VF are derived from the mantle wedge and
~95% from the Pb recycled along the VF are derived from the subduction component.
To calculate AOC and SED content, a similar procedure was used.

Appendix III

Table AIII-1: Blank levels (in ppm) from ICP-MS Analyses. *denotes dissolution Method after Garbe-Schönberg without $HClO_4$.

	blank	blank*
Rb	0.026	0.026
Sr	0.024	0.016
Y	0.003	0.001
Zr	0.014	0.029
Nb	0.000	0.002
Cs	0.001	0.002
Ba	0.040	0.025
La	0.001	0.001
Ce	0.001	0.001
Pr	0.000	0.000
Nd	0.001	0.002
Sm	0.000	0.001
Eu	0.001	0.000
Gd	0.001	0.002
Tb	0.000	0.000
Dy	0.001	0.000
Ho	0.000	0.000
Er	0.000	0.000
Tm	0.000	0.000
Yb	0.002	0.000
Lu	0.000	0.000
Hf	0.000	0.001
Ta	0.001	0.002
Pb	0.007	0.032
Th	0.000	0.000
U	0.000	0.000

Table AIII-2: Trace element analyses (in ppm) of International Rock Standards dissolved and analysed with ICP-MS in Kiel compared to values of Garbe-Schönberg (1993, =Ref. 1). Newer unpublished values of Garbe-Schönberg compare much better to the values of this study.

	BHVO-1 this work	BHVO-1 Ref. 1	Dev. %	JB-2 this work	JB-2 Ref. 1	Dev. %
Rb	5.06	9.15	44.7	6.02	6.25	3.7
Sr	291.83	364.00	19.8	177.75	167.00	6.0
Y	19.45	25.30	23.1	20.82	21.30	2.3
Zr	154.08	168.00	8.3	43.19	44.50	2.9
Nb	16.77	19.70	14.9	0.54	0.76	29.5
Cs	0.02	0.13	81.5	0.72	0.84	14.1
Ba	134.83	121.00	10.3	222.44	207.00	6.9
La	14.84	14.00	5.7	2.21	2.11	4.4
Ce	37.06	34.10	8.0	6.47	5.14	20.6
Pr	5.16	4.81	6.7	1.12	1.10	2.1
Nd	23.54	22.40	4.8	6.24	5.92	5.1
Sm	5.94	5.72	3.8	2.25	2.18	3.1
Eu	1.96	1.88	4.1	0.82	0.79	3.8
Gd	5.86	5.79	1.2	3.11	2.89	7.0
Tb	0.88	0.85	3.3	0.57	0.54	4.6
Dy	5.03	4.82	4.1	3.93	3.70	5.8
Ho	0.91	0.88	2.9	0.85	0.80	5.8
Er	2.30	2.32	0.9	2.48	2.42	2.4
Tm	0.30	0.30	0.8	0.37	0.35	5.4
Yb	1.79	1.84	2.5	2.47	2.40	2.7
Lu	0.24	0.25	2.6	0.37	0.35	6.1
Hf	4.39	4.36	0.7	1.51	1.64	8.0
Ta	1.13			0.06		
Pb	2.01	2.08	3.2	5.08	4.94	2.7
Th	0.99	1.10	10.1	0.27	0.24	10.4
U	0.43	0.43	0.9	0.16	0.15	6.8

Table AIII-3: Trace element analyses (in ppm) dissolved in duplicate to check the reproducibility. *denotes dissolution method of Garbe-Schönberg without $HClO_4$. Reproducibility of both dissolution methods is for most elements better than 3%. For dissolution without $HClO_4$, Rb and Ba show reproducibilities up to 3.5%. For dissolution using $HClO_4$, Nb, Cs and Ta show giant variations up to 44%, the other elements, however, reproduce better than 2%.

	48-4-R*	48-4-R*	Dev. %	49-2-D	49-2-D	Dev. %
Rb	10.21	9.88	3.25	11.10	11.27	1.45
Sr	131.83	129.45	1.81	125.60	125.16	0.35
Y	29.47	29.04	1.45	31.74	31.67	0.22
Zr	123.11	121.82	1.05	125.97	125.32	0.52
Nb	2.05	2.00	2.21	1.02	1.41	27.44
Cs	0.70	0.68	3.63	0.61	0.67	9.33
Ba	167.99	166.83	0.69	180.12	180.26	0.08
La	5.58	5.60	0.41	6.08	6.06	0.38
Ce	15.56	15.60	0.26	16.62	16.55	0.44
Pr	2.41	2.41	0.30	2.56	2.55	0.33
Nd	11.63	11.77	1.19	12.30	12.27	0.20
Sm	3.50	3.53	0.85	3.75	3.69	1.46
Eu	0.98	0.99	1.19	1.04	1.03	1.13
Gd	4.24	4.24	0.13	4.59	4.55	0.84
Tb	0.75	0.76	1.66	0.81	0.80	1.38
Dy	5.15	5.21	1.14	5.57	5.54	0.63
Ho	1.11	1.13	1.80	1.20	1.20	0.02
Er	3.37	3.41	1.13	3.66	3.60	1.54
Tm	0.52	0.53	1.66	0.57	0.57	1.32
Yb	3.61	3.67	1.52	4.00	3.95	1.24
Lu	0.56	0.56	1.17	0.61	0.60	0.29
Hf	3.68	3.74	1.58	3.77	3.72	1.34
Ta	1.42	1.44	1.38	0.26	0.47	43.57
Pb	3.20	3.26	1.68	3.51	3.51	0.02
Th	0.58	0.59	2.35	0.73	0.72	1.12
U	0.31	0.32	3.33	0.35	0.35	0.67

Table AIII-4: Precision of ICP-MS analyses. Replicate analysis (N=4) yield that precision is better or equal than 1% for Zr, Ce, Pr, Nd, Sm, Eu, Tb, Dy, Ho, Er, Tm, Yb, Lu, Ta and Pb and better than 3% for Rb, Sr, Y, Nb, Cs, Ba, La, Gd, Hf, Th and U.

	41-1 B	41-1 B Rep. 1	41-1 B Rep. 2	41-1 B Rep. 3	Precision %
Rb	10.65	11.07	10.73	10.48	2.33
Sr	957.88	956.29	947.74	933.31	1.19
Y	72.35	71.95	71.49	70.52	1.10
Zr	140.68	142.29	141.43	140.87	0.51
Nb	3.86	3.85	3.77	3.79	1.20
Cs	0.53	0.55	0.55	0.56	1.91
Ba	183.44	184.77	187.76	189.76	1.54
La	7.36	7.40	7.63	7.65	2.04
Ce	22.27	22.28	22.62	22.64	0.92
Pr	4.03	4.03	4.08	4.08	0.76
Nd	22.55	22.63	22.66	22.66	0.23
Sm	8.35	8.25	8.33	8.21	0.82
Eu	3.46	3.44	3.44	3.48	0.52
Gd	11.10	11.14	11.40	11.23	1.21
Tb	2.02	2.02	2.03	2.03	0.37
Dy	13.80	13.74	13.87	13.80	0.38
Ho	2.92	2.91	2.94	2.90	0.58
Er	8.42	8.36	8.35	8.33	0.43
Tm	1.24	1.23	1.23	1.25	0.76
Yb	8.13	8.09	8.12	8.18	0.47
Lu	1.21	1.19	1.20	1.19	0.83
Hf	4.61	4.56	4.56	4.46	1.35
Ta	3.67	3.62	3.59	3.60	1.02
Pb	4.46	4.41	4.36	4.41	0.96
Th	0.50	0.50	0.49	0.48	2.38
U	0.31	0.30	0.30	0.30	1.85

Table AIII-5: Replicate analyses SIRMS: $\partial^{18}O$.

$\Delta\ \partial^{18}O$= average external reproducibility.

Sample	Region	$\partial^{18}O$
S-2	VF	6.38
S-2	VF	6.07
$\Delta\ \partial^{18}O$		0.05
49-2d	VF	7.16
49-2d	VF	7.33
$\Delta\ \partial^{18}O$		0.02
3	VF-Tephra	6.03
3	VF-Tephra	6.28
$\Delta\ \partial^{18}O$		0.04
41-1	Rift	6.01
41-1	Rift	5.76
$\Delta\ \partial^{18}O$		0.04
108-6	RA	7.00
108-6	RA	6.72
$\Delta\ \partial^{18}O$		0.04

Table AIII-6: Total Chemistry Blanks TIMS (1pg= 10^{-9} g/g).

Sample	Lab.	Date	Pb (pg)	File
Blank 1	GEOMAR	14.05.1998	198	605
Blank 2	GEOMAR	30.10.1998	256	1322
Blank 3	GEOMAR	17.12.1998	180	1414
Blank 4	GEOMAR	31.08.1999	257	2573
Blank 5	GEOMAR	10.09.1999	613	2738
Blank 6	GEOMAR	27.09.1999	116	2875
Average			270	
2 σ			152	

Table AIII-7: TIMS Standard Measurements MAT 262 GEOMAR - NBS 987

	Date	File	T (°C)	values	$^{87}Sr/^{86}Sr$	2 σ
NBS 987	28.05.98	694	1500	100	0.710290	(18)
NBS 987	25.06.98	811	1450	76	0.710231	(9)
NBS 987	25.06.98	812	1400	78	0.710245	(12)
NBS 987	25.06.98	815	1513	78	0.710234	(10)
NBS 987	25.06.98	821	1360	58	0.710248	(11)
NBS 987	25.06.98	822	1507	56	0.710244	(9)
NBS 987	25.06.98	826	1505	79	0.710223	(14)
NBS 987	25.06.98	830	1511	58	0.710214	(10)
NBS 987	17.07.98	851	1367	137	0.710254	(11)
NBS 987	17.07.98	858	1485	95	0.710238	(11)
NBS 987	04.09.98	1024	1439	114	0.710229	(8)
NBS 987	24.09.98	1074	1308	118	0.710236	(9)
NBS 987	06.11.98	1362	1352	99	0.710250	(10)
NBS 987	07.11.98	1366	1303	80	0.710234	(13)
NBS 987	07.11.98	1366	1425	59	0.710267	(9)
NBS 987	08.11.98	1372	1399	117	0.710255	(9)
NBS 987	06.01.99	1468	1525	98	0.710236	(8)
NBS 987	01.09.99	2574	1475	99	0.710251	(6)
NBS 987	09.09.99	2725	1488	100	0.710247	(8)
NBS 987	10.09.99	2740	1488	98	0.710261	(8)
NBS 987	30.09.99	2896	1487	137	0.710257	(8)
NBS 987	06.10.99	2925	1501	95	0.710259	(7)
Average					0.710246	
2 σ					0.000016	

Table AIII-8: TIMS Standard Measurements MAT 262 GEOMAR - La Jolla, Nd-Spex

	Date	File	T (°C)	Blocks	$^{143}Nd/^{144}Nd$	2 σ
La Jolla	01.07.98	834	1796	6	0.511845	(10)
La Jolla	02.07.98	836	1830	4	0.511839	(7)
La Jolla	02.07.98	842	1775	5	0.511838	(9)
La Jolla	02.07.98	842	1711	3	0.511840	(8)
La Jolla	03.07.98	848	1770	4	0.511850	(6)
La Jolla	06.07.98	849	1691	5	0.511845	(8)
La Jolla	06.07.98	850	1695	4	0.511848	(9)
La Jolla	20.07.98	859	1741	5	0.511848	(8)
La Jolla	02.09.98	1013	1811	6	0.511845	(8)
La Jolla	03.09.98	1019	1860	5	0.511838	(7)
La Jolla	30.09.98	1114	1759	6	0.511839	(9)
La Jolla	16.10.98	1231	1800	5	0.511848	(8)
La Jolla	16.10.98	1235	1828	3	0.511835	(11)
La Jolla	03.11.98	1351	1861	3	0.511840	(11)
La Jolla	04.11.98	1354	1993	6	0.511838	(9)
La Jolla	25.11.98	1381	1861	8	0.511848	(9)
La Jolla	25.11.98	1383	1850	2	0.511850	(14)
La Jolla	26.11.98	1384	1873	4	0.511844	(8)
La Jolla	18.01.99	1547	1919	6	0.511849	(9)
La Jolla	21.01.99	1571	1878	5	0.511852	(9)
La Jolla	09.09.99	2724	1904	6	0.511820	(10)
La Jolla	11.09.99	2744	1935	6	0.511842	(9)
Average					0.511843	
2 σ					0.000007	
Nd-Spex	11.09.99	2745	1947	6	0.511698	(10)
Nd-Spex	12.09.99	2753	1938	5	0.511711	(8)
Nd-Spex	12.09.99	2760	1893	3	0.511699	(5)
Nd-Spex	14.09.99	2771	1937	5	0.511709	(6)
Nd-Spex	28.09.99	2879	1898	6	0.511704	(7)
Nd-Spex	29.09.99	2887	1873	6	0.511702	(7)
Nd-Spex	06.10.99	2935	1831	3	0.511703	(8)
Average					0.511704	
2 σ					0.000005	

Table AIII-9: TIMS Standard Measurements MAT 262 GEOMAR - NBS 981

NBS981* Values from Todt et al. (1996)

	Date	$^{206}Pb/^{204}Pb$	2 σ	% fract/ a.m.u.	$^{207}Pb/^{204}Pb$	2 σ	% fract/ a.m.u.	$^{208}Pb/^{204}Pb$	2 σ	% fract/ a.m.u.
NBS 981*		16.936			15.489			36.701		
NBS 981	14.05.98	16.901	(2)	0.103	15.443	(2)	0.100	36.541	(4)	0.109
NBS 981	24.08.98	16.895	(2)	0.122	15.434	(2)	0.119	36.517	(4)	0.126
NBS 981	31.08.98	16.898	(2)	0.112	15.439	(2)	0.108	36.533	(4)	0.115
NBS 981	31.08.98	16.902	(1)	0.100	15.444	(1)	0.096	36.550	(3)	0.103
NBS 981	01.09.98	16.896	(2)	0.117	15.438	(1)	0.110	36.530	(4)	0.117
NBS 981	13.09.98	16.900	(2)	0.105	15.441	(1)	0.103	36.539	(4)	0.111
NBS 981	27.09.98	16.896	(2)	0.117	15.438	(2)	0.111	36.530	(4)	0.117
NBS 981	29.09.98	16.898	(1)	0.110	15.441	(1)	0.105	36.536	(3)	0.113
NBS 981	30.10.98	16.891	(2)	0.131	15.430	(1)	0.127	36.506	(3)	0.133
NBS 981	03.11.98	16.894	(1)	0.124	15.434	(1)	0.119	36.519	(3)	0.125
NBS 981	16.12.98	16.893	(1)	0.126	15.434	(1)	0.120	36.516	(3)	0.126
NBS 981	17.12.98	16.894	(1)	0.122	15.435	(1)	0.117	36.519	(3)	0.125
NBS 981	18.08.99	16.918	(2)	0.052	15.466	(2)	0.050	36.620	(5)	0.055
NBS 981	18.08.99	16.895	(1)	0.120	15.435	(1)	0.116	36.522	(3)	0.122
NBS 981	31.08.99	16.901	(1)	0.102	15.449	(1)	0.086	36.545	(1)	0.106
NBS 981	09.09.99	16.897	(2)	0.113	15.429	(2)	0.130	36.506	(4)	0.133
NBS 981	09.09.99	16.893	(1)	0.127	15.432	(1)	0.124	36.511	(2)	0.130
NBS 981	10.09.99	16.913	(1)	0.067	15.448	(1)	0.090	36.568	(3)	0.090
NBS 981	10.09.99	16.902	(1)	0.098	15.434	(1)	0.119	36.525	(3)	0.120
NBS 981	27.09.99	16.889	(1)	0.137	15.428	(1)	0.133	36.498	(1)	0.139
NBS 981	10.10.00	16.898	(2)	0.112	15.436	(2)	0.114	36.525	(5)	0.120
NBS 981	10.10.00	16.904	(2)	0.093	15.443	(2)	0.101	36.542	(4)	0.109
NBS 981	19.11.00	16.889	(2)	0.138	15.426	(1)	0.137	36.494	(4)	0.142
NBS 981	19.11.00	16.896	(2)	0.118	15.433	(2)	0.122	36.516	(4)	0.127
Average		16.898			15.438			36.529		
2_		0.007			0.008			0.026		

Table AIII-10: Replicate Analyses TIMS-IC - Sr

$\Delta\ ^{87}Sr/^{86}Sr$= Average external reproducibility

Sample	Date	Treatment	File	T (°C)	Values	$^{87}Sr/^{86}Sr$	2 σ
32-3	28.05.98	unleached	695	1557	118	0.703495	(7)
32-3	04.09.98	unleached	1025	1477	80	0.703483	(7)
32-3	29.06.98	unleached	824	1619	96	0.703003	(20)
32-3	30.06.98	unleached	828	1588	80	0.703495	(9)
59-7	30.06.98	unleached	827	1729	75	0.702993	(14)
59-7	04.09.98	unleached	1028	1510	98	0.702891	(7)
59-7	17.07.98	unleached	852	1532	99	0.702902	(9)
59-7	25.06.98	unleached	814	1669	75	0.702935	(8)
59-7	17.07.98	unleached	857	1560	78	0.702899	(8)
59-7	04.09.98	6N HCl	1029	1480	77	0.702822	(8)
59-7	17.07.98	6N HCl	853	1621	139	0.702846	(9)
$\Delta\ ^{87}Sr/^{86}Sr$						0.000034	
90-1	29.05.98	unleached	700		60	0.703340	(10)
90-1	07.09.98	unleached	1032	1471	119	0.703297	(7)
90-1	26.06.98	unleached	817	1592	60	0.703315	(9)
90	07.01.99	6N HCl	1476	1575	97	0.703640	(8)
90	07.01.99	6N HCl	1477	1519	78	0.703635	(7)
$\Delta\ ^{87}Sr/^{86}Sr$						0.000007	
11-3-a-1	01.09.99	6N HCl	2584	1503	98	0.703073	(8)
11-3-a-1	01.09.99	6N HCl	2583	1554	98	0.703068	(7)
$\Delta\ ^{87}Sr/^{86}Sr$						0.000007	
106	10.09.99	6N HCl	2741	1515	98	0.703514	(9)
106	30.09.99	6N HCl	2900	1480	100	0.703508	(8)
$\Delta\ ^{87}Sr/^{86}Sr$						0.000009	
29	06.10.99	6N HCl	2934	1550	98	0.703557	(9)
29	30.09.99	6N HCl	2905	1465	100	0.703565	(8)
$\Delta\ ^{87}Sr/^{86}Sr$						0.000012	

Table AIII-11: Replicate Analyses TIMS-IC - Nd

$\Delta\ ^{143}Nd/^{144}Nd$ = Average external reproducibility

Sample	Date	Treatment	Filename	T (°C)	blocks	$^{143}Nd/^{144}Nd$	2 σ
32-3	22.05.98	unleached	647	1870	6	0.513126	(6)
32-3	02.07.98	unleached	837	1882	8	0.513115	(8)
32-3	02.09.98	unleached	1014	1832	6	0.513117	(9)
59-7	22.05.98	unleached	646	1870	4	0.513056	(5)
59-7	02.07.98	unleached	839	1802	4	0.513030	(8)
59-7	20.07.98	unleached	860	1760	3	0.513041	(8)
59-7	20.07.98	unleached	865	1773	3	0.513038	(7)
59-7	02.09.98	unleached	1017	1758	7	0.513007	(9)
90-1	22.05.98	unleached	648	1900	7	0.513028	(8)
90-1	03.09.98	unleached	1021	1861	4	0.513011	(8)
90-1	02.07.98	unleached	841	1852	6	0.513016	(8)
59-7	02.09.98	6n HCl	1018	1905	6	0.513053	(9)
59-7	20.07.98	6n HCl	861	1919	4	0.513053	(8)
$\Delta\ ^{143}Nd/^{144}Nd$						0.000001	
1894-9	03.11.98	6n HCl+ 8n HNO_3	1353	1895	6	0.513071	(15)
1894-9	03.11.98	6n HCl+ 8n HNO_3	1352	1861	5	0.513077	(11)
$\Delta\ ^{143}Nd/^{144}Nd$						0.000011	
115-2	18.01.99	5ml 6N HCl	1554	1838	5	0.513006	(6)
115-2	29.09.99	5ml 6N HCl	2895	1845	5	0.513009	(7)
$\Delta\ ^{143}Nd/^{144}Nd$						0.000006	
9-6-6	21.01.99	5ml 6N HCl	1237	1855	5	0.513034	(9)
9-6-6	29.09.99	5ml 6N HCl	2894	1846	5	0.513024	(6)
$\Delta\ ^{143}Nd/^{144}Nd$						0.000018	
69	21.01.99	5ml 6N HCl	1573	1822	5	0.513077	(8)
69	29.09.99	5ml 6N HCl	2890	1859	6	0.513081	(8)
$\Delta\ ^{143}Nd/^{144}Nd$						0.000007	
T-60	21.01.99	5ml 6N HCl	1238	1955	3	0.512999	(17)
T-60	29.09.99	5ml 6N HCl	2893	1867	5	0.513086	(7)
$\Delta\ ^{143}Nd/^{144}Nd$						0.00017	
11-3-a-1	12.09.99	5ml 6N HCl	2754	1919	5	0.513017	(7)
11-3-a-1	12.09.99	5ml 6N HCl	2756	1893	6	0.513032	(7)
$\Delta\ ^{143}Nd/^{144}Nd$						0.000028	
29	28.09.99	5ml 6N HCl	2880	1830	6	0.513101	(8)
29	29.09.99	5ml 6N HCl	2889	1866	6	0.513097	(8)
$\Delta\ ^{143}Nd/^{144}Nd$						0.000006	
111	12.09.99	5ml 6N HCl	2759	1858	5	0.513026	(8)
111	06.10.99	5ml 6N HCl	2936	1849	4	0.513031	(11)
$\Delta\ ^{143}Nd/^{144}Nd$						0.000009	

Table AIII-12: Replicate Analyses TIMS-IC - Pb

Δ% a.m.u.= External reproducibility

Sample	Date	Treatment	File	T (°C)	Blocks	$^{206}Pb/^{204}Pb$	2 σ	$^{207}Pb/^{204}Pb$	2 σ	$^{208}Pb/^{204}Pb$	2 σ
32-3	24.08.98	unleached	997	1222	7	18.396	(2)	15.489	(1)	38.0954	(4)
32-3	14.05.98	unleached	606	1300	5	18.379	(2)	15.478	(2)	38.0604	(5)
Δ% a.m.u.						0.047		0.037		0.046	
59-7	24.08.98	unleached	1000	1227	6	18.166	(2)	15.439	(2)	37.7967	(4)
59-7	31.08.98	unleached	1010	1245	6	18.164	(2)	15.436	(2)	37.7919	(4)
Δ% a.m.u.						0.007		0.011		0.006	
59-7	24.08.98	5ml 6N HCl	1001	1224	5	18.128	(2)	15.420	(2)	37.727	(4)
59-7	01.09.98	5ml 6N HCl	1011	1381	7	18.114	(2)	15.404	(1)	37.671	(4)
Δ% a.m.u.						0.041		0.052		0.074	
90-1	15.05.98	unleached	612	1130	3	18.426	(4)	15.449	(3)	37.924	(7)
90-1	15.05.98	unleached	613		4	18.429	(2)	15.452	(1)	37.932	(3)
90-1	31.08.98	unleached	1004	1178	6	18.439	(2)	15.462	(1)	37.964	(3)
1894-9	13.09.98	$HCl+HNO_3$	1070	1353	4	18.209	(2)	15.429	(1)	37.820	(3)
1894-9	13.09.98	$HCl+HNO_3$	1072	1400	2	18.209	(2)	15.429	(2)	37.816	(4)
Δ% a.m.u.						0.001		0.0002		0.005	
RD 7-3	31.08.99	5ml 6N HCl	2569	1350	5	18.194	(4)	15.471	(4)	37.924	(11)
RD 7-3	27.09.99	5ml 6N HCl	2867	1252	5	18.166	(2)	15.442	(1)	37.828	(3)
Δ% a.m.u.						0.076		0.094		0.126	
106	09.09.99	5ml 6N HCl	2728	1251	5	18.102	(1)	15.413	(1)	37.722	(1)
106	10.09.99	5ml 6N HCl	2735	1254	5	18.105	(1)	15.415	(1)	37.730	(2)
Δ% a.m.u.						0.006		0.007		0.010	
11-3-a-1	18.08.99	5ml 6N HCl	2562	1245	5	18.250	(3)	15.445	(2)	37.924	(6)
11-3-a-1	18.08.99	5ml 6N HCl	2561	1300	5	18.263	(2)	15.462	(2)	37.979	(5)
Δ% a.m.u.						0.036		0.056		0.073	
111	09.09.99	5ml 6N HCl	2730	1300	5	18.129	(3)	15.415	(2)	37.751	(5)
111	10.09.99	5ml 6N HCl	2733	1314	5	18.130	(3)	15.411	(2)	37.739	(5)
Δ% a.m.u.						0.005		0.013		0.015	
29	27.09.99	5ml 6N HCl	2869	1224	5	18.369	(1)	15.481	(1)	38.059	(2)
29	27.09.99	5ml 6N HCl	2878	1242	6	18.364	(2)	15.474	(2)	38.036	(4)
Δ% a.m.u.						0.014		0.021		0.030	
S-10	17.12.98	5ml 6N HCl	1415	1292	5	18.519	(1)	15.477	(1)	38.213	(3)
S-10	27.09.99	5ml 6N HCl	2868	1231	5	18.521	(1)	15.479	(1)	38.217	(2)
S-10	10.10.00	5ml 6N HCl	7981	1330	5	18.517	(1)	15.474	(1)	38.205	(3)

Table AIII-13 : Results of the leaching experiments. HCl (hot) leaching was carried out using 5ml 6N HCl, leaching for 1h at ~70°C; HCl (cold) leaching was carried out using 5ml 6N HCl, leaching for 1h at room temperature; HNO_3 (hot) leaching was carried out using 5ml 8N HNO_3, leaching 1h at ~70°C; HCl + HNO_3 (hot) leaching was carried out using 5ml 6N HCl and 5ml 8N HNO_3; leaching for 1h at 70°C.

Sample	Treatment	weight	$^{87}Sr/^{86}Sr$	2 σ	$^{143}Nd/^{144}Nd$	2 σ	$^{206}Pb/^{204}Pb$	2 σ	$^{207}Pb/^{204}Pb$	2 σ	$^{208}Pb/^{204}Pb$	2 σ
1884-9	unleached	170 mg	0.703074	(9)	0.513083	(7)	-	-	-	-	-	-
1884-9	HCl + HNO_3 (hot)	200 mg	0.702911	(7)	0.513072	(8)	18.209	(1)	15.429	(1)	37.820	(3)
1884-9	leachat	-	0.703218	(7)	0.513086	(11)	18.276	(3)	15.475	(3)	37.967	(7)
32-3	unleached	50 mg	0.703483	(7)	0.513117	(9)	18.396	(2)	15.489	(1)	38.095	(4)
32-3	HCl (hot)	200 mg	0.703471	(6)	0.513093	(8)	18.385	(2)	15.486	(2)	38.092	(4)
32-3	HCl + HNO_3 (hot)	190 mg	-	-	0.513109	(9)	18.381	(2)	15.481	(1)	38.071	(3)
32-3	leachet HCl	-	0.703494	(6)	0.512993	(9)	18.374	(2)	15.481	(2)	38.044	(4)
59-7	unleached	50 mg	0.702891	(7)	0.513007	(9)	18.166	(2)	15.439	(2)	37.797	(4)
59-7	HCl (hot)	200 mg	0.702822	(8)	0.513053	(9)	18.128	(2)	15.420	(2)	37.727	(4)
59-7	leachat HCl	-	0.702973	(7)	0.513043	(16)	-	-	-	-	-	-
59-7	unleached	40 mg	0.702902	(9)	0.513041	(8)	18.164	(2)	15.436	(2)	37.792	(4)
59-7	HCl (hot)	185 mg	0.702846	(9)	0.513053	(8)	18.114	(2)	15.404	(1)	37.671	(3)
59-7	leachet HCl	-	0.702988	(8)	0.513027	(7)	18.156	(2)	15.418	(1)	37.743	(3)
59-7	unleached	50 mg	0.702899	(8)	0.513038	(7)	18.144	(2)	15.422	(1)	37.750	(3)
59-7	HNO_3 (hot)	200 mg	0.702823	(8)	0.513045	(8)	18.143	(2)	15.434	(2)	37.770	(6)
59-7	leachet HNO_3	-	0.702970	(9)	0.513041	(8)	18.150	(2)	15.408	(1)	37.712	(4)
90-1	HNO_3 (hot)	200 mg	0.703164	(8)	-	-	18.272	(2)	15.446	(1)	37.938	(3)
90-1	unleached	50 mg	0.703297	(7)	0.513011	(8)	18.439	(1)	15.462	(1)	37.964	(3)
90-1	HCl (hot)	200 mg	0.703172	(7)	0.513005	(11)	18.271	(1)	15.446	(1)	37.934	(3)
90-1	leachat HCl	-	0.703496	(8)	0.513006	(10)	-	-	-	-	-	-
94-1	HCl + HNO_3 (hot)	200 mg	0.702878	(6)	0.512996	(12)	18.217	(1)	15.443	(1)	37.920	(3)
94-1	unleached	200 mg	0.702990	(9)	0.513001	(8)	-	-	-	-	-	-
S-10	unleached	200 mg	0.703412	(10)	0.513085	(8)	-	-	-	-	-	-
S-10	HCl (hot)	150 mg	-	-	-	-	18.519	(1)	15.477	(1)	38.213	(3)
S-10	HCl + HNO_3 (hot)	200 mg	0.703327	(8)	-	-	18.504	(2)	15.459	(1)	38.153	(3)
SOF-1a	HCl + HNO_3 (hot)	200 mg	0.703556	(7)	0.513103	(11)	18.449	(2)	15.475	(1)	38.100	(3)
SOF-1a	unleached	200 mg	0.703711	(10)	0.513105	(8)	-	-	-	-	-	-
Sof-3	HCl (hot)	200 mg	-	-	-	-	18.494	(3)	15.490	(3)	38.150	(6)
Sof-3	HCl + HNO_3 (hot)	200 mg	0.703675	(10)	0.513097	(10)	18.479	(2)	15.492	(1)	38.148	(4)
T-65	HCl + HNO_3 (hot)	200 mg	0.703460	(8)	0.513104	(13)	18.427	(2)	15.486	(1)	38.132	(3)
T-65	unleached	200 mg	0.706478	(111)	0.513107	(9)	-	-	-	-	-	-
17	unleached	80 mg	0.703600	(9)	0.513100	(9)	18.527	(3)	15.547	(3)	38.269	(6)
17	HCl (hot)	100 mg	0.703508	(9)	0.513108	(9)	18.319	(1)	15.465	(1)	37.987	(3)
17	HNO_3 (hot)	100 mg	0.703507	(8)	0.513082	(9)	18.318	(2)	15.459	(1)	37.962	(3)
17	leachate HNO_3 (hot)	-	0.706421	(16)	-	-	18.645	(1)	15.581	(1)	38.409	(3)
45	unleached	70 mg	0.703608	(8)	0.513078	(8)	18.420	(2)	15.499	(2)	38.201	(3)
45	HCl (hot)	75 mg	0.703597	(8)	0.513046	(15)	18.406	(1)	15.486	(1)	38.155	(3)
45	leachate	-	-	-	0.512885	(80)	18.514	(11)	15.572	(9)	38.487	(23)
54	unleached	90 mg	0.703799	(9)	0.513081	(9)	18.397	(1)	15.500	(1)	38.230	(3)
54	HCl (hot)	90 mg	0.703578	(8)	0.512984	(11)	18.368	(1)	15.477	(1)	38.139	(3)
54	HNO_3 (hot)	90 mg	0.703591	(9)	0.513093	(9)	18.378	(1)	15.490	(1)	38.180	(3)
54	HCl (cold)	85 mg	0.703592	(7)	0.513088	(8)	18.375	(1)	15.484	(1)	38.163	(3)
54	leachate HCl (cold)	-	0.708857	(9)	-	-	18.472	(2)	15.562	(2)	38.463	(4)
54-II	unleached	95 mg	0.703870	(8)	0.513059	(9)	18.398	(1)	15.501	(1)	38.228	(3)
54-II	HCl (hot)	110 mg	0.703587	(9)	0.512984	(8)	18.381	(1)	15.495	(1)	38.196	(3)

Table AIII-14: Common “High Priority” Samples from the Pacific Plate choosen by the ODP Leg 185 Shipboard Scientific Party.

	Sample	Sample Description
1	1149A 1H1 140-150	ash and silica bearing clay, dark brown
2	1149A 4H2 140-150	clay, greenish gray, homogeneous
3	1149A 7H4 140-150	ash-bearing siliceous silty clay, dark greenish gray, homogeneous
4	1149A 10H3 140-150	ash-bearing siliceous clay, very dark graysih brown, black fleck and splotches
5	1149A 14H2 140-150	clay, pale brown, homogeneous
6	1149A 18H3 140-150	stiff clay, deep brown, some orange mottles nearby
7	1149A 20X1 140-150	silt bearing clay, brown with yellow and dark brown mottles
8	1149B 6R1 38-42	chert with strong brown bands that are deformed, lots of well preserved radiolarians
9	1149B 11R1 19-22	radiolarian chert and rad. porcellanite, partly laminated, light brown
10	1149B 12R CC 0-5	chocolate brown clay
11	1149B 16R1 93-98	chalky limestone, orange/brown/pink
12	1149B 22R1 20-25	radiolarian marl, reddish brown
13	1149B 22R1 106-110	chert, irregular banding, some blobs of carbonate, red
14	1149B 27R1 49-55	clayey nannofossil chalk, light reddish brown, laminated
15	1149B 29R1 28-35	calcareous marl, brown with dusky red banding
16	1149B 30R1 61-66	calcite rich interflow material with basalt breccia
17	1149B 30R2 56-62	calcite and smectite vein with halo
18	1149C 10R2 47-51	basalt, very hard
19	1149D 7R1 37-42	smectite matrix
20	1149D 8R2 16-19	calcite and quartz interflow material
21	1149D 9R3 30-32	vein and halo
22	1149D 11R2 86-92	calcite breccia
23	1149D 16R3 2-8	min altered
24	1149D 17R1 92-98	smectite-calcite breccia
25	1149D 19R1 85-88	minimal altered
26	801B 43R1 132-135	minimal altered
27	801C 1R5 80-82	interflow material
28	801C 4R1 72-77	hydrothermal
29	801C 14R2 117-120	interflow material
30	801C 15R1 57-61	interlow material, chert
31	801C 15R7 31-34	minimal altered
32	801C 17R4 15-18	interflow material
33	801C 19R2 24-27	interflow material
34	801C 21R2 69-71	interflowmaterial of massive qartz and calcite (smectite)
35	801C 34R1 93-96	fresh basalt
36	801C 37R5 112-114	smectite vein and halo
37	801C 40R1 24-27	Interflow material/ calcite breccia
38	801C 43R3 50-55	vein and halo
39	801C 44R3 23-26	halo

Angelika Schmidt
Prüne 1
D-24103 Kiel

Lebenslauf

Name		Angelika Schmidt
Alter		geboren am 06. März 1972 in Bremen
Familienstand		ledig
Staatsangehörigkeit		deutsch
Schule	1978 - 1982	Grundschule an der Nordstrasse in Bremen
	1982 - 1984	Orientierungsstufe an der Schule am Waller Ring in Bremen
	1984 - 1988	Gymnasiale Oberstufe, Sekundarstufe I an der Schule am Waller Ring in Bremen
	1988 - 1991	Gymnasiale Oberstufe, Sekundarstufe II an der Schule an der Langen Reihe in Bremen mit Abschluß der allgemeinen Hochschulreife (Abitur)
Studium	Okt. 1991	Beginn des Studienganges Geowissenschaften (Diplom) an der Universität Bremen
	Juli 1994	Vordiplom im Fachbereich Geowissenschaften an der Universität Bremen
	1995 - 1996	Anfertigung der Diplomkartierung im Fachbereich Geowissenschaften bei Prof. Dr. J. Kuss zu dem Thema "Die Kartierung des Struglberges, westlich des Obojnikbaches, Kärnten"
	1996 - 1997	Anfertigung der Diplomarbeit im Fachbereich Geowissenschaften bei Dr. habil R. Klemd zu dem Thema "Rekonstruktion des P-T Pfades von Kalksilikaten und Metapeliten der Central Zone des Limpopo Belts, Südafrika"
	1997 - 1998	Diplom-Hauptprüfungen
	Jan. 1998	Diplom im Fachbereich Geowissenschaften and der Universität Bremen
Promotion	Mai 1998	Beginn der Doktorarbeit am GEOMAR, Abteilung Vulkanologie und Petrologie bei Prof. Dr. K. Hoernle mit dem Titel: „Temporal and Spatial Evolution of the Izu Island Arc, Japan in Terms of Sr-Nd-Pb Isotope Geochemistry“

Teilnahme an Schiffsexpeditionen

Apr.-Jun. 1999	Fahrtteilnehmerin ODP Leg 185: Izu-Mariana Margin
Nov.-Dez.1999	Fahrtteilnehmerin Sonne Ausfahrt SO 144-3a, Paganini 3, Panamá Becken und Galápagos „Plume“

Teilnahme an Tagungen, Kongressen und Workshops

Schmidt, A., Straub, S.M. und Hoernle, K. (1999) Regionale und zeitliche Entwicklung des zentralen Izu-Bonin Arc/ Backarc Systems innerhalb der letzten 15 Millionen Jahre. *Poster*, Kolloquium des DFG-Schwerpunktprogrammes Ocean Drilling Program/ Deep Sea Drilling Project, Bremerhaven, Deutschland

Schmidt, A., Straub, S.M., Hoernle, K.A., Hochstaedter, A.G., Langmuir, C.H. and Gill, J. (1999) Comparative evolution of the central Izu and Mariana volcanic arcs during the past 15 Million years. *Poster*, International Union of Geodesy and Geophysics (IUGG), 22nd General Assembly, Birmingham, UK

Schmidt, A., Straub, S.M., Hoernle, K., Langmuir, C.H., Gill, J.B., Hochstaedter, A.G. (2000) Vergleich von Geochemie und Struktur des Izu- und Mariana Arc / Backarc Systems in den letzten 15 Millionen Jahren. *Poster*, Kolloquium des DFG-Schwerpunktes Ocean Drilling Program/Deep Sea Drilling Project, Jena, Deutschland

Schmidt, A., Straub, S.M., Hoernle, K., Langmuir, C.H., Gill, J.B., Hochstaedter, A.G. (2000) Causes of geochemical differences between the adjacent Izu and Mariana arcs, West Pacific. *Vortrag*, IAVCEI General Assembly, Bali, Indonesia

Schmidt, A., Straub, S.M., Hoernle, K., Langmuir, C.H., Gill, J.B., Hochstaedter, A.G. (2000) Comparison of the Sr-Nd-Pb isotope geochemistry of the Central Izu and Mariana Volcanic Arcs. *Poster*. Workshop: Inside the Subduction Factory, Eugene, Oregon, USA

Schmidt, A., Straub, S.M., Hoernle, K., Langmuir, C.H., Gill, J.B., Hochstaedter, A.G. (2000) The geochemistry of the Izu and Mariana volcanic arcs: joint control of input chemistry and structure? *Vortrag*, Jahrestagung der Deutschen Mineralogischen Gesellschaft, 24.-29. September, Heidelberg, Deutschland

Schmidt, A., Straub, S.M., Hoernle, K. (2001) Modellierung von Subduktionszonenprozessen am Beispiel des Izu Arcs, Japan. *Vortrag*, Kolloquium des DFG-Schwerpunktes Ocean Drilling Program/Deep Sea Drilling Project, Karlsruhe, Deutschland